



Norwegian University of
Science and Technology

Ultimate Compressive Strain and Ductility of LWAC Beams

Henrik Nesje Johannesen
Simon André Petersen

Civil and Environmental Engineering
Submission date: June 2017
Supervisor: Jan Arve Øverli, KT

Norwegian University of Science and Technology
Department of Structural Engineering



MASTER THESIS 2017

SUBJECT AREA: Structural Engineering	DATE: 23 June 2017	NO. OF PAGES: 20+106+49
-----------------------------------------	-----------------------	----------------------------

TITLE:

Ultimate Compressive Strain and Ductility of LWAC Beams

BY:

Henrik Nesje Johannesen
Simon André Petersen



SUMMARY:

The purpose of this master thesis was to investigate confinement and ductility of lightweight aggregate concrete (LWAC) in compression. The main characteristics of LWAC in general are brittleness and uncontrolled crack propagation. Because of this, structural applications of LWAC is reduced compared to structural applications of NDC.

To test confinement of LWAC, seven over-reinforced beams were loaded in four point bending. To achieve confinement of the tested beams, shear reinforcement was introduced. The geometry of the beams was 210 x 550 x 4500 mm (width x height x length). The test setup was designed to produce a constant moment zone of 1 m between the loading points. All the seven beams were designed to fail in compression between the two loading points. To compare results, the geometry of the beams was equal to the geometry used in a previous experimental study. The main test parameters that have been varied in this experimental study were stirrup spacing, amount of compressive reinforcement and size of concrete cover. Stalite with fraction 1/2" was used as aggregate for the whole test programme. All beams and small specimens were casted from the same batch of concrete. The compressive strength and oven-dry density of the concrete used in this study was 65 MPa and 1834 kg/m³ respectively.

Four of the tested beams showed ductile behaviour. The beam without stirrups in the testing zone (between the loading points) did not show any ductile behaviour. All the beams were in the range 88-99 % of the calculated capacity. The beams with smaller stirrup spacing in the testing zone, showed more ductile behaviour. The beams with the largest concrete cover showed the largest capacity drop after the maximum load was reached.

The test results indicated that reduced stirrup spacing gave an increase of ductility, with an exception of results from one beam. An increase of concrete cover decreased the confined area, generally leading to a reduction of ductility. The beam with a larger amount of compressive reinforcement showed an increase of ductility and capacity. Based on the experimental results of this study, it is possible to increase the ductility of LWAC structures and bring the application level of LWAC closer to the application level of NDC.

RESPONSIBLE TEACHER: Jan Arve Øverli
SUPERVISOR(S): Jan Arve Øverli
CARRIED OUT AT: The Department of Structural Engineering, NTNU.



MASTEROPPGAVE 2017

Fagområde: Konstruksjonsteknikk	DAT0: 23 Juni 2017	ANTALL SIDER: 20+106+49
------------------------------------	-----------------------	----------------------------

TITLE:

Bruddtøyning i trykk og duktilitet av lettbetongbjelker

BY:

Henrik Nesje Johannesen
Simon André Petersen



SUMMARY:

Hensikten med denne masteroppgaven var å undersøke omhylling og duktilitet av lettbetong i trykk. De viktigste egenskapene til lettbetong er generelt sprøhet og ukontrollert rissutvikling. På grunn av dette reduseres anvendelsen av lettbetong i konstruksjoner sammenlignet med vanlig betong.

For å teste omhylling av lettbetong ble syv overarmerte bjelker belastet i firepunkts bøyning. For å oppnå omhylling av de testede bjelkene ble det brukt skjærarmering. Geometrien til bjelkene var 210 x 550 x 4500 mm (bredde x høyde x lengde). Testoppsettet ble utformet for å skape en konstant momentsone på 1 m mellom lastpunktene. Alle de syv bjelkene var utformet for å gå til brudd i trykk mellom de to lastpunktene. For å sammenligne resultatene var geometriene til bjelkene lik geometrien som ble brukt i en tidligere eksperimentell studie. De viktigste testparametrene som har blitt variert i denne eksperimentelle studien var bøylevstand, mengde trykkarmering og størrelsen på overdekning. Stalite med en fraksjon på 1/2 tomme ble brukt som tilslag for hele testprogrammet. Alle bjelkene og de små prøvene ble støpt fra samme betongblanding. Trykkapasiteten og ovenstørr densitet til betongen som ble benyttet i denne studien var 65 MPa og 1834 kg/m³.

Fire av de testede bjelkene viste duktil oppførsel. Bjelken uten skjærbøyler i testsonen (mellom lastpunktene) viste ikke duktil oppførsel. Alle bjelkene oppnådde 88-99 % av den beregnede kapasiteten. Bjelkene med kortere avstand mellom skjærbøylene i testsonen viste mer duktil oppførsel. Bjelkene med størst overdekning viste størst kapasitetsfall etter at maksimal belastning var nådd.

Testresultatene indikerte at redusert avstand mellom skjærbøylene ga en økning i duktilitet, med unntak av resultater fra en bjelke. En økning av overdekningen reduserte det omhyllende arealet, som generelt fører til en reduksjon av duktiliteten. Bjelken med mer trykkarmering viste en økning i duktilitet og kapasitet. Basert på eksperimentelle resultater fra denne studien, er det mulig å øke duktiliteten til konstruksjoner av lettbetong og føre anvendbarheten nærmere som for normalbetong.

FAGLÆRER: Jan Arve Øverli
VEILEDER(E): Jan Arve Øverli
UTFØRT VED: Institutt ved konstruksjonsteknikk

Abstract

The purpose of this master thesis was to investigate confinement and ductility of lightweight aggregate concrete (LWAC) in compression. The main characteristics of LWAC in general are brittleness and uncontrolled crack propagation. Because of this, structural applications of LWAC are reduced compared to structural applications of normal density concrete (NDC).

To test confinement of LWAC, seven over-reinforced beams were loaded in four point bending. To achieve confinement of the tested beams, shear reinforcement was introduced. The geometry of the beams was 210x550x4500 mm (width x height x length). The test setup was designed to produce a constant moment zone of 1 m between the loading points. All the seven beams were designed to fail in compression between the two loading points. To compare results, the geometry of the beams was equal to the geometry used in a previous experimental study [18]. The main test parameters that have been varied in this experimental study were stirrup spacing, amount of compressive reinforcement and size of concrete cover. Stalite with fraction 1/2" was used as aggregate for the whole test programme. All the beams and the small specimens were casted from the same batch of concrete. The compressive strength and oven-dry density of the concrete used in this study was 65 MPa and 1834 kg/m³ respectively.

Four of the tested beams showed ductile behaviour. The beam without stirrups in the testing zone (between the loading points) did not show any ductile behaviour. All the beams were in the range 88-99 % of the calculated capacity. The beams with smaller stirrup spacing in the testing zone, showed more ductile behaviour. The beams with the largest concrete cover showed the largest capacity drop after the maximum load was reached.

The test results indicated that reduced stirrup spacing gave an increase of ductility, with an exception of results from one beam. An increase of concrete cover decreased the confined area, generally leading to a reduction of ductility. The beam with a larger amount of compressive reinforcement showed an increase of ductility and capacity. Based on the experimental results of this study, it is possible to increase the ductility of LWAC structures and bring the application level of LWAC closer to the application level of NDC.

Table of Contents

Abstract	i
Table of Contents	v
List of Tables	vii
List of Figures	xii
Abbreviations	xiii
Nomenclature	xv
Acknowledgements	xix
1 Introduction	1
2 Lightweight Aggregate Concrete	3
2.1 Definition	3
2.2 History	4
2.3 Types of LWA	5
2.3.1 Natural LWA	5
2.3.2 Manufactured LWA	5
2.3.3 Stalite	6
2.4 LWAC Mix Design	7
2.5 Properties	7
2.5.1 Grains	7
2.5.2 Water Absorption	7
2.5.3 Thermal Properties	8
2.6 Mechanical Properties	8
2.6.1 Compressive Strength	8
2.6.2 Tensile Strength	8
2.6.3 Shear Strength	9

2.6.4	Young's Modulus	9
2.6.5	Fracture Energy and Fatigue	9
2.7	Creep and Shrinkage	9
2.8	Ductility and Seismic Applications	9
2.9	LWAC in Eurocode 2	10
3	Confinement	13
3.1	Stress-Strain Model	14
3.1.1	Effectively Confined Area of Rectangular Concrete Sections	14
3.1.2	Stress-Strain Curve of Confined Concrete	16
4	Methodology	19
4.1	Test Specimens	19
4.1.1	Small Specimens	19
4.1.2	Beams	22
4.2	Material and Mix Properties	24
4.2.1	Concrete Mix Recipe and Goal	24
4.2.2	Measurement of Moisture and Absorption of Stalite	24
4.2.3	Determination of Sieve Curve for Stalite	25
4.2.4	Final Concrete Recipe	26
4.2.5	Methodology for Concrete Preparation	27
4.2.6	Reinforcement	27
4.3	Test Setup and Procedure	31
4.3.1	Four Point Bending Test	31
4.3.2	Setup of Measuring Devices	32
4.3.3	Calculation of Capacities	35
5	Results	43
5.1	Material Properties	43
5.1.1	Compressive Strength	44
5.1.2	Tensile Splitting Strength	46
5.2	Beams	48
5.2.1	Beam 1 - LWAC65_20_0	49
5.2.2	Beam 2 - LWAC65_20_200	58
5.2.3	Beam 3 - LWAC65_20_60	63
5.2.4	Beam 4 - LWAC65_20_100	68
5.2.5	Beam 5 - LWAC65_40_60	74
5.2.6	Beam 6 - LWAC65_40_100	76
5.2.7	Beam 7 - LWAC65_40_200	81
5.3	Calculated Confined Concrete Capacity Revisited	87
6	Discussion	89
6.1	Stirrup Spacing	89
6.2	Concrete Cover	91
6.3	Amount of Compressive Reinforcement	93
6.4	Confinement	93

6.5 Comparison with Previous Experimental Work	94
7 Summary and Conclusion	99
8 Further Study	101
Bibliography	101
Appendix A Reinforcement Layout	107
A.1 Technical Drawings of Beams	107
A.2 Documentation of Cover and Spacing	116
Appendix B Results	125
B.1 Beam Testing	125
B.2 Crack Development	129
B.3 Material Properties	136
Appendix C Calculations	141
C.1 Moment Capacity	142
C.2 Shear Capacity	145
C.3 Load-Deflection Curve	146
C.4 Confinement	148

List of Tables

4.1	Test programme	23
4.2	Values for sieve curve for Stalite	25
4.3	Final concrete recipe mix	26
4.4	Ratios	27
4.5	Calculated moment capacities and maximum calculated load	37
4.6	Confined compressive capacity	42
5.1	Material properties	43
5.2	Compressive strength of cubes	44
5.3	Compressive Strength of Cylinders	46
5.4	Tensile splitting strength of cylinders	47
5.5	Summary of testing results	49
5.6	73
5.7	Confined concrete compressive capacity	88
6.1	Deflections at peaks and deflection plateaus	91
6.2	Maximum concrete compressive strains on the top surface	92
6.3	Compressive capacities	93
6.4	Aggregate, compressive strength and reinforcement layout of compared beams	94
6.5	Local maximum loads with corresponding deflections for all beams	96
6.6	Maximum concrete compressive strains on the top surface	97
B.1	Beam 1 - Steps, loads, deflections and strains	125
B.2	Beam 2 - Steps, loads, deflections and strains	126
B.3	Beam 3 - Steps, loads, deflections and strains	126
B.4	Beam 4 - Steps, loads, deflections and strains	127
B.5	Beam 6 - Steps, loads, deflections and strains	127
B.6	Beam 7 - Steps, loads, deflections and strains	128

List of Figures

2.1	Stolmabrua [38]	4
2.2	Leca [43]	5
2.3	Liapor [42]	6
2.4	Stalite [11]	6
2.5	Schematic representation of the non-linear stress-strain relation for structural analysis [26]	10
2.6	Parabola-rectangle diagram for concrete under compression [26]	11
2.7	Bi-linear stress-strain relation [26]	12
3.1	Stress-strain relation of unconfined and confined concrete [26]	14
3.2	Confined concrete area [16]	15
3.3	Stress-strain curve of confined concrete [5]	16
4.1	Cube and cylinder in the <i>ToniTechnik</i> machine	20
4.2	Cylinder in the <i>Mohr Federhaff Losenhausen</i> machine	21
4.3	Beam geometries and reinforcement layouts between the loading points. All dimensions are in [mm]	22
4.4	Side of beam marked for DIC	24
4.5	Sieve curve for Stalite	26
4.6	Connection of plate and reinforcement	30
4.7	Four point bending	31
4.8	Setup on the west side of the beam.	32
4.9	Setup on the east side of the beam.	32
4.10	Measuring devices at the middle of the beam	33
4.11	Subareas (or subsets) before and after deformation [21]	34
4.12	Bending of cross section	35
4.13	Simply supported beam loaded symmetrically [41]	39
4.14	Calculated load-deflection curve	40
4.15	Effectively confined concrete core	41
4.16	Calculated stress-strain curve of all tested beams	42

5.1	Development of compressive strength of cubes	45
5.2	Failure of cubes in compression	45
5.3	Failure of cylinders in compression	46
5.4	Failure of cylinders in tension	47
5.5	Location and designated names for each measuring device	49
5.6	Yielding of steel spreader beam for setup 1	50
5.7	First and second setup of beam 1	50
5.8	Load-deflection curves setup 1 for beam 1	51
5.9	Load-deflection curves setup 2 for beam 1	51
5.10	Load-compressive strain curves setup 1 for beam 1	52
5.11	Load-compressive strain curves setup 2 for beam 1	53
5.12	Load-tensile strain curves setup 1 for beam 1	54
5.13	Load-tensile strain curves setup 2 for beam 1	54
5.14	Strain distribution at different load levels for beam 1	55
5.15	Beam 1 - Whole beam, failure	55
5.16	Beam 1 - Test zone, failure	56
5.17	Strain field from DIC	57
5.18	Load-deflection curves for beam 2	58
5.19	Load-compressive strain curves for beam 2	59
5.20	Load-tensile strain curve for beam 2	60
5.21	Strain distribution at different load levels for beam 2	60
5.22	Beam 2 - Whole beam, failure	61
5.23	Beam 2 - Test zone, failure	61
5.24	Strain field from DIC	62
5.25	Load-deflection curves for beam 3	63
5.26	Load-compressive strain curves for beam 3	64
5.27	Load-tensile strain curves for beam 3	64
5.28	Strain distribution at different load levels for beam 3	65
5.29	Beam 3 - Whole beam, failure	66
5.30	Beam 3 - Test zone, failure	66
5.31	Strain field from DIC	67
5.32	Load-deflection curves for beam 4	68
5.33	Load-compressive strain curve for beam 4	69
5.34	Load-tensile strain curves for beam 4	70
5.35	Strain distribution at different load levels for beam 4	70
5.36	Beam 4 - Whole beam, failure	71
5.37	Beam 4 - Test zone, failure	72
5.38	Load-time curves for all the beams	72
5.39	Strain field from DIC	73
5.40	Visual pockets of air in the concrete	74
5.41	Beam 5 - Whole beam, failure	75
5.42	Beam 5 - Test zone, failure	75
5.43	Load-deflection curves for beam 6	76
5.44	Load-compressive strain curves for beam 6	77
5.45	Load-tensile strain curves for beam 6	77

5.46	Strain distribution for different load levels for beam 6	78
5.47	Beam 6 - Test zone, failure	79
5.48	Strain field from DIC	80
5.49	Load-deflection curves for beam 7	81
5.50	Load-compressive strain curves for beam 7	82
5.51	Load-tensile strain curves for beam 7	83
5.52	Strain distribution for different load levels for beam 7	83
5.53	Beam 7 - Whole beam, failure	84
5.54	Beam 7 - Test zone, failure	85
5.55	Strain field from DIC	86
5.56	87
5.57	Updated calculated stress-strain curves for all the tested beams	88
6.1	Load-deflection curves for all the beams	90
6.2	Load-average top strain curves for all the beams	91
6.3	DIC-pictures of max strain longitudinally with accompanying cross sections	92
6.4	Test programme of previous experimental study [18].	95
A.1	Beam 1 - Reinforcement layout.	108
A.2	Beam 2 - Reinforcement layout.	109
A.3	Beam 3 - Reinforcement layout.	110
A.4	Beam 4 - Reinforcement layout.	111
A.5	Beam 5 - Reinforcement layout.	112
A.6	Beam 6 - Reinforcement layout.	113
A.7	Beam 7 - Reinforcement layout.	114
A.8	Recapitulation of total reinforcement for all beams.	115
A.9	Beam 1 - Stirrup spacing	116
A.10	Beam 1 - Concrete cover	116
A.11	Beam 2 - Stirrup spacing	117
A.12	Beam 2 - Concrete cover	117
A.13	Beam 3 - Stirrup spacing	118
A.14	Beam 3 - Concrete cover	118
A.15	Beam 4 - Stirrup spacing	119
A.16	Beam 4 - Concrete cover	119
A.17	Beam 5 - Stirrup spacing	120
A.18	Beam 5 - Concrete cover	120
A.19	Beam 6 - Stirrup spacing	121
A.20	Beam 6 - Concrete cover	121
A.21	Beam 6 - Stirrup spacing	122
A.22	Beam 7 - Concrete cover	122
B.1	Beam 1 - Setup 1 - Load steps with drawn crack development.	129
B.2	Beam 1 - Setup 2 - Load steps with drawn crack development.	130
B.3	Beam 2 - Load steps with drawn crack development.	131
B.4	Beam 3 - Load steps with drawn crack development.	132
B.5	Beam 4 - Load steps with drawn crack development.	133

B.6	Beam 6 - Load steps with drawn crack development.	134
B.7	Beam 7 - Load steps with drawn crack development.	135

Abbreviations

NDC	=	Normal density concrete
NWC	=	Normal weight concrete
LWA	=	Lightweight aggregate
LWAC	=	Lightweight aggregate concrete
PFA	=	Pure fly ash
DIC	=	Digital image correlation
LVDT	=	Linear variable differential transformer
SG	=	Strain gauge
EC2	=	NS-EN 1992-1-1:2004+NA2008

Nomenclature

f_{c0}	: Compressive strength of unconfined concrete
f'_l	: Effective lateral stress of the confinement
f'_{lx}	: Effective lateral stress of the confinement in x-direction
f'_{ly}	: Effective lateral stress of the confinement in y-direction
f_l	: Lateral confinement stress
f_{yh}	: Yield strength of stirrups
k_e	: Effective confinement coefficient
ρ_{cc}	: Longitudinal reinforcement ratio
A_{sp}	: Transverse reinforcement area
A_{cc}	: The area within a stirrup, when subtracting the area of the longitudinal reinforcement
A_i	: ineffectively confined concrete area
A_e	: Effectively confined concrete area
ρ_s	: Volumetric ration of circular stirrups
ρ_x	: Volumetric ration of stirrups in x-direction
ρ_y	: Volumetric ration of stirrups in y-direction
w'_i	: Distance of free concrete between longitudinal bars
E_{slope}	: The slope of the descending curve after peak stress
bc	: Distance between outermost vertical stirrups
dc	: Distance between outermost horizontal stirrups
s'	: Distance of free concrete between stirrups
f_{cc}	: Confined concrete capacity
ε_{c0}	: Unconfined concrete strain corresponding to the peak stress
ε_{cc0}	: Confined concrete strain corresponding to the peak stress
ε_{ccu}	: Confined concrete ultimate strain
ε_c	: Confined concrete strain
ε_{65}	: The strain corresponding to the stress equal to $0.65f_{cc}$
σ_{cc}	: Confined concrete stress
E_{bc0}	: Calculated Young's modulus in the first interval
f_{ctm}	: Mean value of axial tensile strength of concrete
f_{lctm}	: Mean value of axial tensile strength of LWAC
$f_{ctk,0,05}$: Mean characteristic tensile capacity of NDC with a significance level of 5%
$f_{lctk,0,05}$: Mean characteristic tensile capacity of LWAC with a significance level of 5%
ρ	: Oven-dry density
E_{cm}	: Young's modulus of concrete
E_{lcm}	: Young's modulus of LWAC
ε_{c1}	: Compressive strain in concrete at peak stress for non-linear stress-strain relation
ε_{cu1}	: Ultimate compressive strain in concrete at peak stress for non-linear stress-strain relation

f_{cm}	: Mean value of compressive strength of concrete
f_{lcm}	: Mean value of compressive strength of LWAC
ε_{c2}	: Compressive strain in concrete at peak stress for parabola-rectangle stress-strain relation
ε_{cu2}	: Ultimate compressive strain in concrete at peak stress for parabola-rectangle stress-strain relation
ε_{c3}	: Compressive strain in concrete at peak stress for bi-linear stress-strain relation
ε_{cu3}	: Ultimate compressive strain in concrete at peak stress for bi-linear stress-strain relation
f_{lc}	: Compressive strength of LWAC
f_{lct}	: Tensile splitting strength of LWAC
A_c	: Area of concrete subjected to load
F_c	: Compressive force applied to the specimen
F	: Tensile force applied to cylindrical specimen
L	: Length of cylinder specimen
d	: Diameter of cylinder specimen
c_m	: Moisture content
m_w	: Mass of a tested sample before drying
m_d	: Mass of an oven dry tested sample in air
a	: Absorption
m_s	: Mass of a saturated surface dry test sample
ϕ	: Steel bar diameter
f_{yk}	: Characteristic yield strength of steel
$l_{b,rqd}$: Basic required anchorage length
σ_{sd}	: Design stress in the reinforcement at the point where the anchorage is measured from
f_{bd}	: Ultimate bond strength
θ	: Angle between the compression strut and the horizontal axis
ΔF_{td}	: Additional force in the longitudinal reinforcement
A_{sl}	: Sectional area of tensile reinforcement
f_{ctd}	: Concrete tensile strength
A'_s	: Sectional area of compressive reinforcement
h	: Height of cross section
b	: Width of top part of cross section
α	: Compressive zone part of effective height
d	: Effective height
αd	: Neutral axis depth
d'	: Distance from center of compressive reinforcement to top edge
f_{lcm}	: Mean cylinder compressive strength
f_{lck}	: Characteristic compressive strength
η_1	: Reduction factor
E_s	: Young's modulus of reinforcement
ε_s	: Tensile reinforcement strain
ε'_s	: Compressive reinforcement strain

ε_{cu}	:	Ultimate concrete strain
σ_s	:	Tensile reinforcement stress
σ'_s	:	Compressive reinforcement stress
σ_c	:	Concrete stress
F_c	:	Concrete force
F'_s	:	Compressive reinforcement force
F_s	:	Tensile reinforcement force
z_s	:	Moment arm from tensile reinforcement to bottom edge
z'_s	:	Moment arm from the compressive reinforcement to bottom edge
z_c	:	Moment arm from concrete force to bottom edge
M_R	:	Moment capacity
$V_{lRd,c}$:	Shear capacity without shear reinforcement
$V_{lRd,s}$:	Value of the shear force which can be sustained until yielding of the shear reinforcement
$V_{lRd,max}$:	Value of the maximum shear force which can be sustained by the member, limited by crushing of the compression strut.
A_{sw}	:	Cross sectional area of stirrups
s	:	Stirrup spacing from center to center
z	:	Internal moment arm
f_{yk}	:	Characteristic yield strength of shear reinforcement
α_{cw}	:	Value depending on the stress state in the compressive strut
b_w	:	Width of cross section
ν_1	:	Strength reduction factor for concrete exposed to shear forces
I_{c1}	:	The concrete's contribution to the second moment of area
I_{s1}	:	The reinforcement's contribution to the second moment of area
$(EI)_1$:	Bending stiffness of uncracked cross section
δ_I	:	Deflection of uncracked cross section
η	:	Material stiffness ratio
ρ_l	:	Reinforcement ratio
I_c	:	Equivalent second moment of area of the concrete
$(EI)_2$:	Bending stiffness of cracked cross section
δ_{II}	:	Deflection of cracked cross section
δ	:	Deflection when accounting for tension stiffening
P_{cr}	:	Critical load when cracking occurs
M_{cr}	:	Critical moment when cracking occurs
$f_{ctk,0,95}$:	Mean characteristic tensile capacity of NDC with a significance level of 95%
$f_{lctk,0,95}$:	Mean characteristic tensile capacity of LWAC with a significance level of 95%
ε_{lcu1}	:	Ultimate compressive strain in LWAC at peak stress for non-linear stress-strain relation
ε_{lcu2}	:	Ultimate compressive strain in LWAC at peak stress for parabola-rectangle stress-strain relation
ε_{lcu3}	:	Ultimate compressive strain in LWAC at peak stress for bi-linear stress-strain relation

Acknowledgements

We would like to thank our supervisors Professor Jan Arve Øverli and Ph.D. candidate Jelena Zivkovic for guidance and valuable inputs throughout the semester. They have provided us with the necessary theoretical background and critique. Thanks are also due to Senior Scientist Hans Stemland for valuable inputs and Researcher Egil Fagerholt for processing DIC files when time has been a limiting factor. We would also like to thank our colleagues Khaled Bastami and Jonas Andås Belayachi for good collaboration and team work in lab and in the finishing process of the semester. Thanks are also due to all the people working in the laboratory at NTNU, especially Gøran Loraas and Steinar Seehuus. They have provided much help and guidance when constructing and testing the beams.

We would like to give special thanks to Jelena Zivkovic for extra close supervision and valuable discussions. She has spent much more time than expected of her to accommodate for misfortunes we have experienced in the lab work. We would like to express our gratitude as she has made us feel like part of an efficient team when this whole process could have been a race against the clock.

Lastly, we would like to thank our friends, Eirik Bugge Kulsrud, Steffen Hammersvik, Ole Christian Holsen, Sammy Ziedoy, Niklas Amundsen, Aksel Lynum, Jon Magnus Stensjen, Hallvard Hjellvik and Sondre Tuft Thorgerisson for inspiring discussions and good company throughout the semester.

Introduction

Lightweight aggregate concrete (LWAC) has been utilized in construction for more than two thousand years. The Greeks and Romans used natural lightweight aggregates (LWA) to lighten the mortar. LWAs were eventually manufactured and used more commonly after 1917.

The advantageous relationship between weight and strength for LWAC will in various cases lead to more cost-efficient structures. LWAC is usually applied in tall buildings or bridges with long main spans. In spite of many advantageous aspects of LWAC, the use in design is often limited due to the generally brittle behaviour and low ductility.

This thesis is a part of the research project *Durable Advanced Concrete Structures* (DACS), through NTNU's participation. The purpose of the project is to develop knowledge, methods and tools that allow for sustainable and competitive concrete structures in an arctic-marine environment. The project is divided in four work packages. This thesis is a part of the fourth package, Ductile Lightweight Aggregate Concrete.

Stalite is a LWA that is manufactured from expanded argillite slate. The aggregate is less absorptive compared to other LWAs. The pore structure of Stalite is advantageous when mixing and pumping concrete.

The focus of this thesis was to investigate how confinement affects ductile behaviour of LWAC in compression. It was decided to test over-reinforced beams made with Stalite as aggregate. Seven over-reinforced beams were subjected to compression through a four point bending test. They were heavily reinforced to resist shear, tension and anchorage failure. To determine material properties, small cubes and cylinders were tested.

Lightweight Aggregate Concrete

The main difference between lightweight aggregate concrete (LWAC) and normal density concrete (NDC) is the density. By reducing the weight of the concrete by approximately 20 %, LWAC will in many cases be advantageous for use in the construction industry compared to NDC [14].

However, the lower density is not the only difference between LWAC and NDC. The formation of cracks differs in a way that makes failure of LWAC more brittle and explosive compared to NDC. To make LWAC a more competitive material, compressive ductility has to be increased, so that LWAC provides as safe and reliable structures as NDC.

In addition to brittleness, LWAC has more disadvantages compared to NDC. Lower tensile strength makes anchoring and lap lengths longer. Another disadvantage is that the material properties of the concrete strictly depend on the type of LWA.

2.1 Definition

Many codes and standards define LWAC differently. Several of these codes define LWAC as a concrete with an oven-dry density less than 2000 kg/m^3 [14, 28]. Although this is a maximum limit, LWAC can be produced with a variety of densities, cube strengths and thermal conductivities. The density can vary from $300\text{-}2000 \text{ kg/m}^3$ [14, 25][7].

Structural LWAC is covered in the Norwegian Standard NS 3473/1992. In this standard, concrete containing LWA with an oven-dry density in the range from $1200\text{-}2000 \text{ kg/m}^3$ is defined as LWAC.

2.2 History

The utilization of LWA stretches back to before the Christian era. LWA was used both by Greeks and Romans. The first LWA ever used were pumice and scoria with volcanic origin. The Pantheon vault in Rome is one example where pumice was applied to lighten the weight of the mortar. Further examples of magnificent structures built with LWA are the Sophia Cathedral in Istanbul and the St. Peter's Basilica in the Vatican.

The industrial production of bricks containing pumice started in Germany in the middle of the 19th century. Most of the pumice extracted in the world today is exported to Germany where production of building blocks is continuing. Pumice started being a part of the building industry in Iceland in 1923 [14, 3].

LWAC was used more commonly after the introduction of a process by S. J. Hayde in 1917. This industrial process expanded clay using a tubular kiln. Aggregates from this process were used when constructing ship hulls in World War 1. Also, some hotels, business buildings and bridges were constructed with LWAC following world war 1 [14, 36]. In Europe, the first clay processing plant was built in Denmark in 1939 and the U.K. was the first country to produce sintered pure fly ash (PFA) [14, 33].

As world war 2 played out, use of LWAC increased fast. From 1950-1960 structures began to be built exclusively with LWAC, and some partially with LWAC. Some examples are 42 story buildings and airport terminals. During recent years, LWAC has been utilized in construction of parking structures, bridges, floors, roof fills and thin shell structures. LWAC also has pavement and geotechnical applications. In Norway LWAC is applied especially for bridges. One of these bridges is the Stolma Bridge shown in Figure 2.1. This is the longest segmental concrete box girder span bridge in the world. The main span of the bridge stretches 301 m. The main part of this span is 184 m long and is made from LWAC. The Sundøy and Raftsundet bridges are other examples of other bridges with main spans constructed partially from LWAC. LWAC has been applied to balance the weight difference between the main span and the shorter flanking spans of these bridges [6].



Figure 2.1: Stolmabrua [38]

2.3 Types of LWA

2.3.1 Natural LWA

Pumice and scoria are volcanic stones with a cellular structure, and are the two types of natural LWAs that are most commonly used [14, 3]. These LWAs are natural deposits, and are only handled mechanically by crushing and screening [14, 33].

2.3.2 Manufactured LWA

Manufactured LWA consists of three different subgroups, depending on the origin of their raw material. The first subgroup is natural materials. Examples are perlite, clay and shale. The second subgroup is industrial products or by-products. Glass or fly ash being two examples. The last subgroup is industrial by-products themselves and examples include PFA, cinder, or expanded slag [14, 33].

There are two types of production principals when manufacturing LWA. By developing steam or heating minerals to fusion temperature, pyroplasticity and formation of gas will occur to bloat the aggregate (called "expansion"). In addition to this, heating of the materials to temperatures above 1100° C causes some of the material to melt, turning it into aggregate by merging (called "agglomeration") [14].

Leca is a scandinavian LWA based on clay. It is manufactured by the principal of expansion, where the raw material is dried and heated in a rotary kiln to fusion temperature. This results in an expansion of the material, where the product has a porous core and a hard outer surface. Leca is delivered in grain sizes of 2 to 32 mm [39][40][9].



Figure 2.2: Leca [43]

Liapor is a German LWA based on shale. At first, the raw material becomes crushed and dried. It is then powderized and compressed into a homogeneous mass, and later turned into pellets of desirable size and coated in limestone. The final part of the production process involves a rotary kiln where the expansion process of the pellets can be controlled to provide preferred density [9].



Figure 2.3: Liapor [42]

2.3.3 Stalite

Stalite is an LWA that has been proven to be a suitable aggregate in structural concrete. The foothills region of North Carolina is the only place where slate is exhausted as raw material to produce Stalite. The region is called the "Tillery Formation" and contains argillite slate. The argillite slate is a laminated, fine-grained siltstone of clastic rock. The aggregate can achieve up to 30 % less unit weight than an normal density aggregate (NDA). The bulk density ranges from 720-880 kg/m³ for coarse aggregate and 960-1120 kg/m³ for fine aggregate. With the absorption of about 6 % and relatively high particle strength, concrete containing Stalite can achieve over 83 MPa of compressive strength. The low absorption of the aggregate allows for easy mixing and pumping of the concrete. The hardness of the material is equivalent to that of the quartz [14, 19][11].



Figure 2.4: Stalite [11]

2.4 LWAC Mix Design

In general, regular routines and methods for mixing LWAC are the same as for NDC. However, there are some considerations to be made. The density of the LWAC will differ depending on the mix; the aggregate is absorptive by nature and the final LWAC properties depend on the LWA material characteristics [14].

The American Concrete Institute (ACI) provides information and knowledge about alternative ways and important concepts when mixing LWAC. ACI 211.2-91 presents two different methods of mixing LWAC: the "Weight method" and the "Volumetric method". Common for both procedures is that they are based on test and fail trial batching [14, 1].

Another important aspect of LWAC proportioning, is to use presaturated LWA. ACI 304.5R-91 favors use of presaturated LWA. The reason for this is to avoid the LWA absorbing the liquid part of additives [14, 2].

2.5 Properties

2.5.1 Grains

Size, size distribution, and shape of the grains impact strength, the content of cement and mix water and the workability of the LWAC. Strength generally decreases as grain size increases, while the amount of cement and mix water depend on size distribution, shape and the water absorption of the aggregate [14].

When considering bonding between aggregate and paste, it is preferred that the shape of the aggregate is spherical. The external surface of the aggregate should be solid, closed and not perfectly smooth (to increase bonding), while the inside should have high porosity [14, 8]. The reason for this is to create good bonding between aggregate and paste and to prevent paste from infiltrating into the aggregate [14]. Leca and Liapor are examples of LWAs that have a spherical shape and a solid outer surface. Stalite is different from these two. Stalite has a non-spherical shape, and the outer surface is rough and not solid. Later studies show that this uneven geometry, where aggregate is able to soak paste from the concrete mix, leads to increased bonding between aggregate and paste. Because of this, cracking lines can develop through and around the aggregate.

2.5.2 Water Absorption

LWA requires larger amounts of water to be saturated compared to NDA. This is an unique trait for LWAs and should be accounted for in the production process of the concrete mix. If the LWA is not desirably saturated before added to the concrete mix, it will absorb water from the paste. If absorption occurs, workability of the LWAC decreases. However, full saturation of the LWA can not be achieved, due to lack of connection between pores [7][14, 3, 29].

2.5.3 Thermal Properties

The thermal properties of LWAC will in many cases make LWAC a preferable material compared to NDC. The reason for this is that LWAC shows lower heat capacity and higher insulating properties than NDC. It also has a lower coefficient of thermal expansion [7].

2.6 Mechanical Properties

2.6.1 Compressive Strength

Due to the homogeneity of the particle-matrix bond, the matrix is very efficient [14, 25]. As the particle and paste moduli are also similar, the fracture line will go through the aggregate as opposed to a fracture in the mortar going around the grains. This characteristic is usually seen in high strength concrete and not in common concretes [14, 36].

The correlation between cylinder and cube strength of LWAC is related to the type and amount of LWA. For NDC it is more related to the specimen and how it is stressed [14, 35]. For NDC, some standards use a fixed ratio between the cylinder and the cube strengths, which may lead to inaccuracies when calculating LWAC strength, because the correlations are not the same for LWAC and NDC.

The effect of confinement on the compressive strength has been found to be reduced with approximately 50% for high strength concretes [14, 4].

The problem of high curing temperatures of more than 60-70 degrees is worse in LWAC than in NDC because of the low heat capacity of LWAC [14, 30].

Because the LWA is the weaker part of the concrete, a lower increase of strength will be observed by increasing the cement amount. This is when comparing NDC and LWAC [14, 25].

LWAC normally reaches 80 % of the 28-days compressive strength after 7 days. The strength growth in the space 28-90 days is considered low because of the strength limiting effect of the LWA. It is common to exploit the strength properties of the aggregate to the limit to achieve optimal density/strength ratio in the LWAC [14].

2.6.2 Tensile Strength

The tensile strength is important when considering cracking. As discussed earlier, LWAC has a different fracture path, as the paths goes through the aggregate. LWAC also has a higher water content. Because of the higher moisture gradients, a great reduction in tensile strength can be observed. Flexural strength is more affected than the tensile splitting strength [14, 25].

Both flexural and tensile splitting strength of LWAC is inferior to that displayed of NDC, when observing same strength levels for both concretes [14, 44]. LWAC specimens that are exposed to eccentrically concentrated loads also show inferior results, as this capacity depends on the density of the concrete [14, 37].

The splitting tensile strength is affected by curing conditions. The strength of cubes cured in dry conditions are observed to be 10 % lower than for those that are cured under water [14, 17]. The ratio of tensile/compressive strength is normally in the range 5-15

% for LWAC with compressive strength higher than 20 MPa. The compressive strength increases faster compared to the tensile strength [14].

2.6.3 Shear Strength

There is only a small difference between LWAC and NDC when considering shear capacity. Studies have reported that the strength of a LWAC beam is 7 % lower than the strength of a similar NDC beam. The study compares beams with concrete of identical compressive cube strength and a 45° strut angle [14, 17].

2.6.4 Young's Modulus

The Young's modulus is a function of the moduli of all the parts of the concrete, the proportions of each part and the bond strength between the aggregate and the matrix. Most LWAs have a low stiffness which results in a lower modulus for LWAC compared to NDC [14, 44].

2.6.5 Fracture Energy and Fatigue

The energy consumed by creating a unit crack area is defined as the fracture energy. Some studies show that LWAC only has a slightly lower resistance to cracking than that of NDC. Other studies have shown contrary results where the resistance were 50 % lower [14, 13][14, 32].

Most studies show that LWAC performs equally or slightly better than NDC when comparing susceptibility to fatigue. This excludes cyclic tensile-compressive states, where LWAC showed slightly poorer results [14].

2.7 Creep and Shrinkage

LWAC has been considered as a material showing greater creep and shrinkage compared to NDC, assuming materials of equal compressive strength [7]. Later studies show that LWAC that contains porous aggregate has reduced shrinkage. Beyond this, tests on LWAC with higher strength behave more similar to NDC [12][22][10].

2.8 Ductility and Seismic Applications

LWAC's low density compared to NDC will essentially make LWAC a preferable material concerning seismic applications. However, LWAC has shown to be a less ductile material compared to NDC, considering materials of equal compressive strength. This can in many cases be limiting for LWAC, especially for structures demanding ductile behaviour [7].

2.9 LWAC in Eurocode 2

All design rules in every chapter in the standard are applicable for LWAC, unless they are substituted by the rules given in chapter 11 [26]. Tensile strength, ultimate compressive strain and Young's modulus are mechanical properties that are regulated in chapter 11. These parameters are reduced by use of reduction factors and have an additional index l as shown under [26]:

$$f_{lctm} = f_{ctm}\eta_1 \quad (2.1)$$

$$f_{lctk,0.05} = f_{ctk,0.05}\eta_1 \quad (2.2)$$

$$f_{lctk,0.95} = f_{ctk,0.95}\eta_1 \quad (2.3)$$

where

$$\eta_1 = 0.40 + 0.60 \frac{\rho}{2200}$$

$$E_{lcm} = E_{cm}\eta_E \quad (2.4)$$

where

$$\eta_E = \left(\frac{\rho}{2200}\right)^2$$

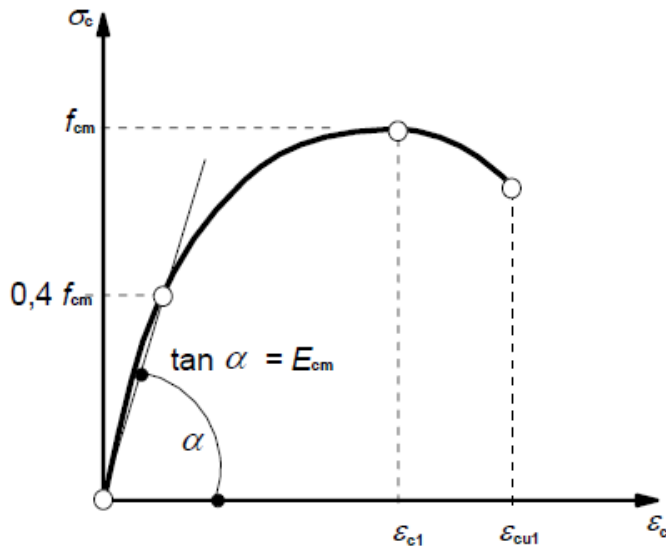


Figure 2.5: Schematic representation of the non-linear stress-strain relation for structural analysis [26]

$$\varepsilon_{lcu1} = \varepsilon_{lc1} = \frac{k f_{lcm}}{E_{lcm} \eta_E} \quad (2.5)$$

where $k = 1.1$ for sanded LWAC and $k = 1.0$ for all other LWACs.

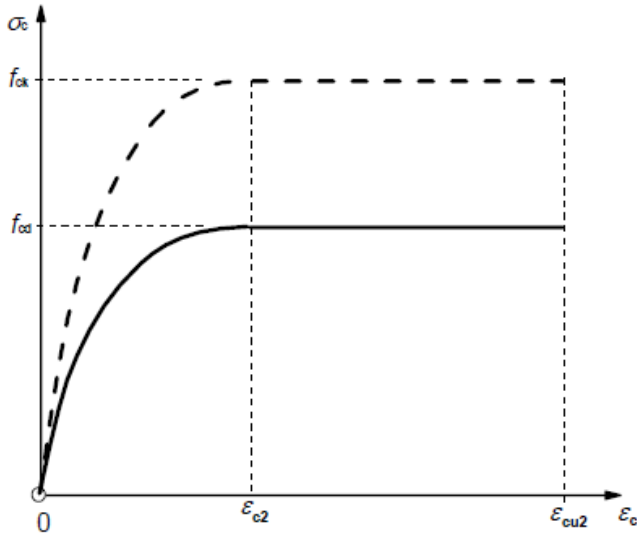


Figure 2.6: Parabola-rectangle diagram for concrete under compression [26]

$$\varepsilon_{lcu2} = \varepsilon_{cu2} \eta_1 \quad (2.6)$$

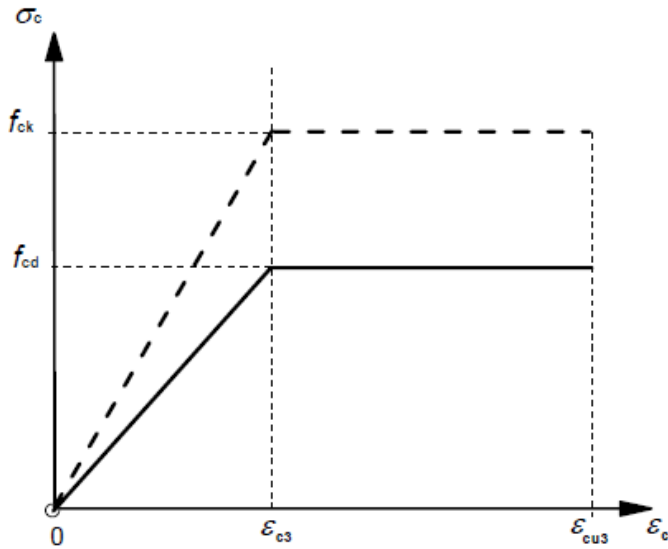


Figure 2.7: Bi-linear stress-strain relation [26]

$$\varepsilon_{lcu3} = \varepsilon_{cu3}\eta_1 \quad (2.7)$$

In addition to the reduction of the mechanical properties shown above, other design rules are also regulated in chapter 11. Rules for creep and shrinkage, concrete cover, shear capacity, torsional capacity and punching shear capacity of slabs and foundations are, in addition to some other parameters, regulated in chapter 11 [26].

Confinement

Designing of structures is closely related to the term ductility. Ductility is the ability for a structural member to deform inelastically without significant loss of strength [20]. Concrete itself is not characterized as a ductile material, and reinforcement is introduced in concrete to provide a certain ductility.

The main characteristics of confined concrete is that both strength and ductility increase with increased confinement. Confinement gives a lateral stress response to a material stressed in compression. When concrete is loaded in compression, the material expands laterally. As concrete has low tensile capacity, the introduction of a lateral constraint will increase the compressive capacity and the ultimate strain.

Confinement is an improvement of the performance of the concrete by utilization of various confinement parameters. Examples are: transverse reinforcement (amount, yield strength, form and diameter), diameter of the longitudinal reinforcement, compressive strength of the concrete, cross section geometry and concrete cover [16][5].

Figure 3.1 illustrates the difference between the stress-strain relation of unconfined and confined concrete. Unconfined concrete fail at both lower stress and strain level compared to confined concrete. The ability to maintain a certain stress level for increasing strains, after reaching peak stress, shows the increase in ductility of confined concrete.

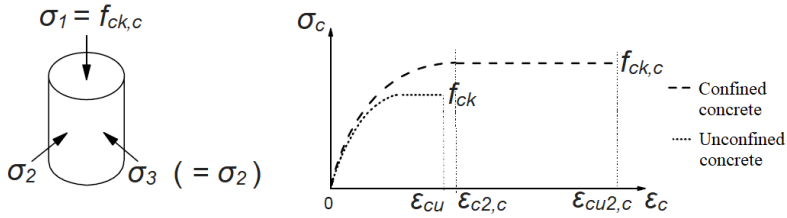


Figure 3.1: Stress-strain relation of unconfined and confined concrete [26]

3.1 Stress-Strain Model

To begin with, the compressive strength of confined concrete can be defined as [5]:

$$f_{cc} = f_{c0} \left(-1.254 + 2.254 \sqrt{1 + \frac{7,94 f'_l}{f_{c0}} - \frac{2 f'_l}{f_{c0}}} \right) \quad (3.1)$$

The confined compressive strength is a function of the unconfined compressive strength f_{c0} , and the effective lateral stress f'_l . The effective lateral stress due to confinement is defined differently for circular and rectangular cross sections. Only the rectangular cross section will be covered here.

3.1.1 Effectively Confined Area of Rectangular Concrete Sections

The area within a stirrup, when subtracting the area of the longitudinal reinforcement A_{sl} , is called the confined concrete area A_{cc} . The area within the stirrup is given as $b_c d_c$ measured from centre to centre of the stirrup. Only a part of the confined concrete area will be effectively confined. This area is called the effectively confined concrete area A_e . The area that is not affected by the confinement is called the ineffectively confined concrete area A_i [5][16].

$$A_{cc} = b_c d_c (1 - \rho_{cc}) \quad (3.2)$$

where

$$\rho_{cc} = \frac{A_{sl}}{b_c d_c}$$

For a section with n longitudinal reinforcement bars, the ineffectively confined concrete area can be defined as [5][16]:

$$A_i = \sum_{i=1}^n \frac{(w'_i)^2}{6} \quad (3.3)$$

The accompanying effectively confined concrete area can be defined as [5][16]:

$$A_e = \left(b_c d_c - \sum_{i=1}^n \frac{(w'_i)^2}{6} \right) \left(1 - \frac{s'}{2b_c} \right) \left(1 - \frac{s'}{2d_c} \right) \quad (3.4)$$

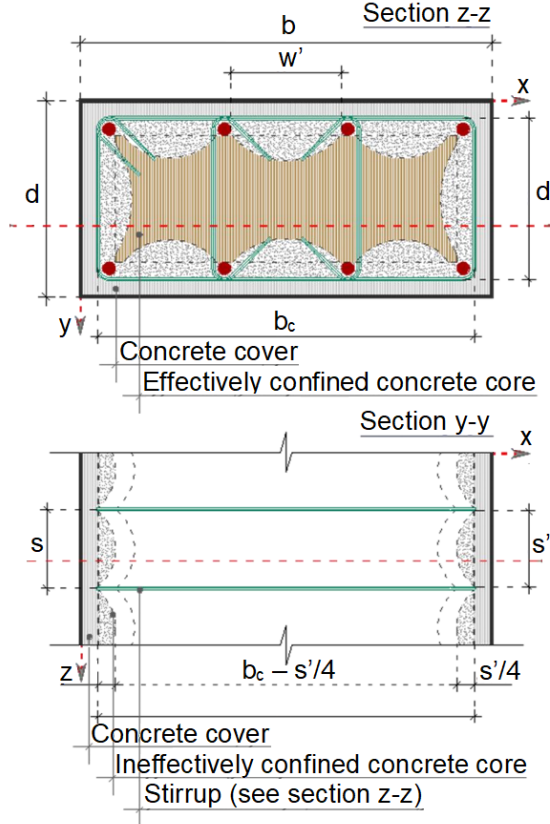


Figure 3.2: Confined concrete area [16]

The lateral confining stress f_l from the transverse reinforcement will fully develop only in the section of the concrete that is surrounded by a stirrup. The lateral stress from the transverse reinforcement decreases in parts of the concrete between stirrups. In Figure 3.2, the change in stress is illustrated from the parabolic line separating the effectively and ineffectively confined concrete area. The initial angle of the parabolas is 45° . In the middle of the span between two transverse stirrups, the area of ineffectively confined concrete will be the largest [16].

The effective confinement coefficient k_e is introduced to modify the lateral stress into effective lateral stress, such that [5][16]:

$$f'_l = k_e f_l \quad (3.5)$$

where

$$k_e = \frac{A_e}{A_{cc}} = \frac{\left(1 - \sum_{i=1}^n \frac{(w'_i)^2}{6b_c d_c}\right) \left(1 - \frac{s'}{2b_c}\right) \left(1 - \frac{s'}{2d_c}\right)}{1 - \rho_{cc}} \quad (3.6)$$

The lateral effective stresses in x- and y-direction are respectively defined as [5][16]:

$$f'_{lx} = k_e \frac{A_{sx}}{s d_c} f_{yh} = k_e \rho_x f_{yh} \quad (3.7)$$

and

$$f'_{ly} = k_e \frac{A_{sy}}{s b_c} f_{yh} = k_e \rho_y f_{yh} \quad (3.8)$$

where ρ_x and ρ_y is the reinforcement ratio in the respective directions. Finally the effective lateral stress is defined as the mean value of the effective stresses in each direction and can be defined as [5][16]:

$$f'_l = \frac{f'_{lx} + f'_{ly}}{2} \quad (3.9)$$

3.1.2 Stress-Strain Curve of Confined Concrete

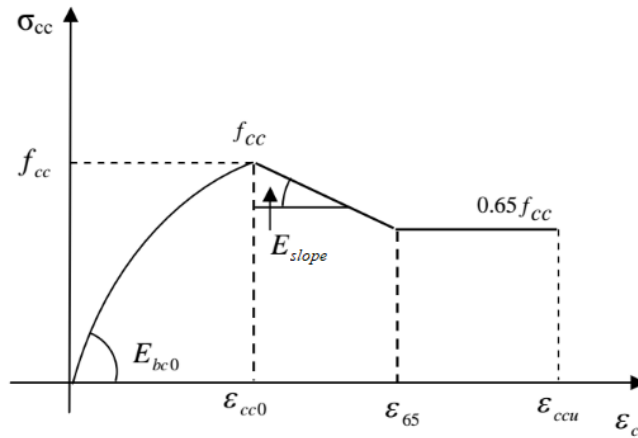


Figure 3.3: Stress-strain curve of confined concrete [5]

The stress-strain curve consists of three intervals. Figure 3.3 depicts a simplistic graphical representation of the stress-strain relation. The first interval starts in the origin with an initial slope E_{bc0} , and grows towards the peak stress f_{cc} and the corresponding strain ε_{cc0} . The stress in this region can be defined as [5, 31]:

$$\sigma_{cc} = f_{cc} \frac{k_c \bar{\varepsilon}_c + (k'_c - 1) \bar{\varepsilon}_c^2}{1 + (k_c - 2) \bar{\varepsilon}_c + k'_c \bar{\varepsilon}_c^2} \quad \text{for } 0 \leq \varepsilon_c \leq \varepsilon_{cc0} \quad (3.10)$$

where

$$\begin{aligned} \bar{\varepsilon}_c &= \frac{\varepsilon_c}{\varepsilon_{cc0}} \\ \varepsilon_{cc0} &= \varepsilon_{c0} \left[1 + 5 \left(\frac{f_{cc}}{f_{c0}} - 1 \right) \right] \\ k_c &= \frac{E_{bc0} \varepsilon_{cc0}}{f_{cc}} \\ E_{bc0} &= 11000 \sqrt[3]{f_{cc}} \\ k'_c &= k_c - 1 \end{aligned}$$

Following this peak, the curve declines with the slope E_{slope} [16] until it reaches 65 % of the stress f_{cc} . The strain at this point is ε_{65} [5].

$$\sigma_{cc} = f_{cc} - E_{slope}(\varepsilon_c - \varepsilon_{cc0}) \quad \text{for } \varepsilon_{cc0} < \varepsilon_c \leq \varepsilon_{65} \quad (3.11)$$

where

$$\begin{aligned} E_{slope} &= \frac{f_{cc}}{\varepsilon_{cc0}} \\ \varepsilon_{65} &= \frac{0.35 f_{cc}}{E_{slope}} + \varepsilon_{cc0} \end{aligned}$$

After the third and final interval is reached, the curve remains at a constant stress level as the strain increases towards the ultimate strain ε_{ccu} . The confined ultimate strain ε_{ccu} can be defined as [5]:

$$\varepsilon_{ccu} = \varepsilon_{cu} + 0.4 \frac{f'_l}{f_{c0}} \quad (3.12)$$

The effective transverse lateral stress f'_l , the unconfined compressive strength f_{c0} and the ultimate unconfined concrete strain ε_{cu} determines the confined concrete ultimate strain.

As mentioned earlier, there are several factors that affect how effectively the concrete is confined. In this research study, the amount of transverse reinforcement, the diameter of the compressive reinforcement and the concrete cover will be varied to observe each parameter's influence on the ductility of the LWAC beams.

Methodology

To investigate the ductility of LWAC beams, it was decided to subject 7 over-reinforced beams to compression through a four point bending test. This testing produced a constant moment zone of 1 meter in the middle of each beam. For comparison, the geometry of the beams were equal to what has been used in previous experimental work [18]. A detailed description of cross section and reinforcement layout for each beam is given in appendix A.1.

All the beams were subjected to the same loading. The main testing parameter was the spacing of the stirrups in the constant moment zone. In addition to this, the effect of different concrete covers and compressive reinforcement were investigated.

Small specimens were tested to find the material properties of the LWAC.

4.1 Test Specimens

4.1.1 Small Specimens

Cubes with dimensions 100x100x100 mm and cylinders with dimensions $\phi 100 \times 200$ mm were tested to find the density, compressive strength and tensile splitting strength. Both the small specimens and all the beams were casted from the same batch of concrete.

The small specimens were demoulded 24 hours after casting and kept under water until the day of testing. They were removed from the water just before testing and the surface was dried. The cylinders were additionally grained on both sides to create smooth and parallel surface areas.

The procedures described in NS-EN 12390-3:2009, NS-EN 12390-6:2009 and NS-EN 12390-7:2009 were followed in testing. The specimens were tested 7, 28, 38, 44, 49, 55 and 59 days after casting.

Compressive Strength

The compressive strength of the LWAC f_{lc} , was determined from equation 4.1. A_c was the surface area subjected to loading and F_c was the applied force. The units were MPa, mm² and N respectively.

$$f_{lc} = \frac{F_c}{A_c} \quad (4.1)$$

The computerized *ToniTechnik* machine preloaded the specimens to about 1 % of the failure load. Thereafter, the test continued without pause with a loading speed of 0.8 MPa/s. The cylinders were tested in the same way as the cubes to determine compressive strength.



Figure 4.1: Cube and cylinder in the *ToniTechnik* machine

Young's Modulus

EC2 gives equation 4.2 for calculation of the Young's modulus of LWAC. The formula is based on a correlation between the compressive strength and the Young's modulus. f_{cm} was the mean value of the compressive strength and ρ was the oven-dry density of the LWAC.

$$E_{lcm} = E_{cm}\eta_E \quad (4.2)$$

where

$$E_{cm} = 22 \left[\frac{f_{cm}}{10} \right]^{0.3}$$

$$\eta_E = (\rho/2200)^2$$

From a previous similar study [23], it was discovered that the measured Young's modulus for this type of concrete differed significantly from the calculated value using equation 4.2. The Young's modulus used in this experimental study will be the value measured in the previous study. The previous study used a LWAC with the same aggregate and the same compressive strength.

Tensile Splitting Strength

The tensile splitting strength of the LWAC f_{lct} , was determined from equation 4.3. F was the force applied, L was the length of the cylinder and d was the diameter of the cylinder's cross section. The units were MPa, N, mm and mm respectively.

$$f_{lct} = \frac{2F}{\pi Ld} \quad (4.3)$$

To measure the capacity, a *Mohr Federhaff Losenhausen* compression machine was used. To ensure correct loading, the specimens were placed centrally in the machine and wooden pieces were placed beneath and above the specimens. The loading rate was 0.06 MPa/s.



Figure 4.2: Cylinder in the *Mohr Federhaff Losenhausen* machine

Oven-Dry Density

The volume of the test specimens were found by submerging them in water. The volume was calculated using equation 4.4. m_a was the specimen mass in air. m_w was the submerged specimen mass. The density of water ρ_w was 998 kg/m³.

$$V = \frac{m_a - [(m_{st} + m_w) - m_{st}]}{\rho_w} = \frac{m_a - m_w}{\rho_w} \quad (4.4)$$

The density D of the specimens were calculated using the following formula:

$$D = \frac{m_a}{V} \quad (4.5)$$

The oven-dry density ρ of the specimens were found by drying the specimens at 105°C. When the mass of the specimen did not change more than 0.2 % from the last measuring, this mass was used to calculate the oven-dry density. The specimens were dried in the oven 24 hours between each measuring of the mass.

4.1.2 Beams

The test programme included seven over-reinforced LWAC beams. The geometry of the beams were 210x550x4500 mm (width x height x length). Detailed technical drawings of the beam geometries and reinforcement layouts are given in appendix A.1. The beam geometries and reinforcement layouts were equal to what was used in a previous experimental study [18].

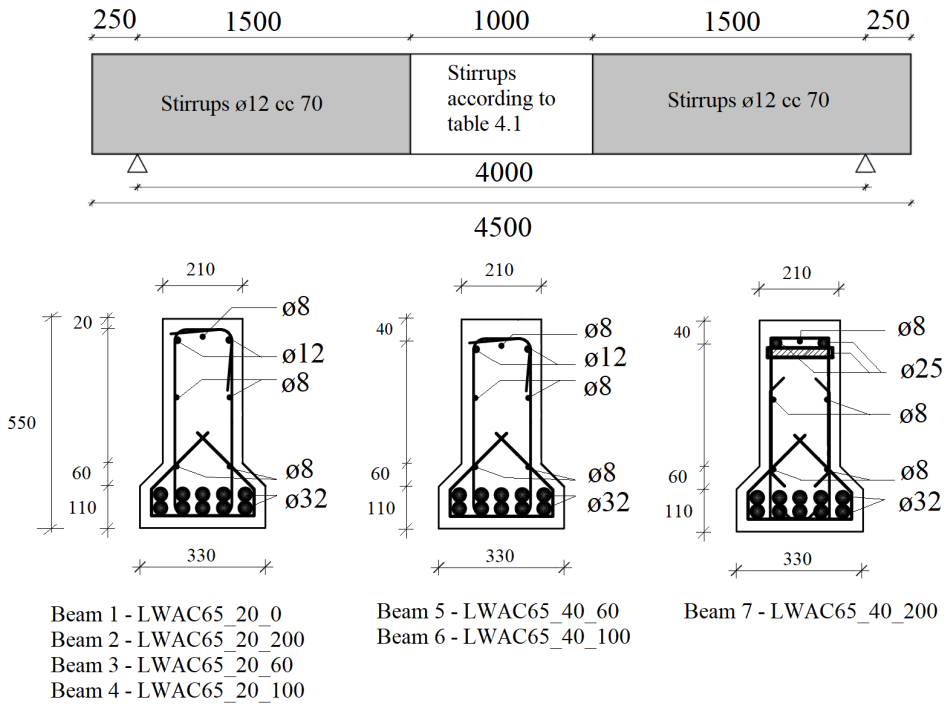
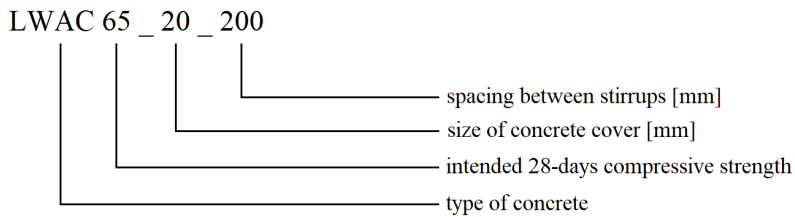


Figure 4.3: Beam geometries and reinforcement layouts between the loading points. All dimensions are in [mm]

The numbering system of the beams is as follows:



The beams were subjected to a four point bending test. The load situation was chosen to produce a constant moment zone in the middle part of the beams. The beams were designed to fail in bending and were over-reinforced as in the previous experimental study [18]. The complete beam test programme is given in Table 4.1.

Table 4.1: Test programme

Beam number	Beam identification	Size of concrete cover [mm]	Stirrup spacing [mm]	Longitudinal reinforcement	Compressive reinforcement	Stirrups reinforcement diameter [mm]
1	LWAC65_20_0	20	-	10 ϕ 32	2 ϕ 12	12
2	LWAC65_20_200	20	200	10 ϕ 32	2 ϕ 12	12
3	LWAC65_20_60	20	60	10 ϕ 32	2 ϕ 12	12
4	LWAC65_20_100	20	100	10 ϕ 32	2 ϕ 12	12
5	LWAC65_40_60	40	60	10 ϕ 32	2 ϕ 12	12
6	LWAC65_40_100	40	100	10 ϕ 32	2 ϕ 12	12
7	LWAC65_40_200	40	200	10 ϕ 32	2 ϕ 25	12

Beam 1-4 had concrete cover 20 mm. Beam 5-7 had concrete cover 40 mm. All the beams were reinforced with ϕ 12 stirrups. Outside the constant moment zone the stirrup spacing for all the beams was 70 mm all the way out to the supports.

Between the loading points the stirrup spacing was 200 mm, 60 mm and 100 mm respectively for beam 2, 3 and 4. Beam 1 was created without shear reinforcement between the loading points. The stirrup spacing was 60 mm, 100 mm and 200 mm respectively for beam 5, 6 and 7.

In beam 7 the diameter of the compressive reinforcement was increased to ϕ 25. The beam had additional transverse reinforcement of ϕ 25 bars attached to the stirrups between the loading points. Detailed drawings are given in appendix A.1.

All the beams were casted from the same batch of concrete. The concrete was poured in wooden forms in three layers because of the beam height. The concrete was vibrated to ensure that it filled the forms adequately. The beams were covered with plastic sheets immediately after casting. The beams were demoulded after 24 hours and kept covered with wet burlaps under plastic sheets for 31 days. The beams were then painted white in order to better observe cracking. On the east side of each beam, an area was marked with black dots for strain field observation using DIC. This is shown in Figure 4.4.

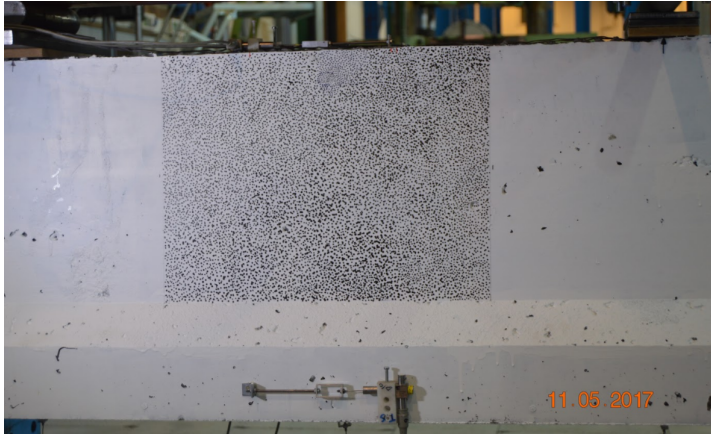


Figure 4.4: Side of beam marked for DIC

4.2 Material and Mix Properties

4.2.1 Concrete Mix Recipe and Goal

Expected oven-dry density was 1900 kg/m^3 and expected compressive strength was 65 MPa. The required amount of LWAC used in this project, including small specimens and beams, was 5.7 m^3 . In order to calculate the concrete mix recipe, moisture content and absorption of the LWA were measured. The sieve curve for the LWA was also determined.

Since the concrete was prepared at a stationary plant, the sieve curve and data concerning moisture content for sand (both 0-2 mm and 0-8 mm) were determined at the plant. For 0-2 mm and 0-8 mm sand, the moisture content was 5.5 % and 7.7 % respectively. The sieve curves are given in appendix B.3.

4.2.2 Measurement of Moisture and Absorption of Stalite

The type of LWA used in this project was Stalite. Since Stalite is an absorptive LWA, measurement of moisture and absorption is necessary when designing the concrete mix. In order to obtain the values for moisture and absorption, 750 g of Stalite were taken from each batch (there were four batches in total) and mixed into one sample of 3000 g, in accordance with ASTM C127-07 [27].

For measurement of the moisture content of the LWA, two samples of 3000 g each were dried at 110°C for 24 hours. The samples were weighed after drying, and equation 4.6 was used to calculate the moisture content:

$$c_m = \frac{m_w - m_d}{m_d} \cdot 100\% \quad (4.6)$$

where c_m was the moisture content, m_w was the mass of a tested sample before drying and m_d was the mass of an oven-dry test sample in air. The average moisture content was 11.4%.

The same samples used for measurement of moisture content were later used to measure the absorption. The samples were sieved and washed in a 4 mm sieve in order to eliminate fine particles. Later, the samples were dried for approximately 19 hours. After drying, the samples were weighed and put in water. After 24 and 100 hours in water, the samples were surface dried and absorption was calculated using equation 4.7:

$$a = \frac{m_s - m_d}{m_d} \cdot 100\% \quad (4.7)$$

where a was the absorption, m_s was the mass of a saturated surface dry test sample and m_d was the mass of an oven-dry test sample in air.

The average absorption after 24 and 100 hours were 6.5% and 8.3% respectively.

4.2.3 Determination of Sieve Curve for Stalite

The same samples used for measurement of moisture content and absorption were used to determine the sieve curve. The samples were sieved by machine for 10 minutes, with sieve sizes 16, 11.2, 8, 4, 2, 1, 0.5, 0.25, 0.125 and 0.063 mm. See Table 4.2 and Figure 4.5 for detailed results.

T27/C136, which is a standard method of testing for sieve analysis of both fine and coarse aggregate, was used.

The obtained result for the sieve curve matched well with the technical sheet from Stalite. The technical sheet is given in appendix B.3.

Table 4.2: Values for sieve curve for Stalite

Sieve size [mm]	Rest [%]	Passing [%]
16	0	100
11.2	0.3	99.7
8	22.0	78.0
4	76.8	23.2
2	94.4	5.6
1	96.1	3.9
0.5	96.8	3.2
0.25	97.3	2.7
0.125	97.9	2.1
0.063	98.4	1.6

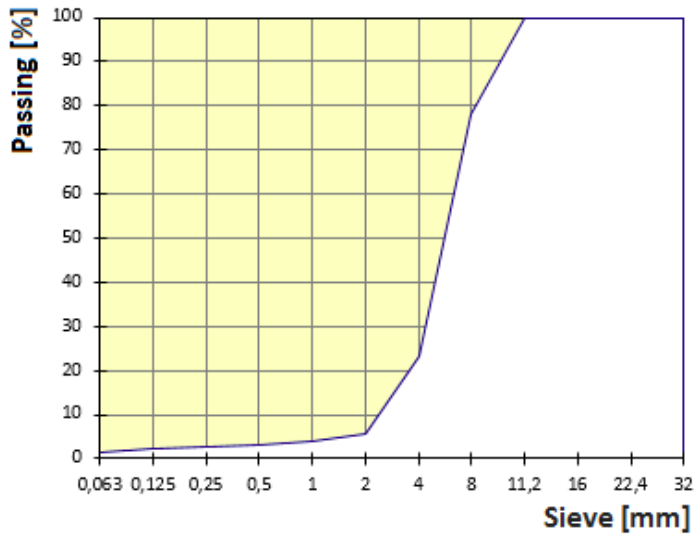


Figure 4.5: Sieve curve for Stalite

4.2.4 Final Concrete Recipe

The final concrete recipe is shown in Table 4.3. All measurements mentioned above were included in an Excel calculation sheet given in appendix B.3. Table 4.4 shows the different ratios between water, cement and binder.

Table 4.3: Final concrete recipe mix

Constituent	Weight [kg/m ³]
Cement (Norcem Anlegg FA)	430.75
Silica fume (Elkem Microsilica)	22.38
Water (free)	123.33
Water (absorbed)	55.17
Sand (Ramlo 0-8mm)	595.31
Sand (Ramlo 0-2mm)	249.65
Aggregate (Stalite 1/2")	550
Superplasticizer (Mapei Dynamon SR-N)	5.40

Table 4.4: Ratios

Ratios	Value
$\frac{\text{water}}{\text{cement}}$	0.29
$\frac{\text{water} + \text{absorbed water}}{\text{cement}}$	0.41
$\frac{\text{water}}{\text{binder}}$	0.39

4.2.5 Methodology for Concrete Preparation

The truck was filled with Stalite at the lab at NTNU before taking mortar at the stationary plant. First, the truck was sprinkled with water and later filled with completely saturated Stalite. There was no mixing of the Stalite during the transport to the stationary plant.

The whole amount of mortar was prepared at the stationary plant. First, all dry particles (sand, cement and silica fume) were added in a twin shaft pedal mixer and mixed for 30 seconds. Then, water and superplasticizer were added during continuously mixing. The mixing process of the mortar took three minutes in total.

The mortar was poured in the truck and the concrete mix was mixed with maximum velocity for six minutes (approximately one minute pr. m^3). During the 20 minutes long transport back to NTNU the concrete mix was mixed continuously, followed up by three minutes of mixing with maximum velocity upon arrival.

The prepared concrete was very flowable, similar to self-compacting concrete. The paste was able to move the LWA and there was enough paste for compaction. In addition, the concrete was pumpable.

Slump, saturated density and air content were measured before casting. Slump was 23 cm, saturated density was 2013 kg/m^3 and air content was 1.4 %.

4.2.6 Reinforcement

S500 was the quality of the reinforcement for the beams. Because there was no tensile testing of the reinforcement, the yield strength was set to be 550 MPa. From previous experience with this steel, the yield strength was set to be this value. This value was used for all the reinforcement in all calculations of capacities. Because of the total reinforcement weight for each beam being approximately 450 kg, the beams had to be lifted with crane. To avoid altering any aspect of the reinforcement layout when lifted, the longitudinal bars were welded to the stirrups. In order to have the testing zone (between the loading points) act appropriately, the reinforcement was attached with steel wires between the loading point and approximately 50 cm beyond each loading point.

The tensile reinforcement requires a certain anchoring length. The longitudinal bars extended 230 mm beyond the support. To ensure enough anchoring capacity, the required anchoring length was verified. The procedure from EC2 was followed. Characteristic values were used in calculations to get a capacity close to expected capacity in laboratory. Equation 4.8 was applied when calculating the basic required anchoring length:

$$l_{b,rqd} = \frac{\phi \sigma_{sd}}{4 f_{bd}} \quad (4.8)$$

From EC2, the additional force in the longitudinal reinforcement was calculated as:

$$\Delta F_{td} = 0.5V_{Ed}(\cot\theta - \cot\alpha) \quad (4.9)$$

where $\cot\theta$ was in the range 1-2.5. It was in this verification conservatively assumed to be 2.5. α is the angle between the shear reinforcement and the beam axis perpendicular to the shear load. In this experiment α was 90° as the stirrups were not tilted.

$$\lim_{\alpha \rightarrow 90^\circ} \cot\alpha = 0$$

The function above shows that $\cot\alpha = 0$ in this experiment. The shear force $V = P$ was here conservatively assumed to be 900 kN. The additional force in the reinforcement was calculated:

$$\begin{aligned} \Delta F_{td} &= 0.5V_{Ed}(\cot\theta - \cot\alpha) \\ &= 0.5 \cdot 900 \cdot (2.5 - 0) \\ &= \underline{1125 \text{ kN}} \end{aligned}$$

σ_{sd} is the design stress in the longitudinal reinforcement at the point where the anchoring is measured from. It is given by equation 4.10:

$$\sigma_{sd} = \frac{\Delta F_{td}}{A_s} \quad (4.10)$$

The longitudinal reinforcement consists of 10 $\phi 32$ bars, leading to a stress in the reinforcement at the support equal to:

$$\begin{aligned} \sigma_{sd} &= \frac{\Delta F_{td}}{A_s} \\ &= \frac{1125 \cdot 10^3}{10 \cdot \pi \cdot 16^2} \\ &= \underline{140 \text{ MPa}} \end{aligned}$$

The ultimate bond stress is given by:

$$f_{bd} = 2.25\eta_1\eta_2f_{ctd} \quad (4.11)$$

$\eta_1 = \eta_2 = 1.0$ for normal conditions. For LWAC the tensile strength is given by:

$$f_{lctd} = \frac{0.85f_{lctk,0.05}}{1.5} \quad (4.12)$$

where

$$f_{lctk,0.05} = f_{ctk,0.05} \cdot \eta_1$$

and

$$\eta_1 = 0.40 + 0.60 \frac{\rho}{2200}$$

With an expected compressive strength of 65 MPa and expected oven-dry density of 1900 kg/m³ characteristic tensile strength was calculated:

$$\begin{aligned} \eta_1 &= 0.40 + 0.60 \frac{\rho}{2200} \\ &= 0.40 + 0.60 \cdot \frac{1900}{2200} \\ &= \underline{0.918} \end{aligned}$$

$$\begin{aligned} f_{lctk,0.05} &= f_{ctk,0.05} \eta_1 \\ &= 3.15 \cdot 0.918 \\ &= \underline{2.89MPa} \end{aligned}$$

As mentioned, characteristic values were used, leading to the following calculation of the ultimate bond strength:

$$\begin{aligned} f_{bk} &= 2.25 \eta_1 \eta_2 f_{lctk,0.05} \\ &= 2.25 \cdot 1.0 \cdot 1.0 \cdot 2.89 \\ &= \underline{6.50MPa} \end{aligned}$$

Lastly, the basic required anchoring length was calculated

$$\begin{aligned} l_{b,rqd} &= \frac{\phi \sigma_{sd}}{4 f_{bk}} \\ &= \frac{32}{4} \cdot \frac{140}{6.50} \\ &= \underline{172mm} \end{aligned}$$

To acquire additional anchoring capacity, so that anchorage failure would not occur, the longitudinal bars were welded to steel plates with dimensions 30x60x330. Each pair of longitudinal bars were welded together at several points to act as one member. Each bar was welded to the plate in two points as shown in Figure 4.6.

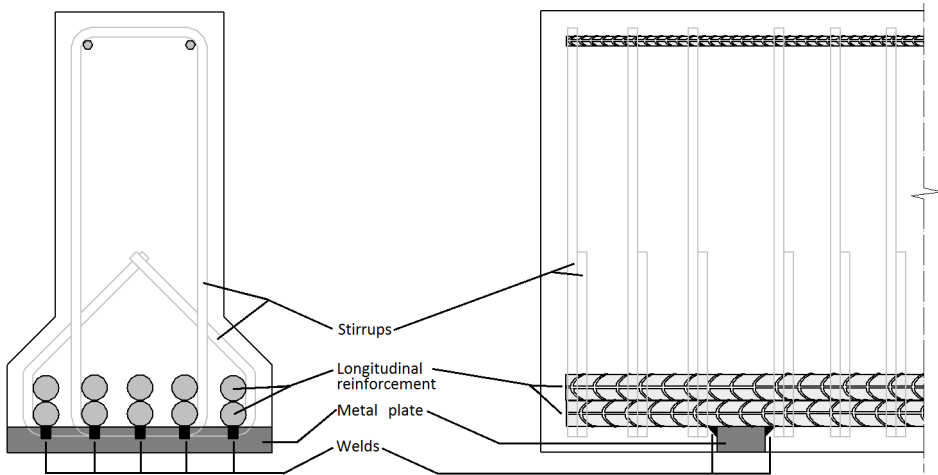


Figure 4.6: Connection of plate and reinforcement

4.3 Test Setup and Procedure

4.3.1 Four Point Bending Test

The static load situation for the LWAC beams in four point bending is illustrated in Figure 4.7. This load situation results in a constant moment $M = P \cdot 1500$ mm between the loading points and a constant shear force $V = P$ between the supports and the point loads.

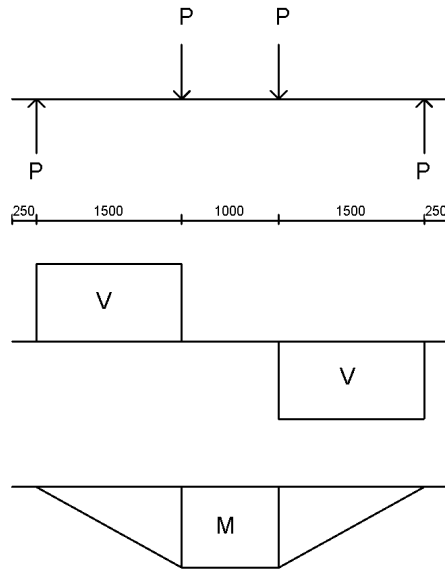


Figure 4.7: Four point bending

The LWAC beams were subjected to the two point loads by a mechanical jack with maximum capacity of 1800 kN. The force from the jack was distributed by a stiff steel spreader beam through two supports. The stiff steel spreader beam was supported by a roller support and a fixed support. The distance between the supports of the steel spreader beam was 1 meter. The LWAC beams were supported by a roller support and a spherical support. The distance between the supports of the LWAC beams was 4 meters. Figure 4.8 and 4.9 illustrate the setup.

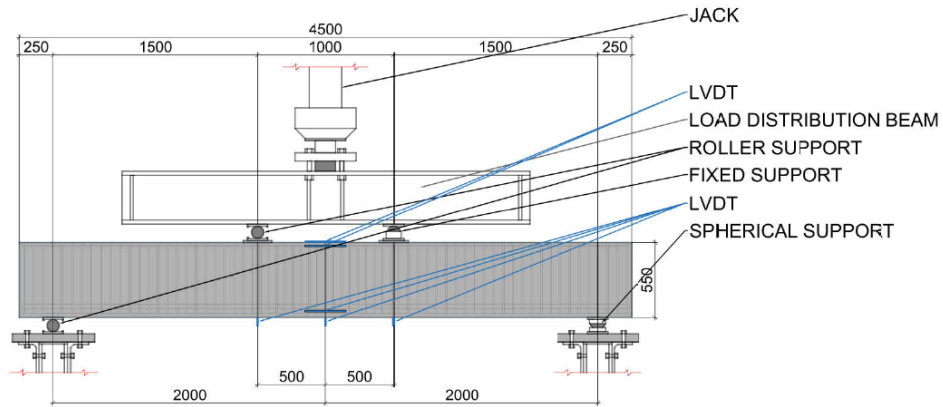


Figure 4.8: Setup on the west side of the beam.

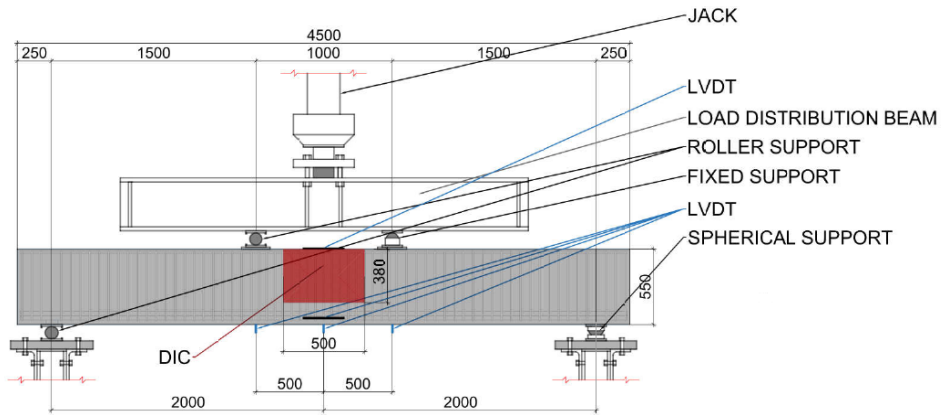


Figure 4.9: Setup on the east side of the beam.

The load was applied step-wise like shown in appendix B.1. At each load step, a three minute break was made before adding the next load increment. The loading rate of the jack was deflection controlled with a speed of 1.2 mm/min.

4.3.2 Setup of Measuring Devices

Strain Gauges and Linear Variable Differential Transformers

The beams were equipped with six strain gauges attached to the middle longitudinal bars for strain measurement of the reinforcement. Both the compressive and the tensile zone had three strain gauges each. In the compressive zone, one strain gauge was placed at the midspan of the beam, while the two others were placed one on each side, 400 mm from the

midspan. In the tensile zone, all three strain gauges were placed at the midspan. Two were placed on the lower bar and one on the top bar. The strain gauges were of the type FLA-6-11-5L and were 6 mm long. The gauge factor was $2,12 \pm 1\%$ and the gauge resistance was $119,5 \pm 0,5 \Omega$. In addition to strain gauges, five linear variable differential transformers (LVDT) were used for strain measurement of the concrete. The LVDTs measured deflection over a distance of 200 mm. In total, five LVDTs were used, three for measurement of strains in the compressive zone and two for measurement of strains in the tensile zone. Additionally, three LVDTs measured deflections under the beams. See Figure 4.10 for detailed illustration.

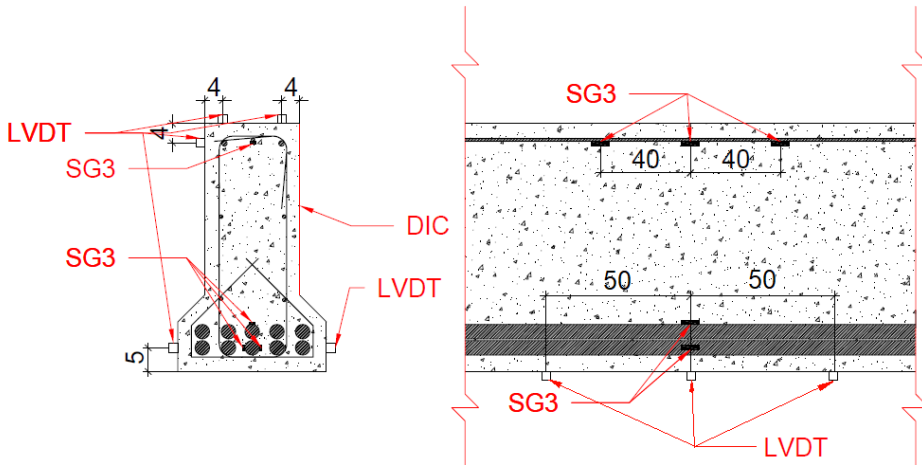


Figure 4.10: Measuring devices at the middle of the beam

Digital Image Correlation

Digital image correlation (DIC) is a method for measuring surface deformations of an object subjected to forces. This method involves comparison of images taken of a predetermined area during loading. An image of the predetermined area of inspection is divided into small subareas (also called "subsets"). By registering the change in position and deformation of the subareas during loading, the full deformation field can be measured [15, 24, 21]. The strain field can be calculated from the deformation field. See Figure 4.11 for illustration.

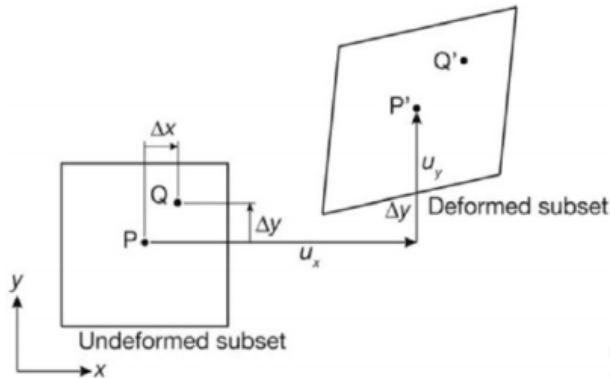


Figure 4.11: Subareas (or subsets) before and after deformation [21]

The predetermined areas on the beams were dotted with black markers. Two cameras were used for the observation. One camera was placed orthogonally on the concrete surface (providing a 2D-observation) while the other was placed with a certain angle (providing a 3D-observation). The computer controlling the cameras was connected to the mechanical jack by an analog signal. This connection ensured that the pictures that was taken could follow the load-deflection curve. The cameras registered one photo every two seconds.

4.3.3 Calculation of Capacities

For all calculations of capacities, strength values measured from small specimen testing were used to get calculated capacities as close to laboratory results as possible.

Moment Capacity

The moment capacity calculation was based on EC2 [26]. The stress-strain relation shown in figure 2.6 was used. Figure 4.12 shows the strain distribution and the forces that are acting on the cross section during bending. It is assumed linear strain distribution and neglectable tensile capacity of the concrete. The real parabolic stress distribution of the concrete is approached by a stress block which height depends on the scaling factor λ , the effective height d , the ultimate concrete strain ε_{cu} and the tensile reinforcement strain ε_s . It is assumed that failure will occur when the concrete reaches ultimate compressive strain ε_{cu} .

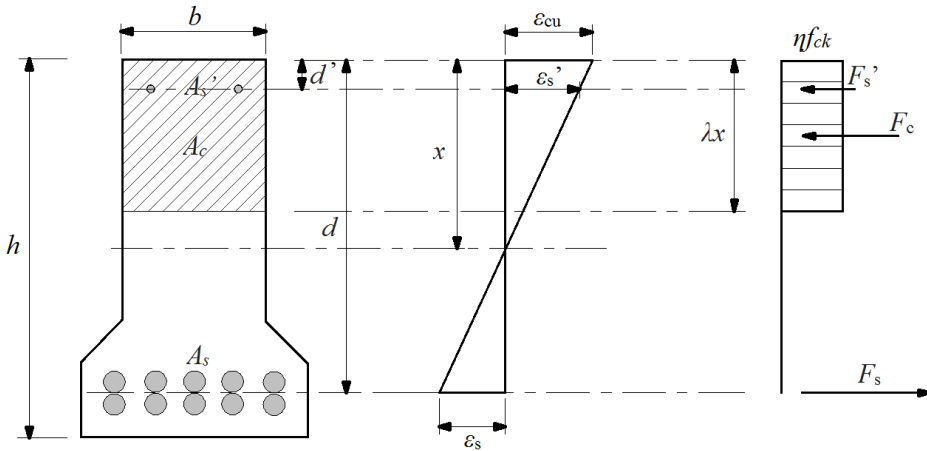


Figure 4.12: Bending of cross section

From the strain distribution in figure 4.12 we get

$$\frac{\varepsilon_{cu}}{x} = \frac{\varepsilon_s}{d-x}$$

$$\downarrow$$

$$x = \frac{\varepsilon_{cu}}{\varepsilon_{cu} + \varepsilon_s} d$$

and by introducing

$$\alpha = \frac{\varepsilon_{cu}}{\varepsilon_{cu} + \varepsilon_s}$$

we get

$$x = \alpha d. \quad (4.13)$$

The value for x is introduced in the relation

$$\frac{\varepsilon_{cu}}{x} = \frac{\varepsilon'_s}{x - d'}$$

gives

$$\varepsilon'_s = \frac{\varepsilon_{cu}}{\alpha d} (\alpha d - d'). \quad (4.14)$$

The characteristic compressive strength f_{ck} was found from small specimen testing. The stresses σ_c , σ'_s and σ_s were calculated from:

$$\sigma_c = \eta f_{ck} \quad (4.15)$$

$$\sigma'_s = \varepsilon'_s E_s \quad (4.16)$$

$$\sigma_s = \varepsilon_s E_s \quad (4.17)$$

The forces F_c , F'_s and F_s were calculated from:

$$F_c = \lambda b \alpha d \sigma_c \quad (4.18)$$

$$F'_s = \sigma'_s A'_s \quad (4.19)$$

$$F_s = \sigma_s A_s \quad (4.20)$$

where

$$\lambda = 0.8 - \frac{f_{ck} - 50}{400}$$

and

$$\eta = 1 - \frac{f_{ck} - 50}{200}$$

To achieve horizontal force equilibrium, the value of ε_s at failure was calculated using Excel. The moment capacity of the cross section was calculated by moment equilibrium about the bottom edge of the cross section:

$$M_R = F_c z_c + F'_s z'_s - F_s z_s \quad (4.21)$$

where z_c , z'_s and z_s are the internal moment arms between the respective forces and the bottom edge of the cross section.

The moment capacity M_R of the different cross sections and the maximum calculated load P_{calc} are presented in Table 4.5. The accompanying tensile reinforcement strains ε_s are also presented. All the strain values are smaller than the yield strain $\varepsilon_{yk} = 2.5 \text{ ‰}$ which implies over-reinforced cross sections [34]. All calculations are given in appendix C.1.

Table 4.5: Calculated moment capacities and maximum calculated load

Beam	Concrete cover [mm]	Compr. reinf.	M_R [kNm]	P_{calc} [kN]	ε_s [‰]
1 - 4	20	$2\phi 12$	1093	729	1.71
5 - 6	40	$2\phi 12$	1088	726	1.71
7	40	$2\phi 25$	1200	800	1.84

Shear Capacity

The shear capacity was calculated in accordance with EC2 [26].

The shear capacity for LWAC for cross sections without shear reinforcement is the larger value of following formulas:

$$V_{lRd,c} = C_{lRd,c} \eta_1 k (100 \rho_l f_{lck})^{\frac{1}{3}} b_w d \quad (4.22)$$

and

$$V_{lRd,c} = v_{l,min} b_w d \quad (4.23)$$

where

$$C_{lRd,c} = k_2$$

$$k = 1 + \sqrt{\frac{200}{d}} \leq 2.0$$

$$\rho_l = \frac{A_{sl}}{b_w d} \leq 0.02$$

$$v_{l,min} = 0.466 MPa$$

$$\eta_1 = 0.4 + 0.6 \frac{\rho}{2200}$$

A_{sl} is the cross sectional area of the tensile reinforcement. Calculated shear capacity for cross sections without shear reinforcement was 764 kN. The calculation is given in appendix C.2. The shear capacity for cross sections with shear reinforcement is the smaller value of following formulas:

$$V_{lRd,s} = \frac{A_{sw}}{s} z f_{yw} d \cot \theta \quad (4.24)$$

and

$$V_{lRd,max} = \frac{\alpha_{cw} b_w z \nu_1 f_{cd}}{\cot \theta + \tan \theta} \quad (4.25)$$

where

$$\nu_1 = 0.5 \left(1 - \frac{f_{ck}}{250}\right)$$

$$z = 0.9d$$

A_{sw} is the cross sectional area of the shear reinforcement, s is the stirrup spacing, z is the internal moment arm, f_{ywd} is the design yield strength of the shear reinforcement, θ is the angle between the compression strut and the horizontal axis, α_{cw} depends on the stress state in the compression strut, b_w is the width of the cross section and ν_1 is a strength reduction factor for concrete exposed to shear forces.

Equation 4.24 was used to calculate the required stirrup spacing. By assuming $V_{lRd,s} = P = 900$ kN, the required stirrup spacing s was 72 mm. By applying stirrup spacing $s = 70$ mm the shear capacity was 925 kN. All calculations are given in appendix C.2.

Load-Deflection Curve

Before testing the beams, a model of the load-deflection relation was established. For relatively small loads, the stresses in tension will be smaller than the tensile capacity and the concrete will not crack. This is defined as stadium I. As the load increases, the concrete tensile capacity will be exceeded and the concrete will crack. This is defined as stadium 2. It was assumed in this model that the concrete did not have any tensile capacity. The bending stiffness for both stadiums were calculated by using appropriate equations and parameters. The transition between uncracked and cracked state is represented by tension stiffening. The model used in calculations of the load-deflection curve was based on EC2 and is presented in "Betongkonstruksjoner" [34].

First, the material stiffness ratio and reinforcement ratio was calculated:

$$\eta = \frac{E_s}{E_{cm}} \quad (4.26)$$

$$\rho_l = \frac{A_{sl}}{bd} \quad (4.27)$$

Then, the bending stiffness of uncracked cross section was calculated.

The neutral axis depth was calculated as:

$$\alpha d = \frac{0.5A_c h + \eta A_{sl} d}{A_c + \eta A_{sl}} \quad (4.28)$$

The concrete's contribution to the second moment of area was calculated as:

$$I_{c1} = \frac{bh^3}{12} + bh \left(\alpha d - \frac{h}{2} \right)^2 \quad (4.29)$$

The reinforcement's contribution to the second moment of area was calculated as:

$$I_{s1} = A_{sl} (d - \alpha d)^2 \quad (4.30)$$

This led to the expression for the bending stiffness of uncracked cross section:

$$(EI)_1 = E_c I_{c1} + E_s I_{s1} \quad (4.31)$$

This in turn led to the expression for deflection of uncracked cross section [41]:

$$\delta_I = \frac{Pa}{24(EI)_1} (3L^2 - 4a^2) \quad (4.32)$$

The deflection is based on a general case where a simply supported beam is exposed to two symmetrical point loads, shown in Figure 4.13:

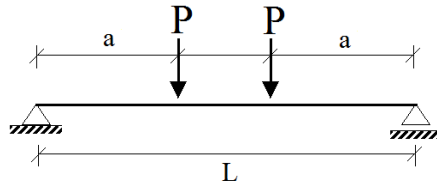


Figure 4.13: Simply supported beam loaded symmetrically [41]

The bending stiffness of cracked cross section was then calculated. Compressive zone part of effective height was calculated as:

$$\alpha = \sqrt{(\eta\rho_l)^2 + 2\eta\rho_l} - \eta\rho_l \quad (4.33)$$

The equivalent second moment of area of the concrete was calculated as:

$$I_c = \frac{1}{2}\alpha^2\left(1 - \frac{\alpha}{3}\right)bd^3 \quad (4.34)$$

This led to the expression for the bending stiffness of cracked cross section:

$$(EI)_2 = E_c I_c \quad (4.35)$$

leading to the deflection of cracked cross section being [41]:

$$\delta_{II} = \frac{Pa}{24(EI)_2}(3L^2 - 4a^2) \quad (4.36)$$

When tension stiffening is taken into account, the deflection can be expressed as:

$$\delta = \zeta\delta_{II} + (1 - \zeta)\delta_I \quad (4.37)$$

where

$$\zeta = 1 - \beta\left(\frac{M_{cr}}{M}\right)^2$$

and

$$M_{cr} = \frac{I_{c1} + \eta I_{sl}}{h - \alpha d} f_{ctm}$$

$\beta = 1, 0$ for a single short term load

$\beta = 0, 5$ for a long term or cyclic load

Lastly, critical load when cracking occurs was calculated as:

$$P_{cr} = 2 \frac{M_{cr}}{a} \quad (4.38)$$

a being the distance from support to the point load. Figure 4.14 shows graphically the calculated relation between load and deflection of the beams. The tension stiffening curve represents the load-deflection relation of the beams. All calculations are given in appendix C.3.

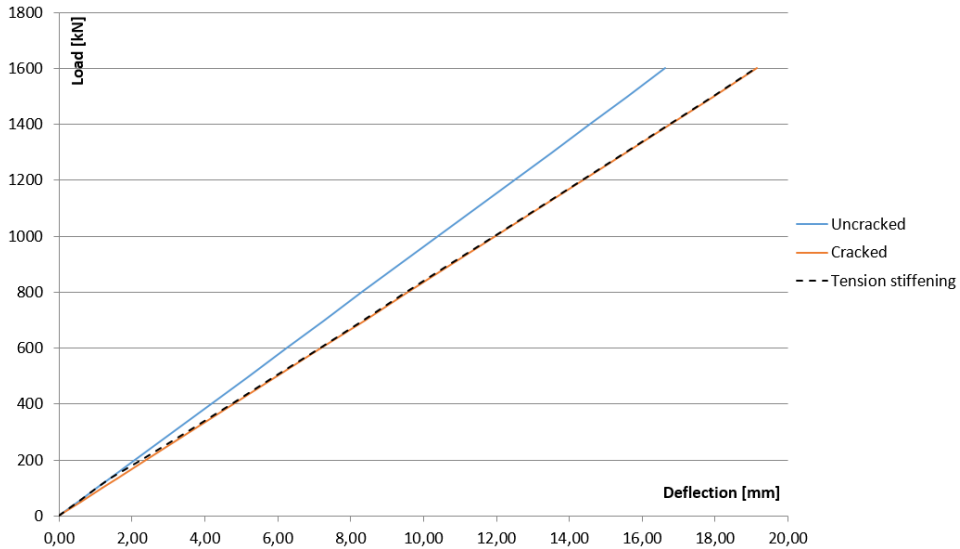


Figure 4.14: Calculated load-deflection curve

Compressive Capacity of Confined Concrete

In order to predict the magnitude of increase in compressive capacity from confinement, the formulas for confined concrete were utilized. Since the configuration of the cross section of the tested beams were different than what was presented in chapter 3, modifications regarding the confined area were applied. The presented equations in chapter 3, cover concrete cross sections in compression. As the tested beams were exposed to bending, only a part of the cross section was subjected to compression, making it impossible to directly apply some of the formulas. Figure 4.15 explains visually how the effectively confined concrete area was calculated.

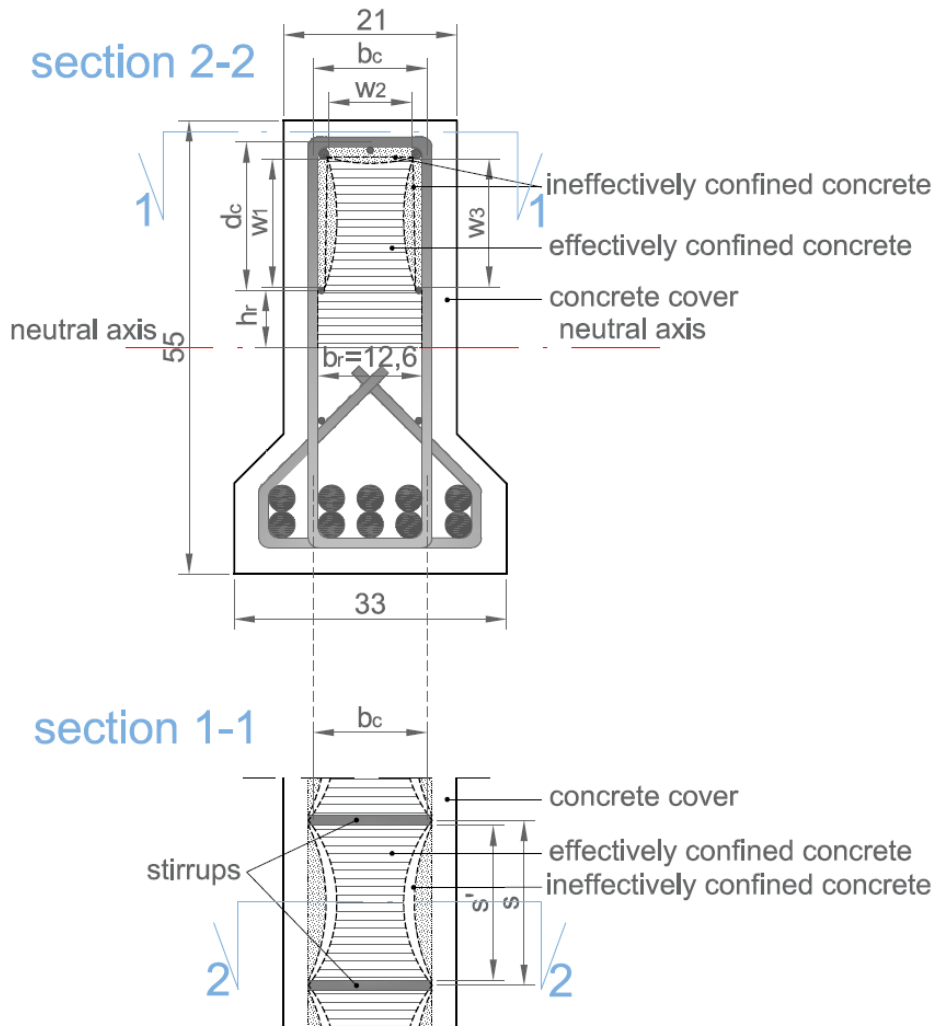


Figure 4.15: Effectively confined concrete core

When applying the formulas, the first step consisted of calculating the confined compressive capacity of the concrete. This was done for each beam and is summarized in Table 4.6.

Table 4.6: Confined compressive capacity

Beam number	Beam identification	Confined compressive capacity [MPa]	Increase of capacity [%]
1	LWAC65_20_0	65	0
2	LWAC65_20_200	67.6	4
3	LWAC65_20_60	99.4	53
4	LWAC65_20_100	81.4	25.3
5	LWAC65_40_60	101.9	56.8
6	LWAC65_20_100	82.4	26.7
7	LWAC65_20_200	67.3	3.5

The next step was to calculate the stress-strain curve for all the beams. These curves are all given in Figure 4.16. The formulas and procedure from chapter 3 were utilized in calculation of these curves.

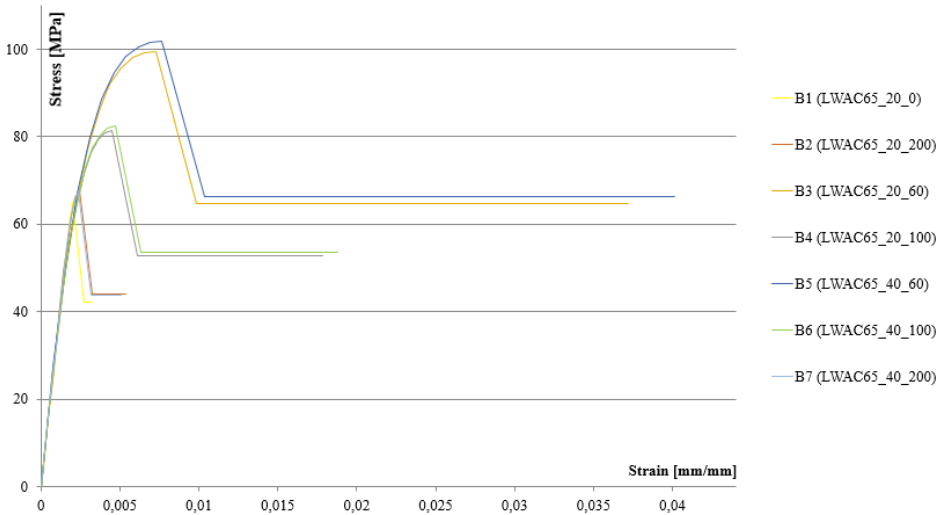


Figure 4.16: Calculated stress-strain curve of all tested beams

Results

This chapter will present the results of all testing done in the laboratory. All small specimens and beams were casted from the same batch of concrete at the same day. This made all material properties representative for all beams. The recipe introduced in chapter 4 was utilized in the final concrete mix. The procedures presented in chapter 4 was followed to achieve the results presented.

5.1 Material Properties

Table 5.1: Material properties

Saturated density	$\rho_{cs} = 2013 \text{ kg/m}^3$
Oven-dry density	$\rho_{cv} = 1834 \text{ kg/m}^3$
Cube - compressive strength after 7 days	$f_{lcm,7} = 56.7 \text{ MPa}$
Cube - compressive strength after 28 days	$f_{lcm,28} = 74.2 \text{ MPa}$
Cylinder - compressive strength after 28 days	$f_{lcm} = 65.1 \text{ MPa}$
Tensile strength	$f_{lctm} = 4.03 \text{ MPa}$
Young's modulus	$E_{lcm} = 24175^* \text{ MPa}$

* Value was taken from previous experimental work [23].

Table 5.1 gives an overview of all average material properties of the concrete mix utilized in testing. All experiments were conducted between 28 and 59 days after casting, with the exception of compressive strength after 7 days.

5.1.1 Compressive Strength

Cubes

Cubes were given identification numbers in the order they were tested. Only cubes that showed adequate failure modes were included in this study. Most of the tested specimens showed a symmetrical hourglass failure shape. This implies centric loading.

Table 5.2: Compressive strength of cubes

Specimen number	t [days]	f_{lc} [MPa]
1	7	56.20
2	7	57.32
3	7	56.52
4	28	72.86
5	28	76.21
6	28	73.48
7	38	74.45
8	38	74.63
9	38	77.13
10	44	76.30
11	44	77.88
12	44	76.99
13	49	78.02
14	49	79.15
15	49	77.78
16	55	80.75
17	55	81.73
20	59	80.06
21	59	77.60
22	59	75.27

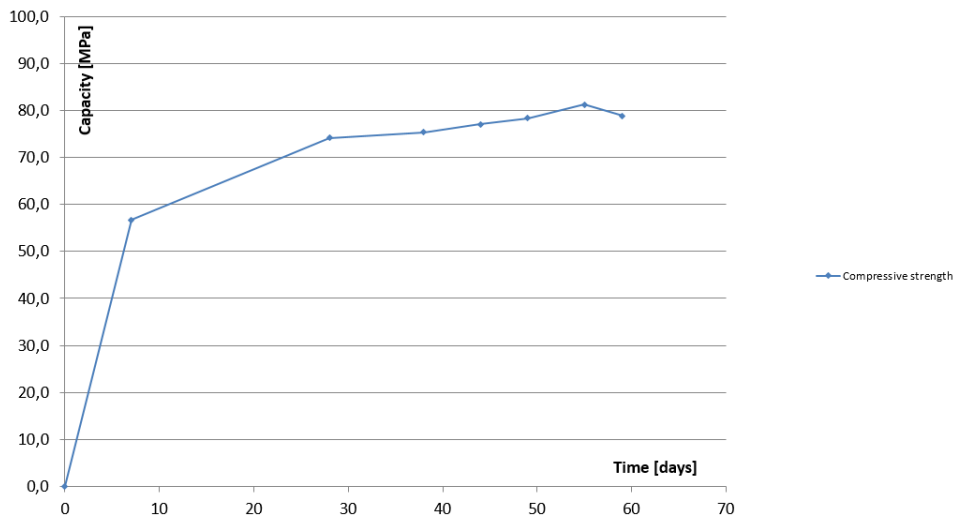


Figure 5.1: Development of compressive strength of cubes

Table 5.2 and Figure 5.1 show how the compressive strength of cubes developed over time. The capacity did not change dramatically after 28 days. Figure 5.1 shows average values of the cubes tested each day.



Figure 5.2: Failure of cubes in compression

Cylinders

Cylinders were given identification number in the order they were tested. Four cylinders were tested after 28 days to measure average compressive capacity. All tested cylinders were grained on the top and the bottom surface to make sure both sides were parallel. All four specimens showed adequate failures.

Table 5.3: Compressive Strength of Cylinders

Specimen number	t [days]	f_{lc} [MPa]
1	28	64.71
2	28	63.83
3	28	66.71
4	28	65.16



Figure 5.3: Failure of cylinders in compression

5.1.2 Tensile Splitting Strength

Four cylinders were tested to find the tensile splitting strength. All specimens displayed adequate failures. The fracture line propagated through the whole diameter. The test was conducted 28 days after casting.

Table 5.4: Tensile splitting strength of cylinders

Specimen number	t [days]	f_{lct} [MPa]
1	28	3.96
2	28	4.18
3	28	3.96
4	28	4.00

**Figure 5.4:** Failure of cylinders in tension

5.2 Beams

The beams were unwrapped 31 days after casting, and later painted white in order to see crack propagation clearer during testing. On the day of testing, each beam was placed in the test rig and the steel spreader beam was connected to provide the desired load situation. In some of the graphs in the following section, some LVDTs or strain gauges did not work. In these cases, the values of the measuring devices will be registered until destruction.

Compressive and tensile strains in both concrete and reinforcement were measured during the tests. Vertical deflections were also measured.

Peak one was defined as the load level when the concrete cover on top between the loading points spalled. Immediately after the beams reached this peak, the LVDTs on top of the beams were not able to record strains. Some of the beams were able to redistribute the forces and continue to deflect, for an increased or a constant load level, after peak one. Failure occurred when the concrete cover on the sides spalled. This was defined as peak two.

The same development of cracks occurred for beam 1-6. The first bending crack was observed in the tensile zone between the loading points. As the load was increased, new bending cracks propagated symmetrically until they reached the top of the beam flange. Development of bending cracks slowed down when shear cracks appeared. The first shear cracks appeared in the middle of the shear zone, between the neutral axis and the beam flange. Additional loading lead to further crack propagation of both bending and shear cracks. In beam 7, shear cracks appeared from bending cracks, which was different than for the other beams. Figure B.1 - B.7 show crack propagation and loading steps for each beam.

Linear strain distributions over the height of the cross section were calculated for all the beams at different load levels. The lines were created from measured strain values in compression and tension using linear interpolation. The strains measured in the reinforcement was used to create the lines.

With the exception of beam 5, all the beams failed in compression between the loading points. This type of failure is defined as compressive failure in the bending moment zone.

By using DIC, it was possible to observe the marked strain field just before spalling of each beam. It can be noticed that the strains measured by the DIC in general showed larger strains than the strains measured by LVDTs. The maximum strains on top of the beams measured by DIC were between 4 and 4.5 ‰ for all the beams. It can be observed from the pictures that the strains were localized in small areas.

Detailed tables of loading steps and accompanying deflections and strains for each beam is given in table B.1 - B.6. Table 5.5 gives a summary of the testing results.

Table 5.5: Summary of testing results

Beam number	Beam identification	Stirrup spacing s [mm]	Compressive cube strength $f_{cm,28}$ [MPa]*	Bending crack P_{cr} [kN]	Shear crack $P_{cr,V}$ [kN]	Max load registered P_{max} [kN]	Failure load P_u [kN]	Calculated max load P_{calc} [kN]	$\frac{P_{max}}{P_{calc}}$
1	LWA65_20_0	-	74.2	53	318	724	717	729	0.99
2	LWA65_20_200	200	74.2	107	350	645	629	729	0.88
3	LWA65_20_60	60	74.2	78	319	707	687	729	0.97
4	LWA65_20_100	100	74.2	69	324	700	691	729	0.96
5	LWA65_40_60	60	74.2	-	-	505	505	726	0.69
6	LWA65_40_100	100	74.2	64	339	663	589	726	0.91
7	LWA65_40_200	200	74.2	64	250	750	653	800	0.94

* Mean cube strength after 28 days.

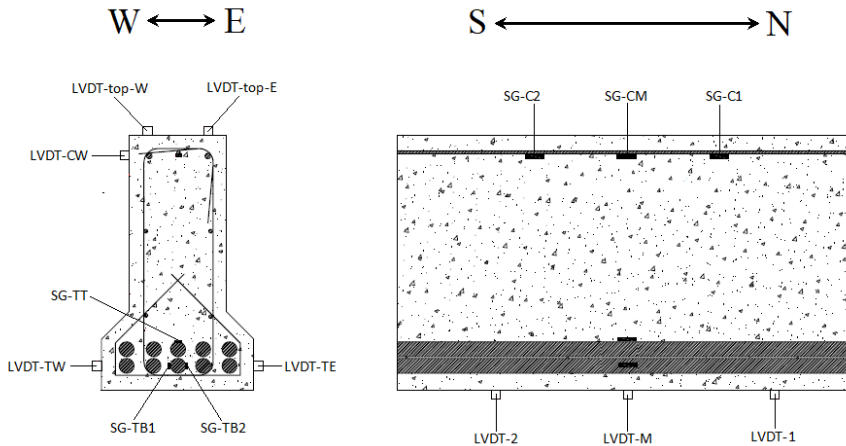
**Figure 5.5:** Location and designated names for each measuring device

Figure 5.5 shows the location and the designated names for each measuring device. All devices will be referred to in this way throughout this chapter.

5.2.1 Beam 1 - LWAC65_20_0

The first beam was tested 37 days after casting with a loading rate of 1 mm/min. As a precaution, more loading steps than necessary were used. The first bending crack appeared at load level $P = 53$ kN. The first shear crack appeared at load level $P = 318$ kN.

The north support of the steel spreader beam of setup 1 was not sufficiently constructed. This led to yielding of the bottom flange making the load situation eccentric, in turn leading to torsion of the concrete beam. The test was then stopped and continued after correct installation of the steel spreader supports. When the load P approached 550 kN, it was apparent that the steel beam did not have sufficient capacity to transfer the load. Moments after, the web of the steel spreader beam started to yield.



(a) Yielding of bottom flange



(b) Yielding of web

Figure 5.6: Yielding of steel spreader beam for setup 1

The test was stopped at approximately $P = 650$ kN. There was also observed local spalling of the concrete under the north support. The beam was left in the rig for 12 days. During these days, a new steel spreader beam was constructed to transfer the load from the jack. No plastic deformations or further propagation of cracks were observed after the resting days. Figure 5.8, 5.10 and 5.12 was created from data of setup 1. Figure 5.7a and 5.7b show setup 1 and 2 of beam 1.



(a) Setup 1



(b) Setup 2

Figure 5.7: First and second setup of beam 1

When testing was continued, beam 1 was loaded without pause to $P = 650$ kN. The loading

rate was changed to 1.2 mm/min. Beam 1 failed in compression between the loading points during the relaxation period after load level $P = 725$ kN. The failure was very explosive and brittle.

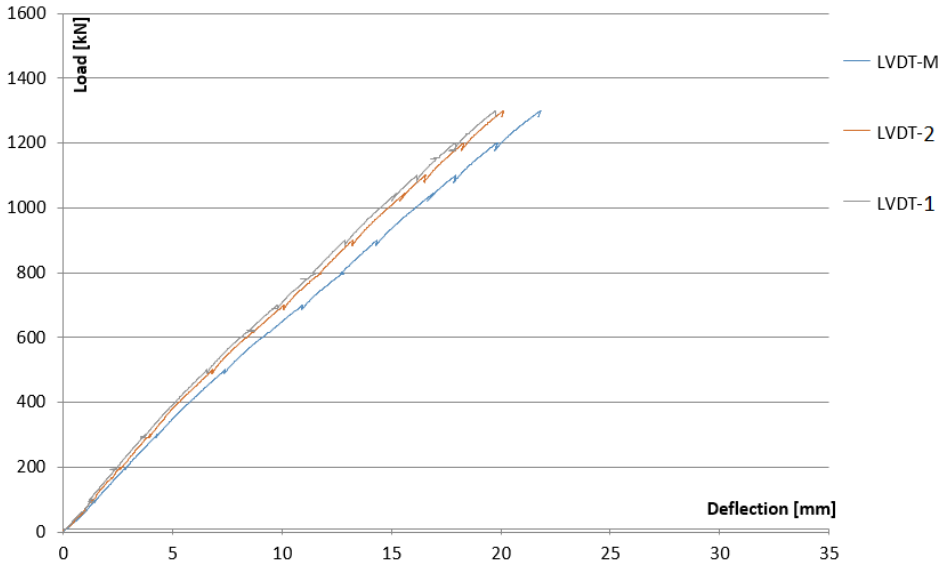


Figure 5.8: Load-deflection curves setup 1 for beam 1

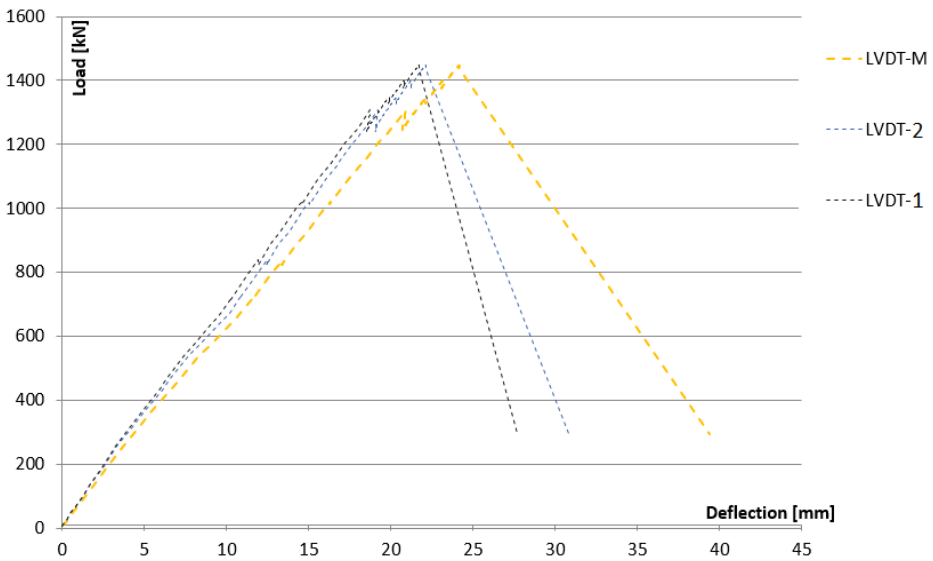


Figure 5.9: Load-deflection curves setup 2 for beam 1

Figure 5.8 and 5.9 show the load-deflection curves. The deflection under each loading point was almost equal throughout the test. This implies symmetrical loading of the beam and that a constant moment zone was achieved between the loading points. The displacement at midspan was larger than under both loading points. The same situation is seen in figure 5.9. However, some spalling under the north support occurred. This indicates that the loading was not symmetrical or that the concrete was locally weaker at this support. It can be seen that beam 1 was not able to resist any loading after reaching peak 1, as the failure happened immediately. The beam showed no ductile behaviour.

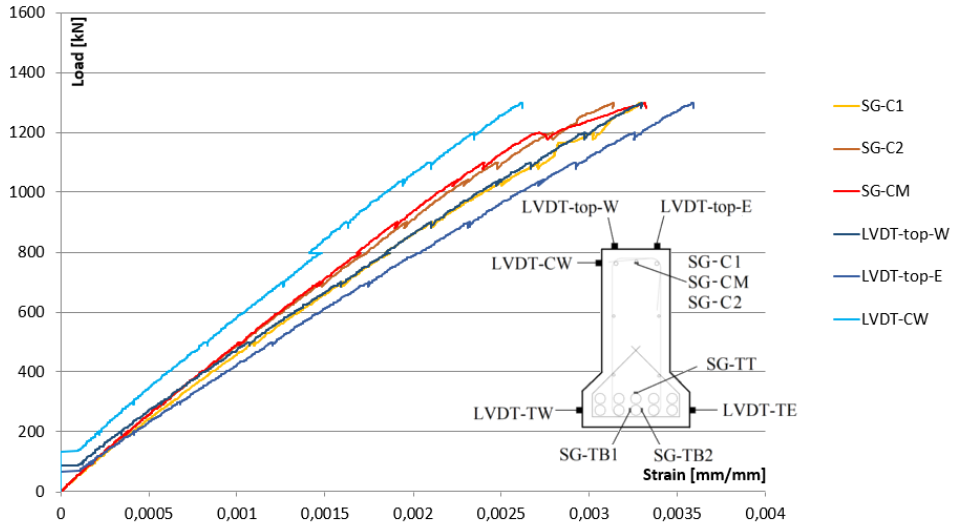


Figure 5.10: Load-compressive strain curves setup 1 for beam 1

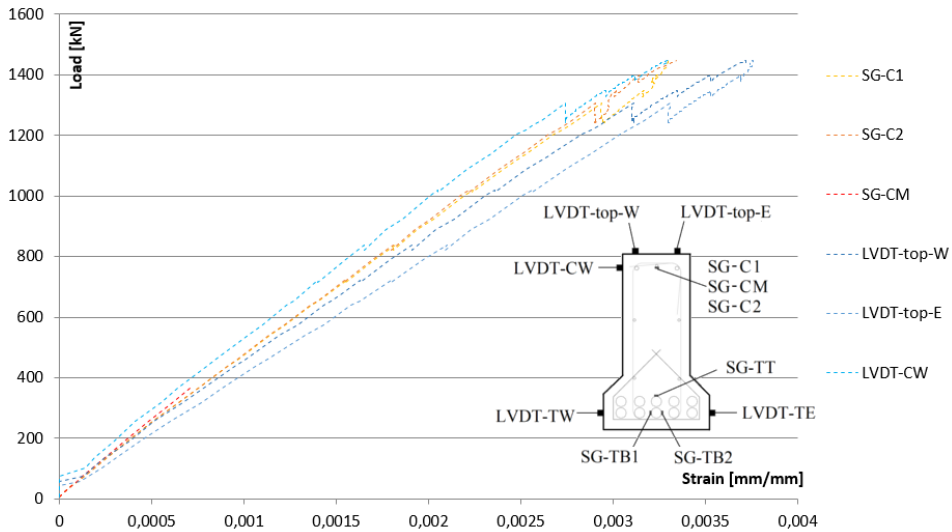


Figure 5.11: Load-compressive strain curves setup 2 for beam 1

Figure 5.10 and 5.11 show the load-compressive strain curves. Unequal strain values were measured at different points along the beam axis. The strain was higher closer to the support where the spalling of the concrete occurred. A difference in strains was also observed for the strains measured at the same height of the cross section. The strains on the east side were larger. This is in accordance with the fact that the beam was subjected to torsion when tested with the first setup. The strains in the compressive bar in the second setup was more equal along the beam axis. This implies more symmetrical loading the second time.

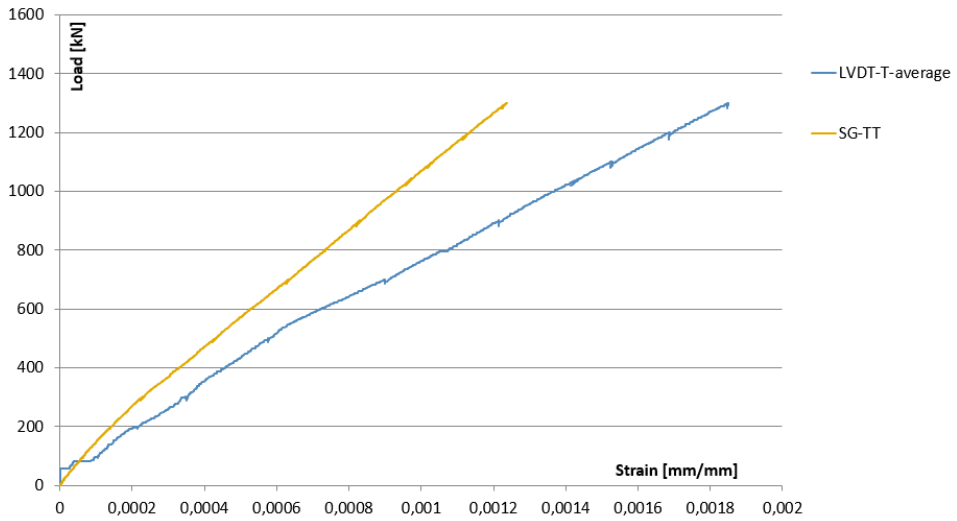


Figure 5.12: Load-tensile strain curves setup 1 for beam 1

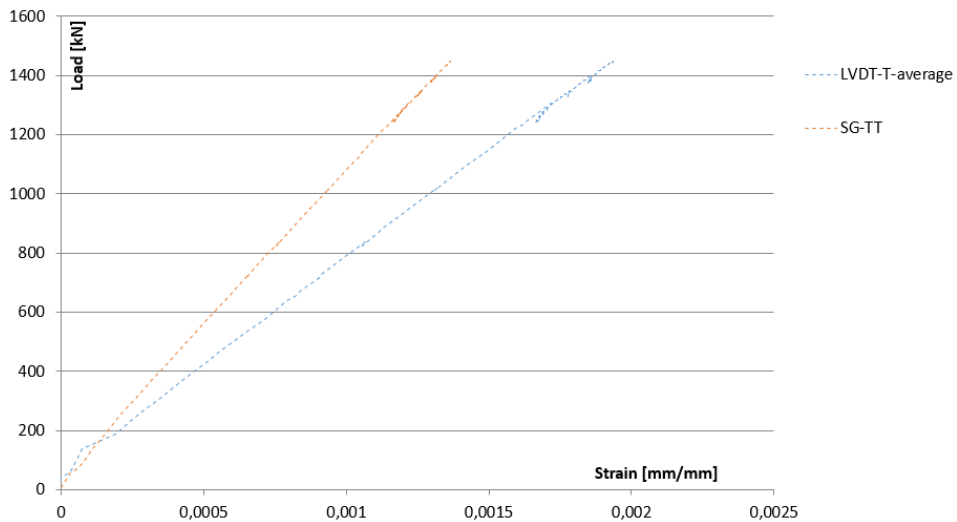


Figure 5.13: Load-tensile strain curves setup 2 for beam 1

Figure 5.12 and 5.13 show the load-tensile strain curves. The tensile strains for the west and east side of the beam differed significantly, as seen in table B.1. This implies torsion during testing. The strains decreased closer to the neutral axis. The tensile reinforcement did not yield as the maximum strain was lower than 2.5 ‰.

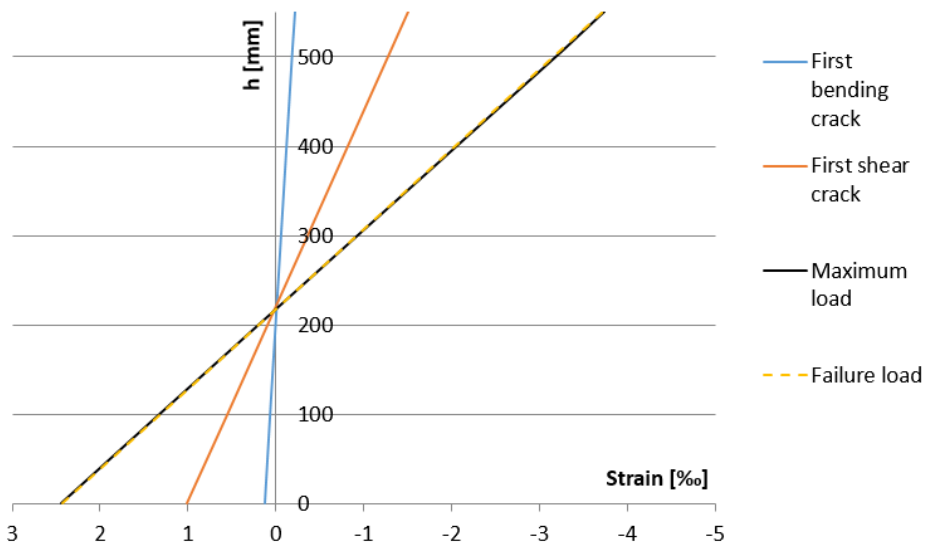


Figure 5.14: Strain distribution at different load levels for beam 1

Figure 5.14 shows the strain distribution over the height of the cross section calculated from strain measurements at different load levels.

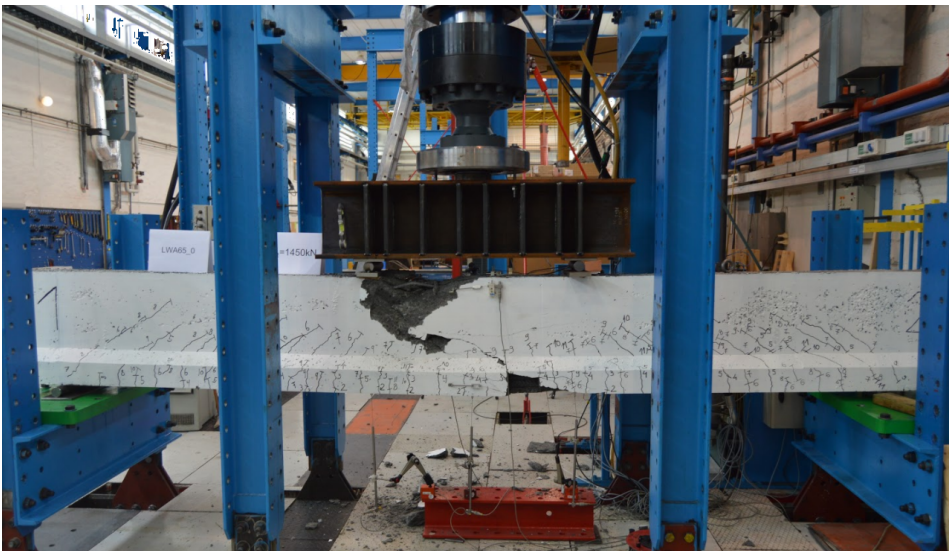


Figure 5.15: Beam 1 - Whole beam, failure

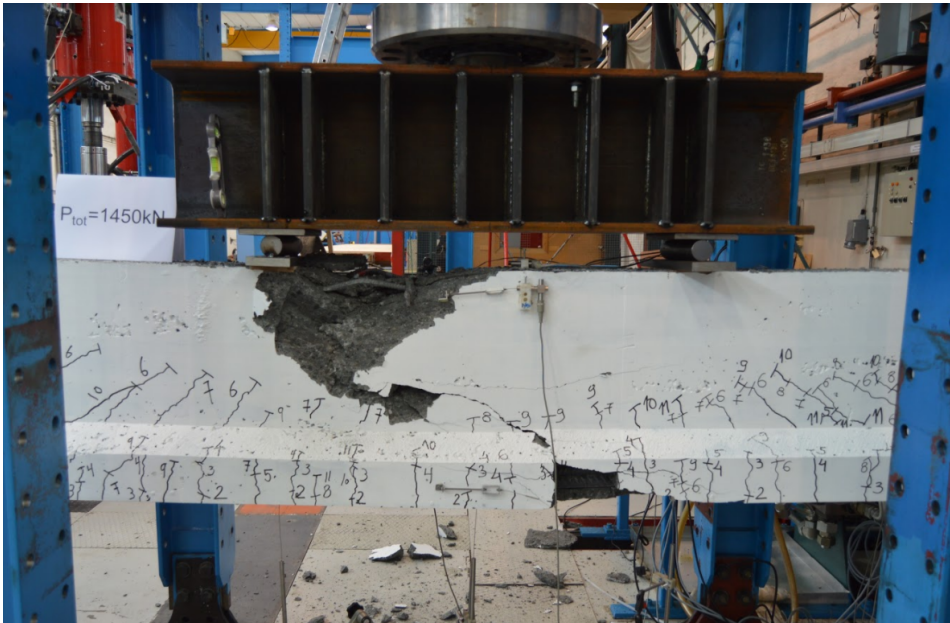


Figure 5.16: Beam 1 - Test zone, failure

Figure 5.15 and 5.16 show beam 1 after failure as well as step wise crack development.

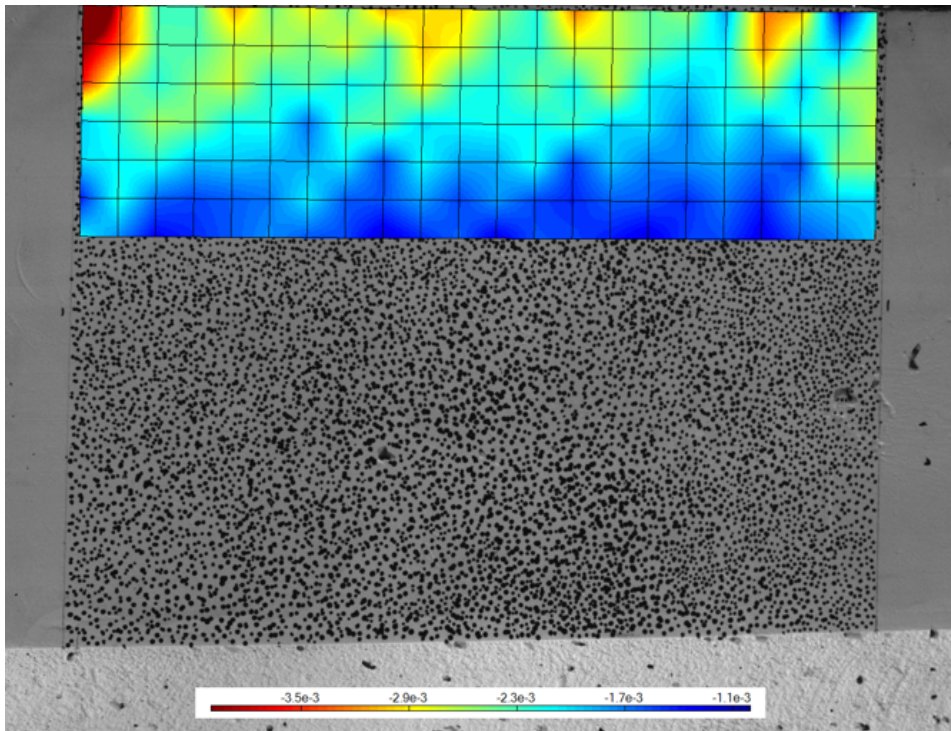


Figure 5.17: Strain field from DIC

Figure 5.17 shows the strain field of the compressive zone from DIC just before peak one.

5.2.2 Beam 2 - LWAC65_20_200

The second beam was tested 50 days after casting with a loading rate of 1.2 mm/min. The first bending crack appeared at load level $P = 107$ kN. The first shear crack appeared at load level $P = 350$ kN. The beam failed in compression between the loading points at load level $P = 645$ kN.

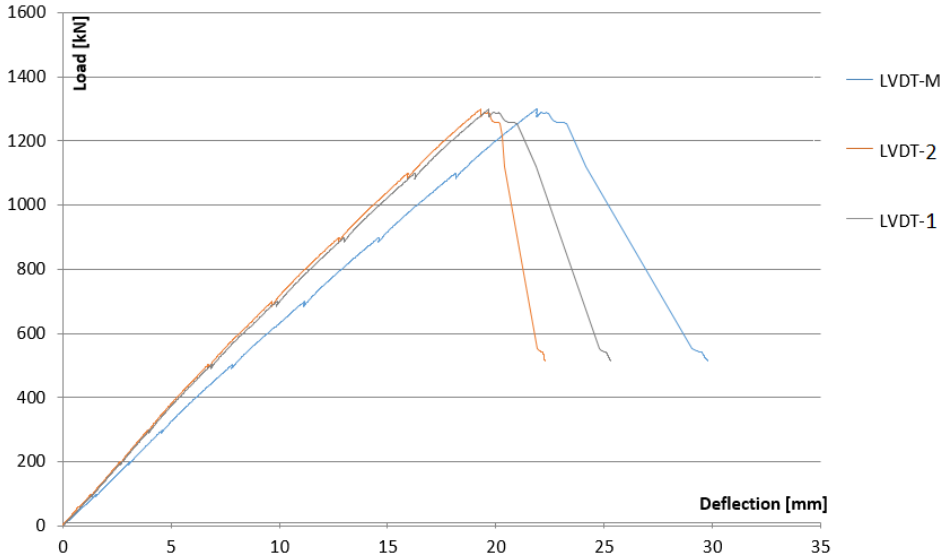


Figure 5.18: Load-deflection curves for beam 2

Figure 5.18 shows the load-deflection curves. The deflections under the loading points developed almost identically. This indicates that the load situation was symmetrical and that a constant moment zone was achieved between the loading points. The figure shows that the deflection at midspan was larger than under both loading points. From figure 5.18, it can be seen that after the maximum load was reached, the displacement increased for a nearly constant load. The figure shows a small displacement plateau before reaching failure load. This indicates a certain ductile behaviour of the beam.

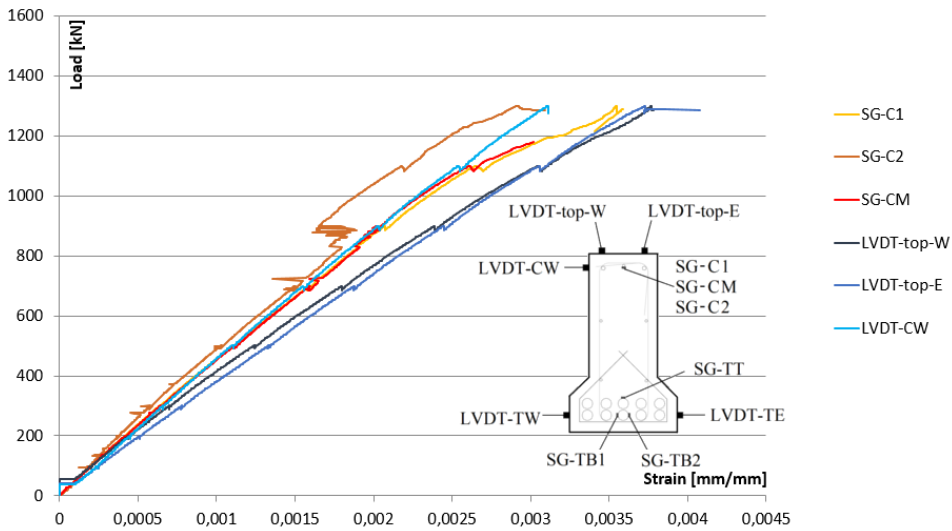


Figure 5.19: Load-compressive strain curves for beam 2

Figure 5.19 shows the load-compressive strain curves. The figure shows good agreement between the strains measured at the same height of the cross section. The strains measured at different points along the beam axis also show good agreement. It can be noticed that SG-C2 stopped working at load level $P \approx 415$ kN. The agreements of strains both laterally and longitudinally show that torsion did not occur and that a constant moment zone was achieved between the loading points. Smaller strains were observed closer to the neutral axis. After reaching strain level 2.5 ‰, the reinforcement yielded.

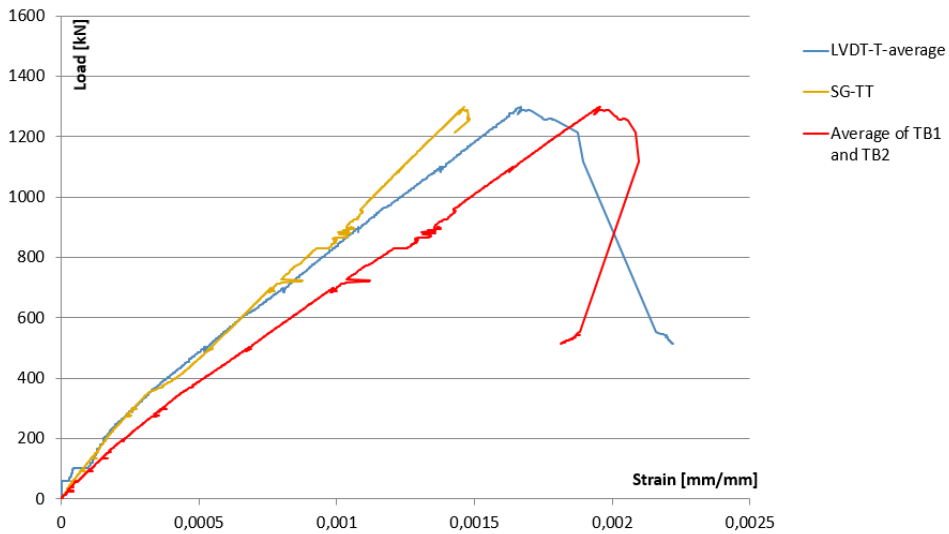


Figure 5.20: Load-tensile strain curve for beam 2

Figure 5.20 shows the load-tensile strain curves. The figure shows different strains for the same height of the cross section. The tensile reinforcement did not yield as the maximum strain was lower than 2.5 ‰.

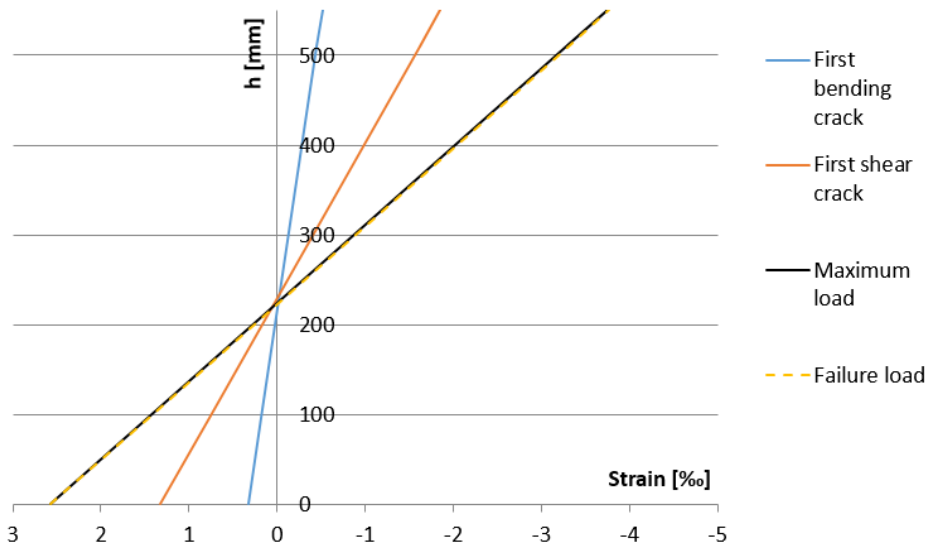


Figure 5.21: Strain distribution at different load levels for beam 2

Figure 5.21 shows the strain distribution over the height of the cross section calculated

from strain measurements at different load levels.



Figure 5.22: Beam 2 - Whole beam, failure



Figure 5.23: Beam 2 - Test zone, failure

Figure 5.22 and 5.23 shows beam 2 after failure as well as step wise crack develop-

ment.

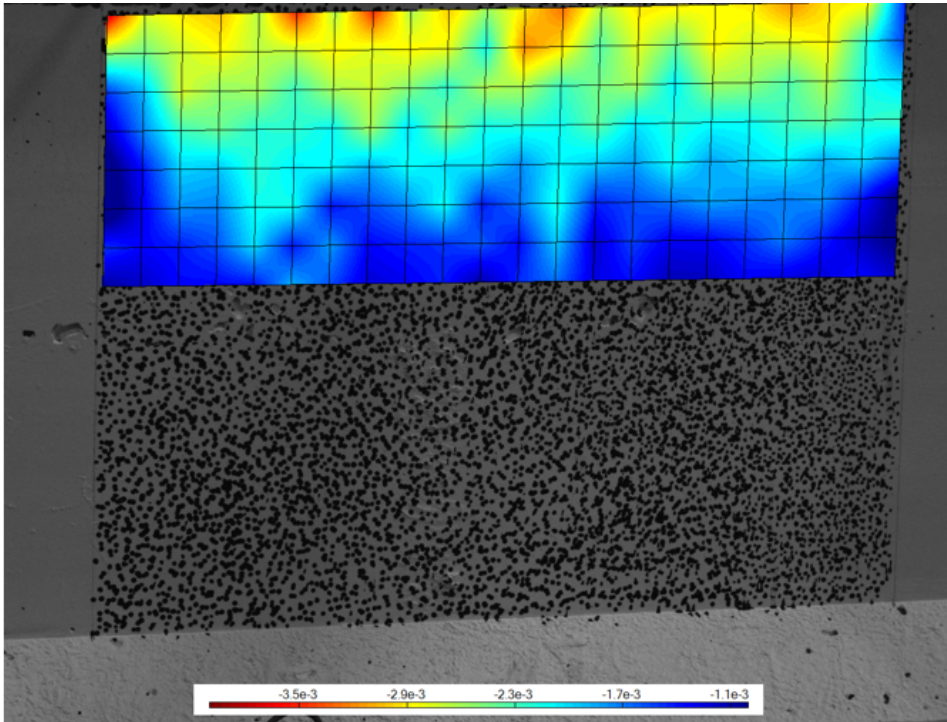


Figure 5.24: Strain field from DIC

Figure 5.24 shows the strain field of the compressive zone from DIC just before peak one.

5.2.3 Beam 3 - LWAC65_20_60

The third beam was tested 50 days after casting with a loading rate of 1.2 mm/min. The first bending crack was observed at load level $P = 78$ kN. The first shear crack was observed at load level $P = 319$ kN. The beam failed in compression between the loading points at load level $P = 687$ kN.

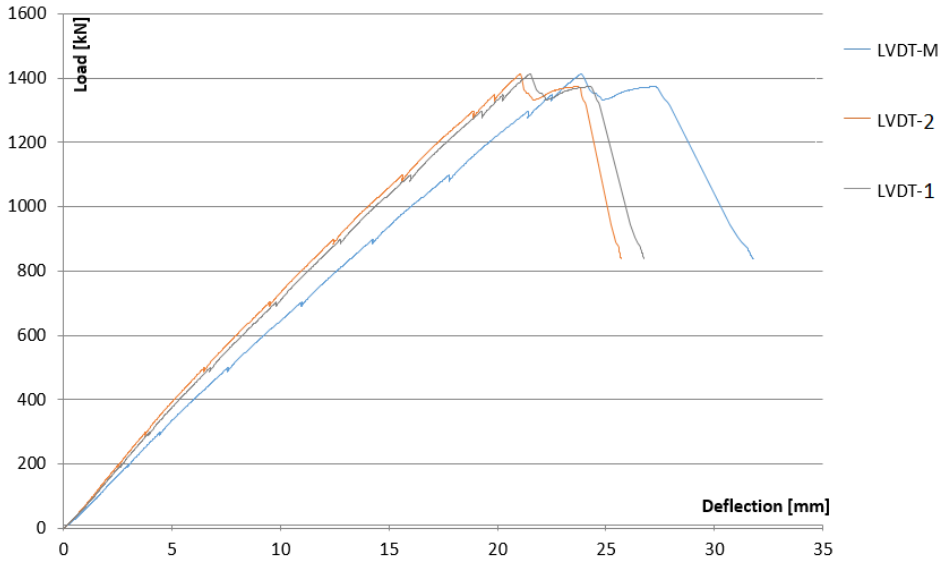


Figure 5.25: Load-deflection curves for beam 3

Figure 5.25 shows the load-deflection curves. The figure indicates that a constant moment zone was achieved as the deflections under both loading points were close to equal. The deflection at midspan was larger than under the loading points. From the figure we observe a deflection plateau after the maximum load level was reached. The deflections increased for a minor increase of the load, shown as two peaks on the curves. The failure of the beam was ductile.

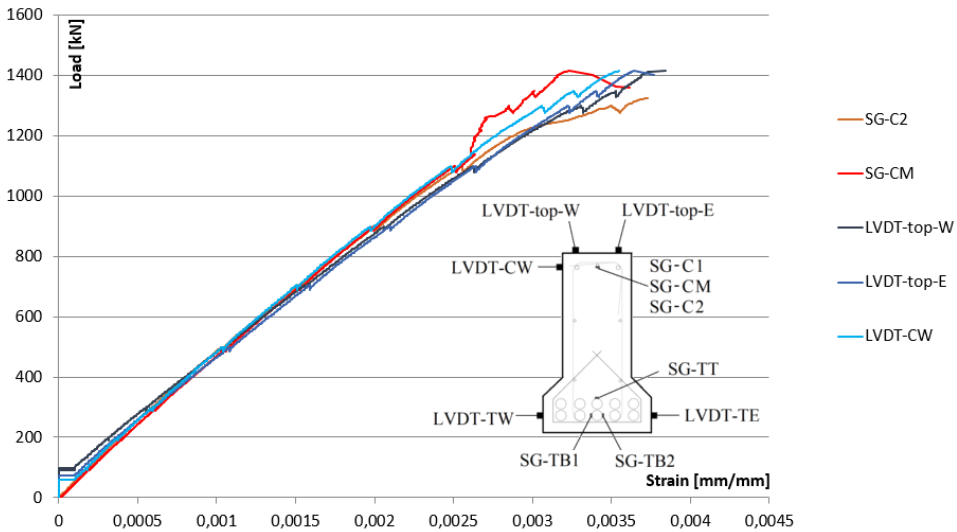


Figure 5.26: Load-compressive strain curves for beam 3

Figure 5.26 shows the load-compressive strain curves. The strains measured at different points along the beam axis were equal. This indicates that a constant moment zone was achieved between the loading points. The strains measured at the same height of the cross section were also equal. This indicates that the beam was not exposed to torsion. The compressive reinforcement yielded after 2.5 ‰.

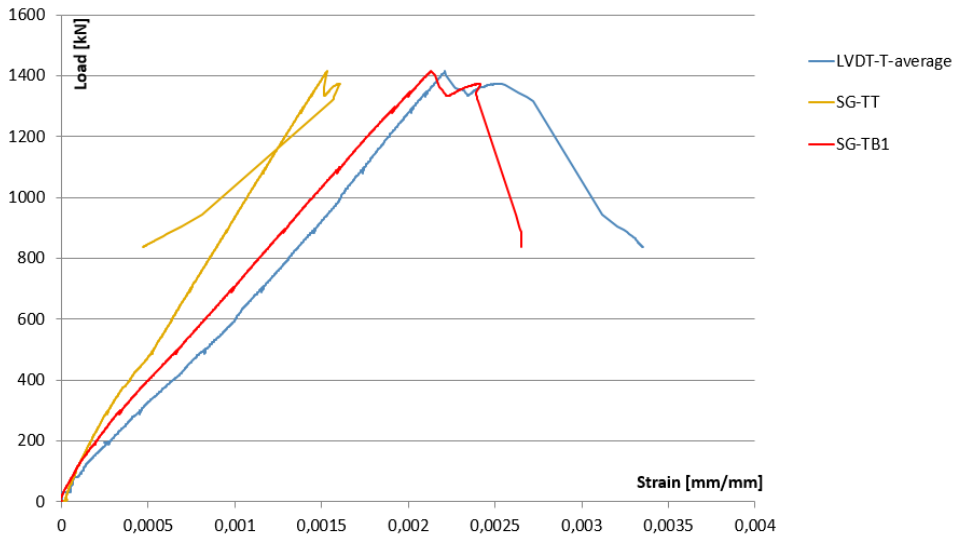


Figure 5.27: Load-tensile strain curves for beam 3

Figure 5.27 shows the load-tensile strain curves. From Table B.3 it can be seen that the concrete strains measured at the same height of the cross section differed significantly. The strains on the west side of the beam were larger than on the east side. This indicates that the beam was exposed to torsion. The average concrete strains were quite similar to the reinforcement strains measured at the same height. The strains decreased closer to the neutral axis. The tensile reinforcement did not yield as the strains were lower than 2.5 ‰.

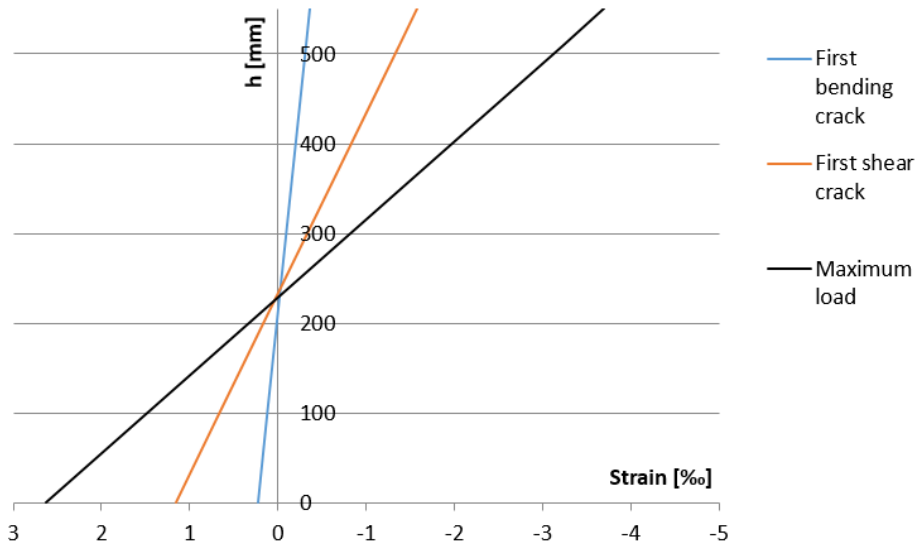


Figure 5.28: Strain distribution at different load levels for beam 3

Figure 5.28 shows the strain distribution over the height of the cross section calculated from strain measurements at different load levels. There was no available strain measurements to calculate the linear strain distribution at failure load.

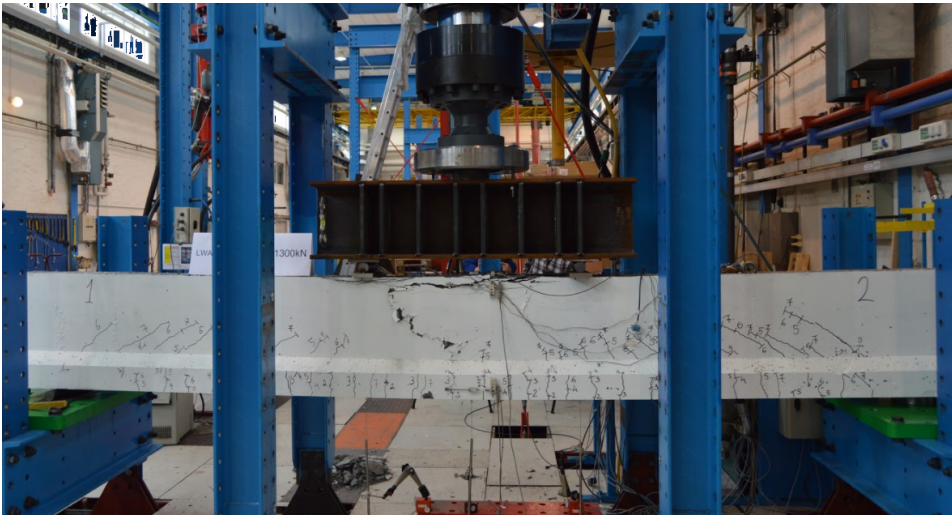


Figure 5.29: Beam 3 - Whole beam, failure

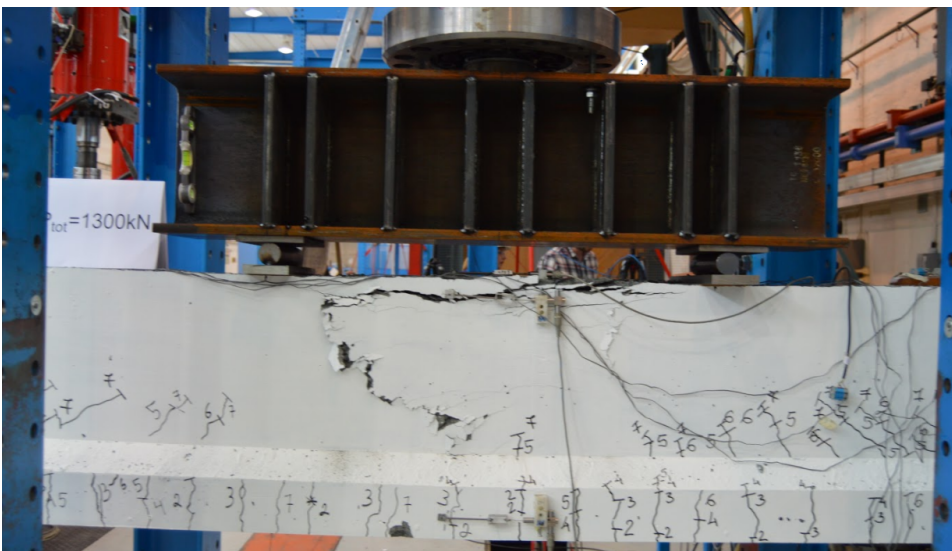


Figure 5.30: Beam 3 - Test zone, failure

Figure 5.29 and 5.30 show beam 3 after failure as well as step wise crack development.

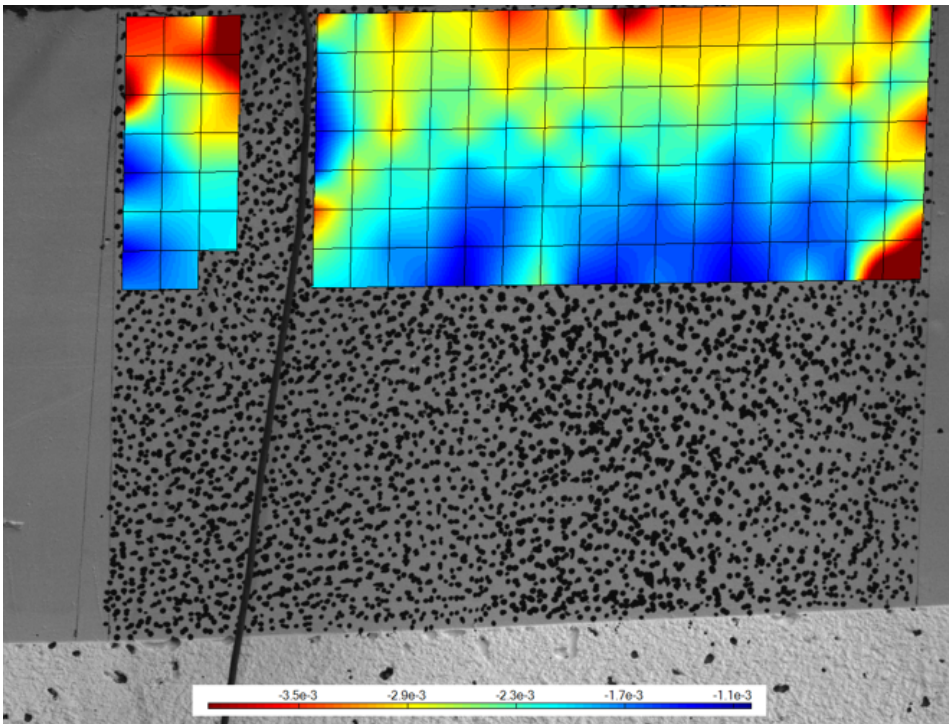


Figure 5.31: Strain field from DIC

Figure 5.39 shows the strain field of the compressive zone from DIC just before peak one.

5.2.4 Beam 4 - LWAC65_20_100

The fourth beam was tested 55 days after casting with a loading rate of 1.2 mm/min. The first bending crack was observed at load level $P = 69$ kN. The first shear crack was observed at load level $P = 324$ kN. The beam failed in compression between the loading points at $P = 690$ kN.

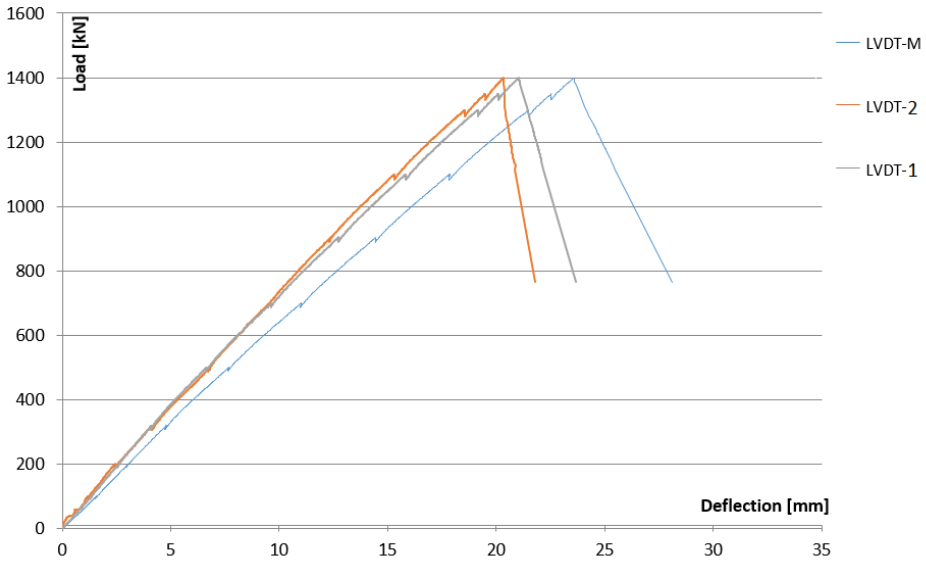


Figure 5.32: Load-deflection curves for beam 4

Figure 5.32 shows the load-deflection curves. The deflection under each loading point were almost equal. This indicates that a constant moment zone was achieved between the loading points. The deflection at midspan was larger than under both loading points. After reaching the maximum load, the load dropped as the deflection increased. The curves do not show a deflection plateau, but a force redistribution can be observed.

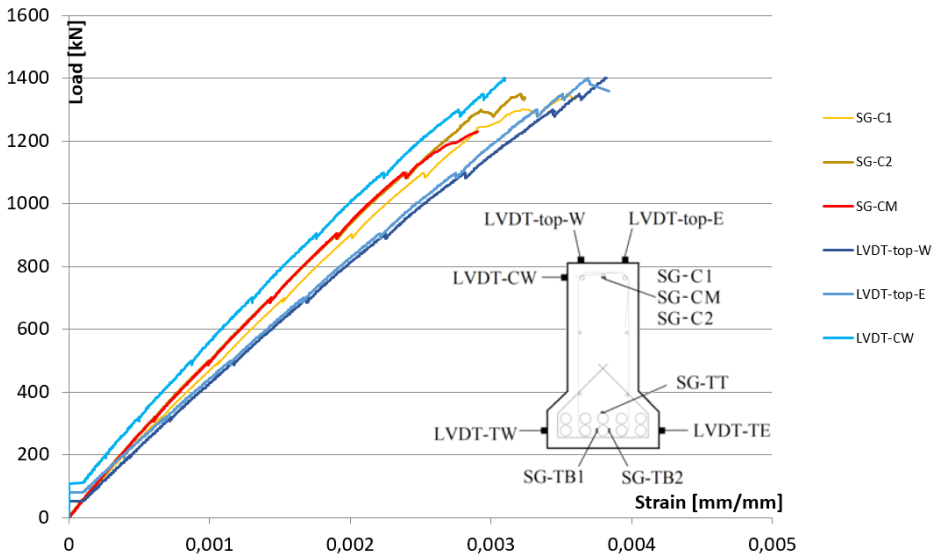


Figure 5.33: Load-compressive strain curve for beam 4

Figure 5.33 shows the load-compressive strain curves. The figure shows good agreement between the strains at the same height of the cross section. However, the strains in the reinforcement differed compared to the strains in the concrete. The agreement between the strains measured at different points along the beam axis indicates that a constant moment zone was achieved between the loading points. The compressive reinforcement yielded after 2.5 ‰.

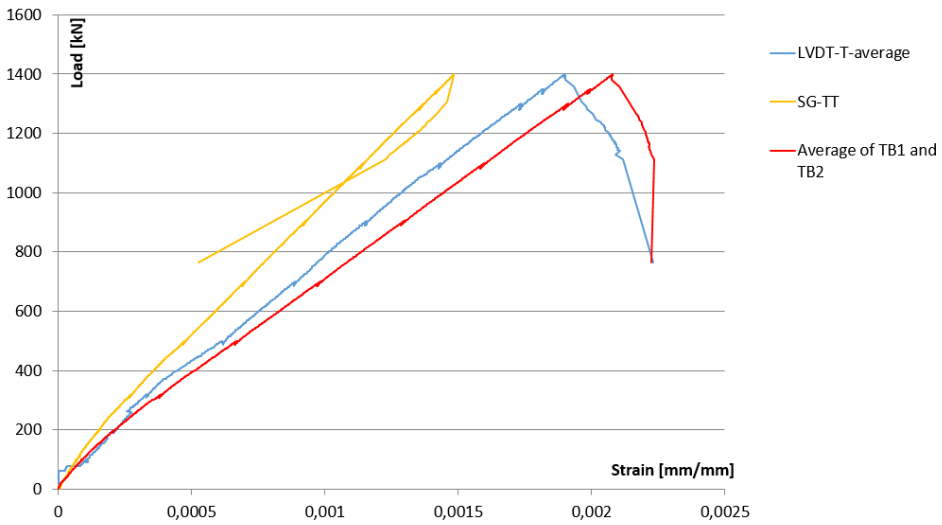


Figure 5.34: Load-tensile strain curves for beam 4

Figure 5.34 shows the load-tensile strain curves. The tensile strains measured at the same height of the cross section differed in the concrete and in the reinforcement. The strains decreased closer to the neutral axis. The tensile reinforcement did not yield as the strains were lower than 2.5 ‰.

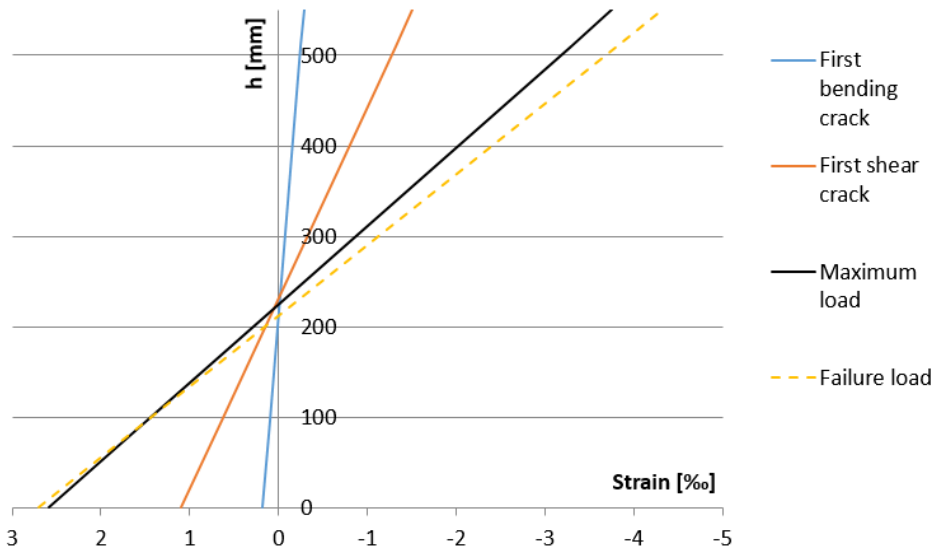


Figure 5.35: Strain distribution at different load levels for beam 4

Figure 5.35 shows the strain distribution over the height of the cross section calculated from strain measurements at different load levels.



Figure 5.36: Beam 4 - Whole beam, failure

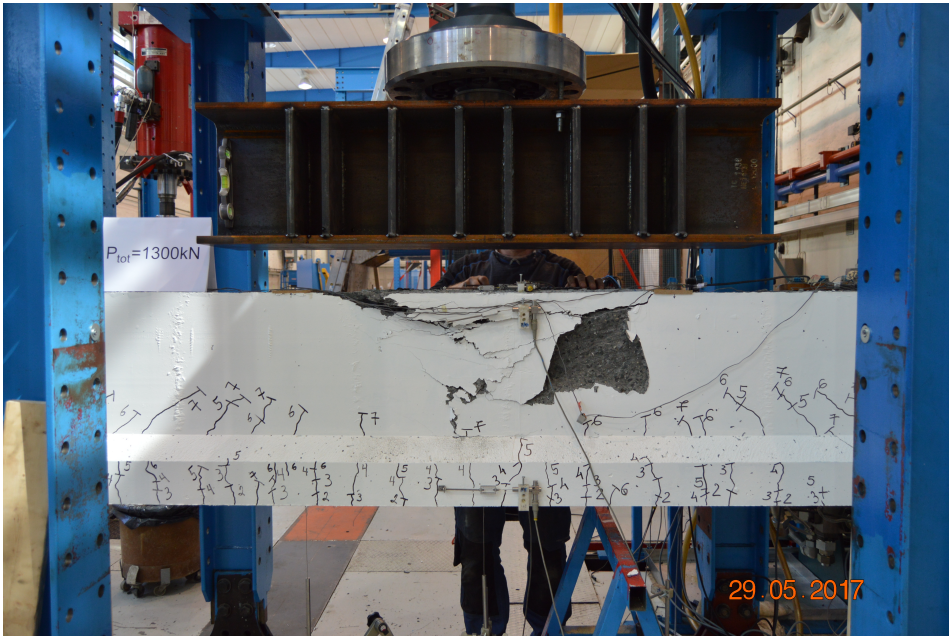


Figure 5.37: Beam 4 - Test zone, failure

Figure 5.36 and 5.37 shows beam 4 after failure as well as step wise crack development.

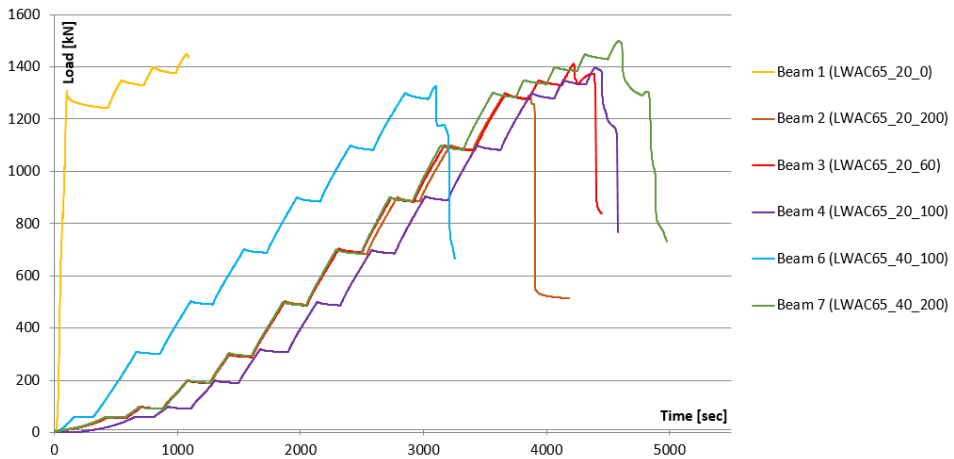


Figure 5.38: Load-time curves for all the beams

Table 5.6

Beam number	Beam identification	First peak T_1 [s]	Second peak T_2 [s]	Time difference $T_2 - T_1$ [s]
1	LWAC65_20_0	1070	-	-
2	LWAC65_20_200	3858	3894	36
3	LWAC65_20_60	4224	4380	156
4	LWAC65_20_100	4448	4564*	116
6	LWAC65_40_100	3100	3164	64
7	LWAC65_40_200	4614	4816	202

* Not considered as a peak, only a second vertical drop in the load-time curve

Figure 5.38 shows the load-time curves for the beams. Table 5.6 shows at what time each peak occurred and the time difference between them. Beam 4 did not reach a second peak. From Figure 5.38 and Table 5.6, a certain time interval between the first peak and the load level where the load drops vertically a second time, can be observed. This shows that beam 4 resisted a certain load level over a certain time interval after reaching peak one, even though the load was constantly decreasing. By visual inspection during testing of beam 4, the concrete on top spalled at T_1 and the concrete on the sides spalled at T_2 .

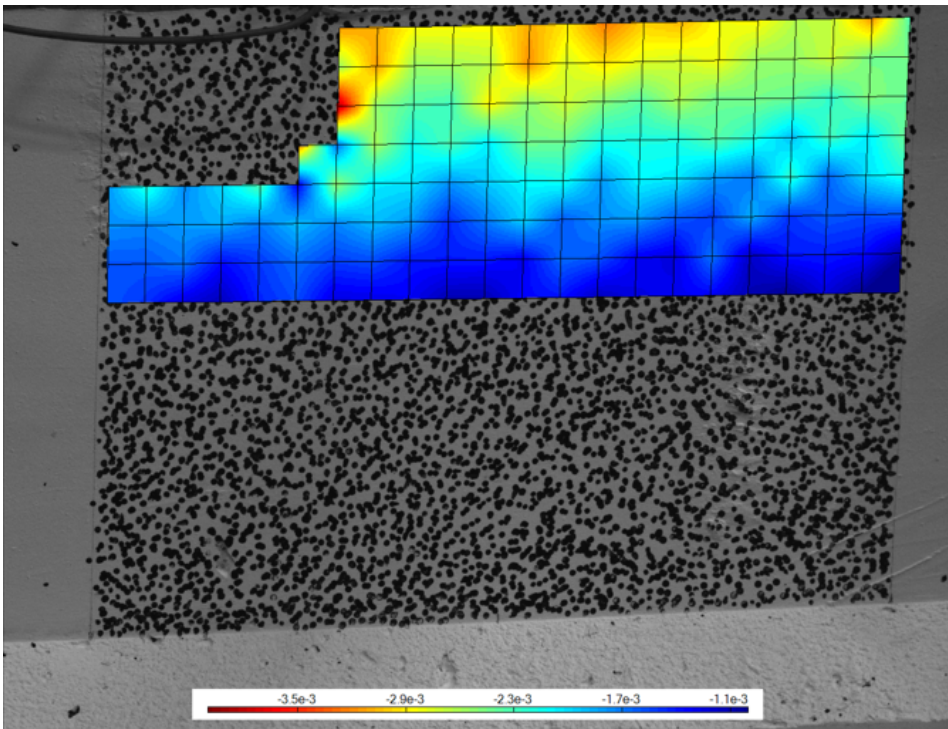
**Figure 5.39:** Strain field from DIC

Figure 5.39 shows the strain field of the compressive zone from DIC just before peak one.

5.2.5 Beam 5 - LWAC65_40_60

The fifth beam was tested 56 days after casting with a loading rate of 1.2 mm/min. At load level $P = 505$ kN the beam unexpectedly failed between the loading point and the north support. This fracture is defined as a compressive failure in the shear zone. After further investigation of the fracture area, it was apparent that the casting of the beam was not adequate. Big air pockets were discovered in the part of the cross section where the beam failed. This is shown in Figure 5.40. It was decided that the results would not be representative for the further investigation of the beam.



Figure 5.40: Visual pockets of air in the concrete



Figure 5.41: Beam 5 - Whole beam, failure

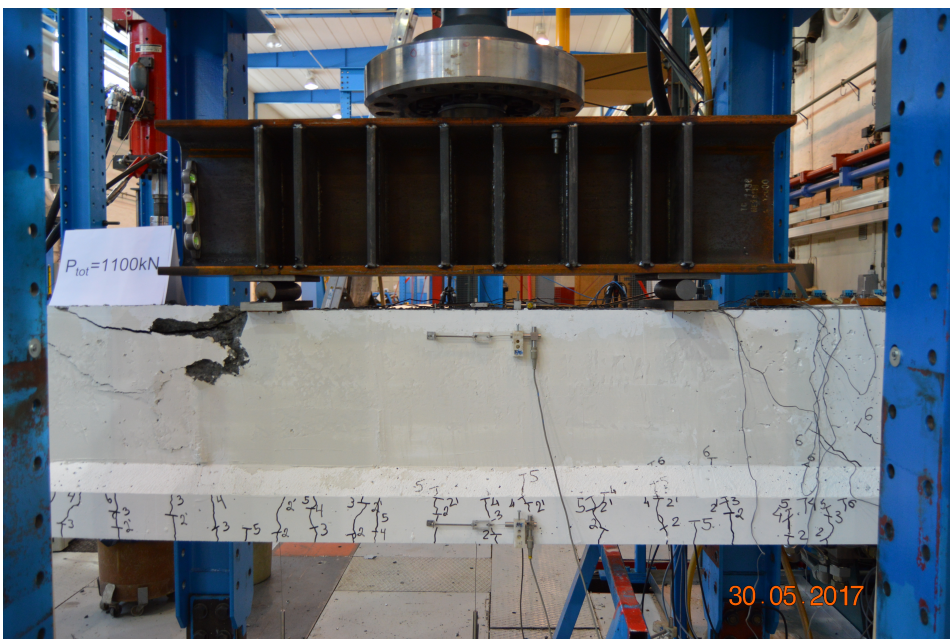


Figure 5.42: Beam 5 - Test zone, failure

5.2.6 Beam 6 - LWAC65_40_100

The sixth beam was tested 57 days after casting with a loading rate of 1.2 mm/min. The first bending crack was observed at a load level $P = 64$ kN. The first shear crack was observed at load level $P = 339$ kN. The beam failed in compression between the loading points at load level $P = 589$ kN.

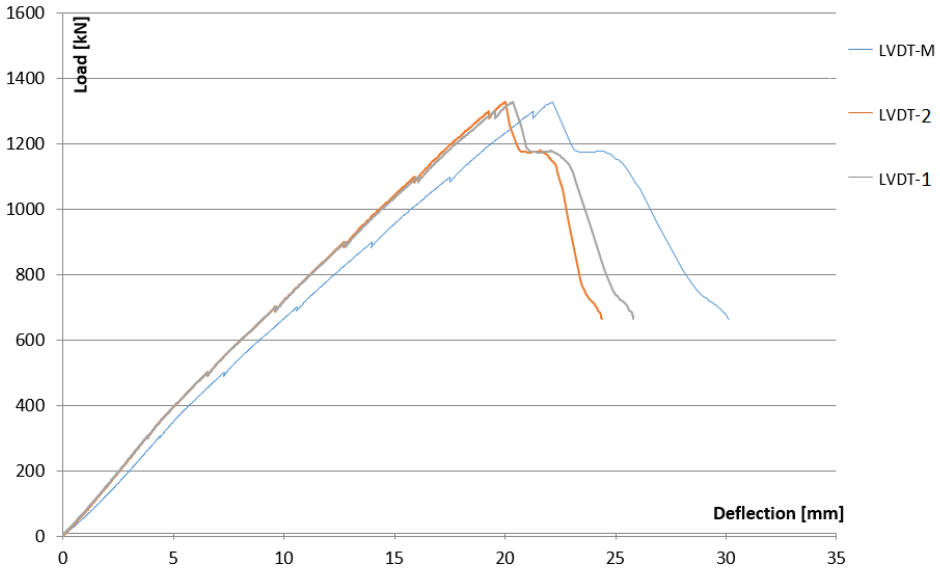


Figure 5.43: Load-deflection curves for beam 6

Figure 5.43 shows the load-deflection curves. The deflection under both loading points coincide until reaching the maximum load. This indicates that a constant moment zone was achieved between the loading points. The deflection at midspan was larger than under both loading points. After reaching the maximum load, the load dropped before the beam continued to deflect at a constant load level until failure. From the graphs, two load peaks and a deflection plateau can be observed. The failure of the beam was ductile.

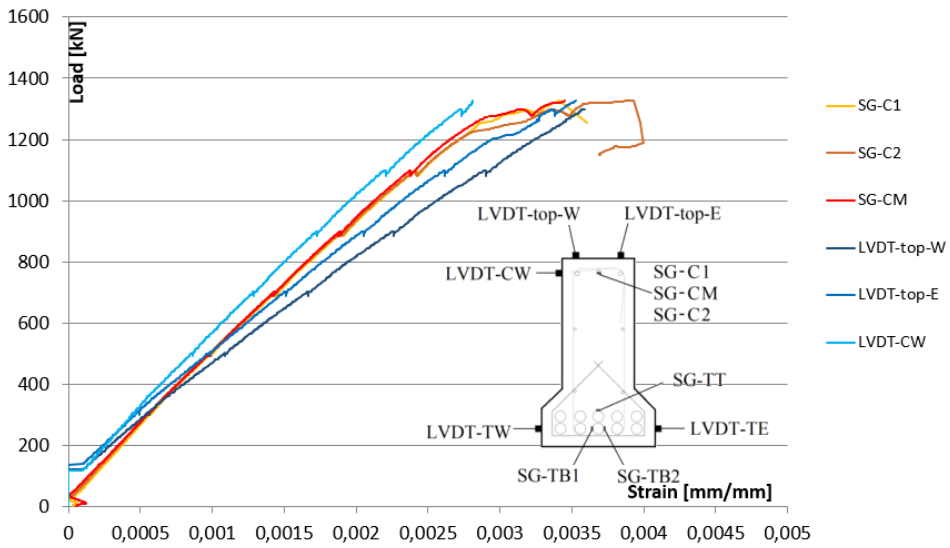


Figure 5.44: Load-compressive strain curves for beam 6

Figure 5.44 shows the load-compressive strain curves. The agreement between the strains measured at different points along the beam axis shows that a constant moment zone was achieved between the loading points. The compressive reinforcement yielded after 2.5 ‰. The strains measured at the same height of the cross section differed significantly. This indicates that the beam was subjected to torsion.

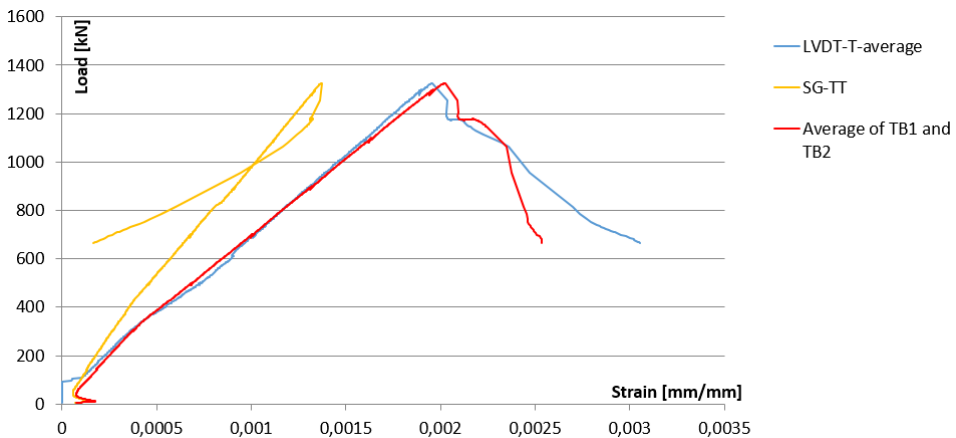


Figure 5.45: Load-tensile strain curves for beam 6

Figure 5.45 shows the load-tensile strain curves. The average values of the strain in the concrete and reinforcement coincide well. However, the strains on each side of the beam

did not match, as seen in Table B.5. This also indicates that the beam was subjected to torsion. The strains decreased closer to the neutral axis.

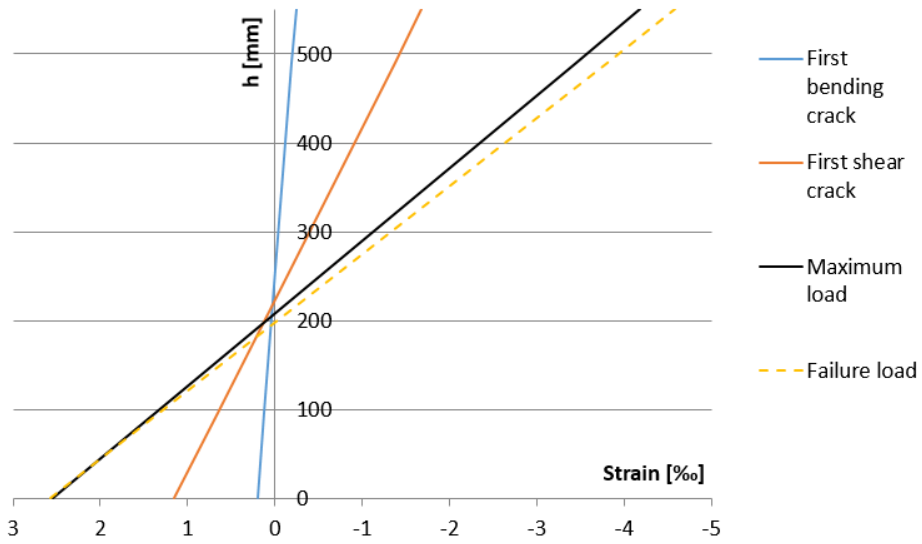


Figure 5.46: Strain distribution for different load levels for beam 6

Figure 5.46 shows the strain distribution over the height of the cross section calculated from strain measurements at different load levels.



Figure 5.47: Beam 6 - Test zone, failure

Figure 5.47 shows beam 6 after failure as well as step wise crack development.

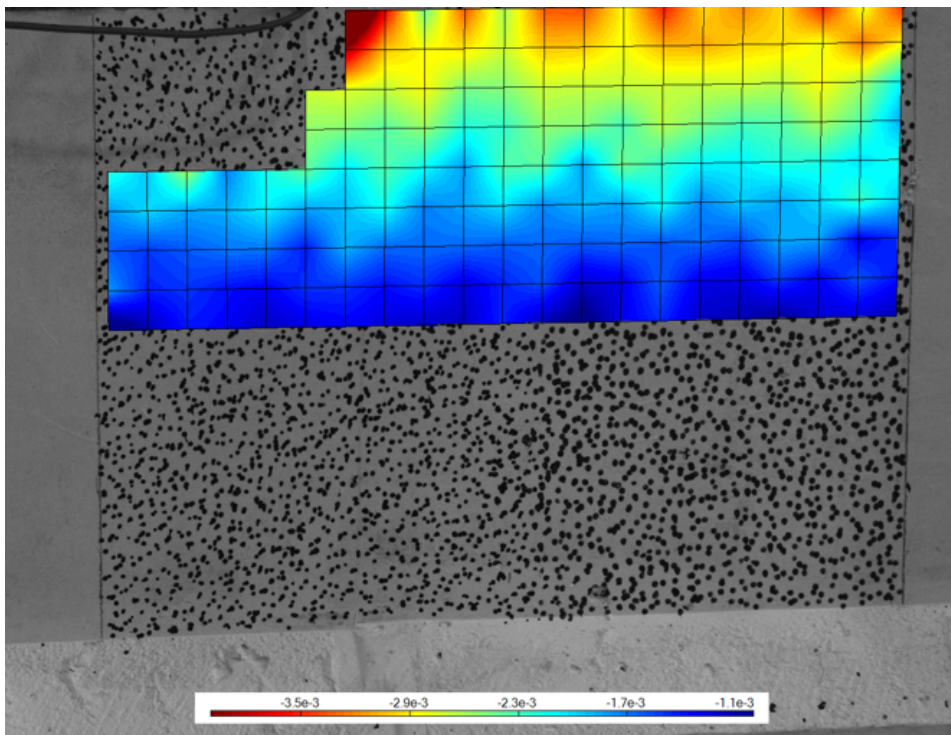


Figure 5.48: Strain field from DIC

Figure 5.48 shows the strain field of the compressive zone from DIC just before peak one.

5.2.7 Beam 7 - LWAC65_40_200

The seventh beam was tested 59 days after casting with a loading rate of 1.2 mm/min. The first bending crack was observed at load level $P = 64$ kN. The first shear crack was observed at load level $P = 250$ kN. Spalling was observed under the south support at load level $P = 550$ kN. The beam failed in compression between the loading points at load level $P = 653$ kN.

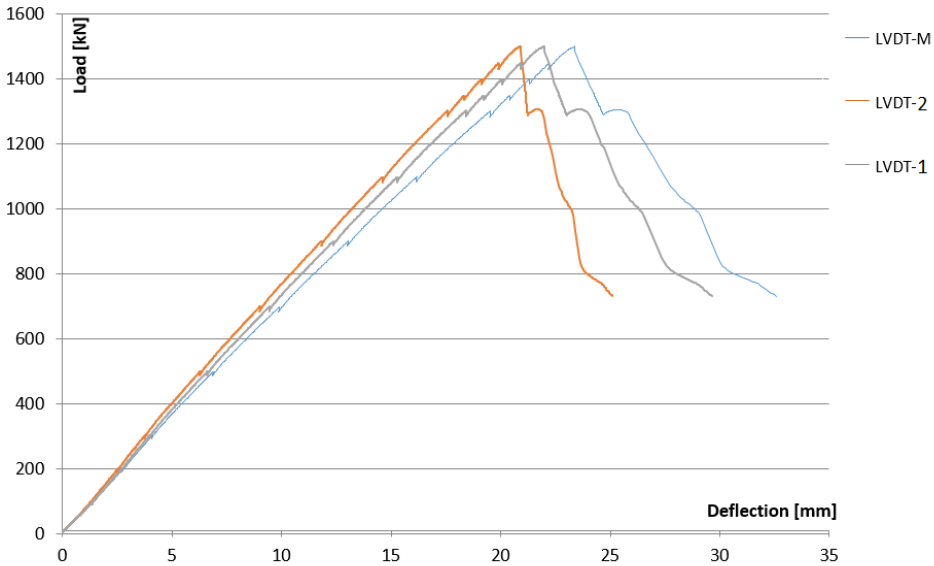


Figure 5.49: Load-deflection curves for beam 7

Figure 5.49 shows the load-deflection curves. The deflection under each loading point differed. This implies minor asymmetrical loading of the beam and that the moment zone was nearly constant between the loading points. The displacement at midspan was larger than under the loading points. After reaching the maximum load, the load dropped before the beam continued to deflect at a nearly constant load level until failure. Two load peaks and a certain deflection plateau can be observed from the curves. The failure of the beam was ductile.

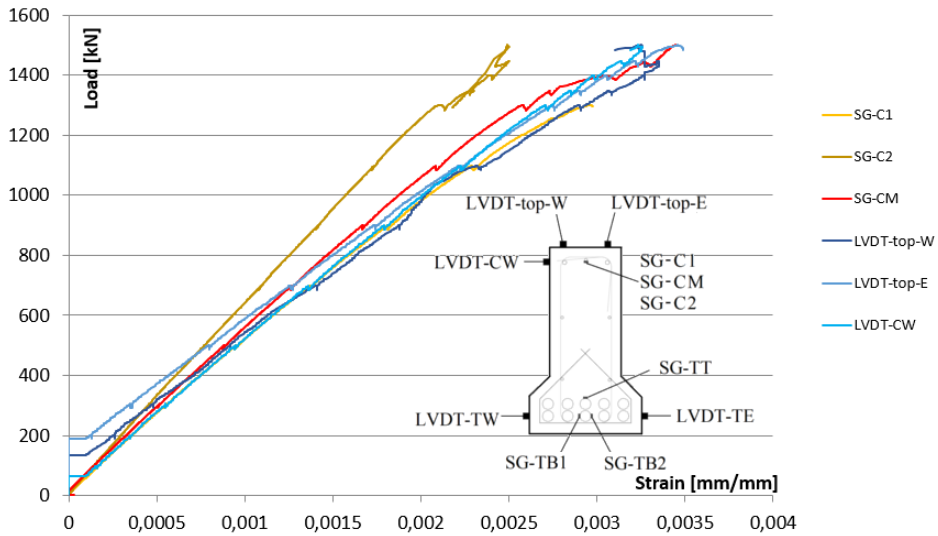


Figure 5.50: Load-compressive strain curves for beam 7

Figure 5.50 shows the load-compressive strain curves. The strains measured at different points along the beam axis differed significantly. The reason for this might be the short transversal reinforcement acting as supports for the longitudinal reinforcement. Asymmetrical loading might also be the reason for this. The amount of compressive reinforcement was very large. This led to a unique behaviour of the compressive zone, resulting in matching concrete strains for the top and the sides of the beam. The compressive reinforcement yielded after 2.5 ‰. It can be observed that SG-C2 stopped working at load level $P \approx 250$ kN.

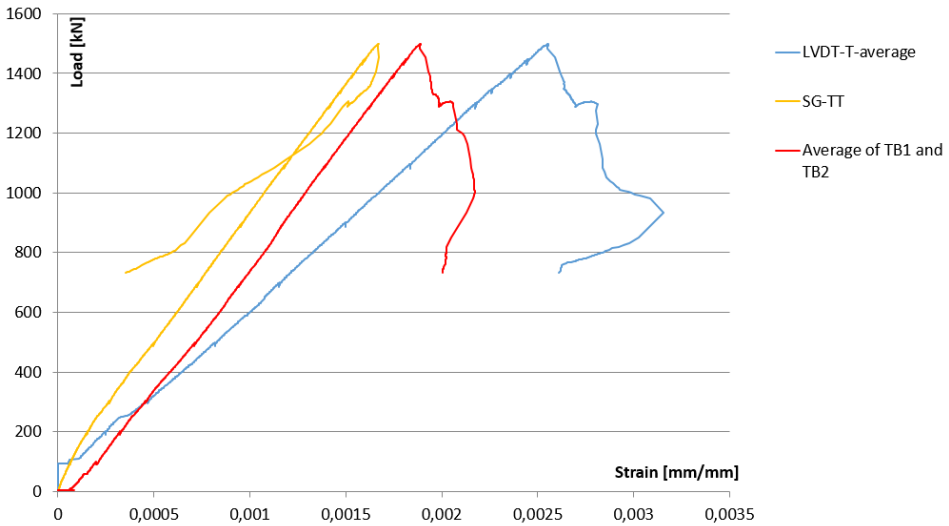


Figure 5.51: Load-tensile strain curves for beam 7

Figure 5.51 shows the load-tensile strain curves. The strains decreased closer to the neutral axis. The average strains in the concrete differed a lot from the average strains in the reinforcement at the same cross-sectional height. The concrete strains on each side of the beam also differed, as seen in Table B.6. This implies that the beam was subjected to torsion during testing.

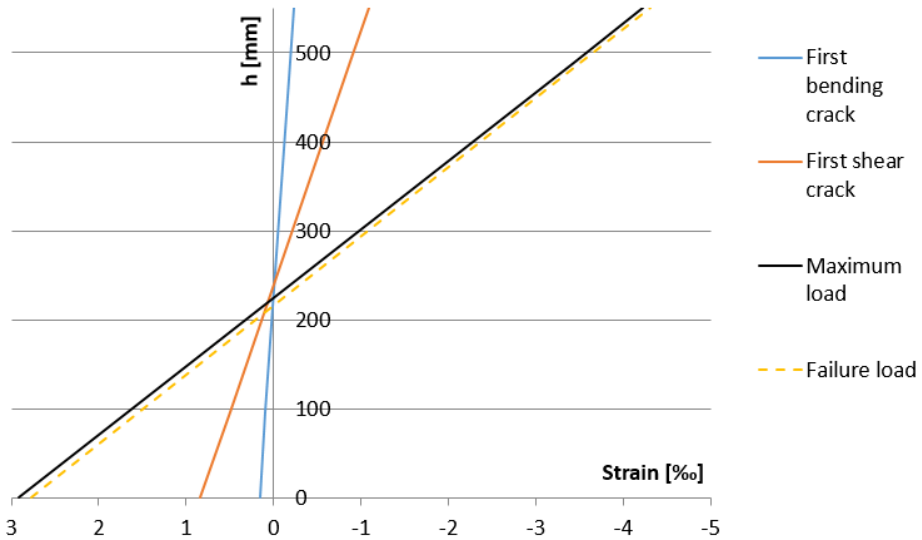


Figure 5.52: Strain distribution for different load levels for beam 7

Figure 5.52 shows the strain distribution over the height of the cross section calculated from strain measurements at different load levels.



Figure 5.53: Beam 7 - Whole beam, failure

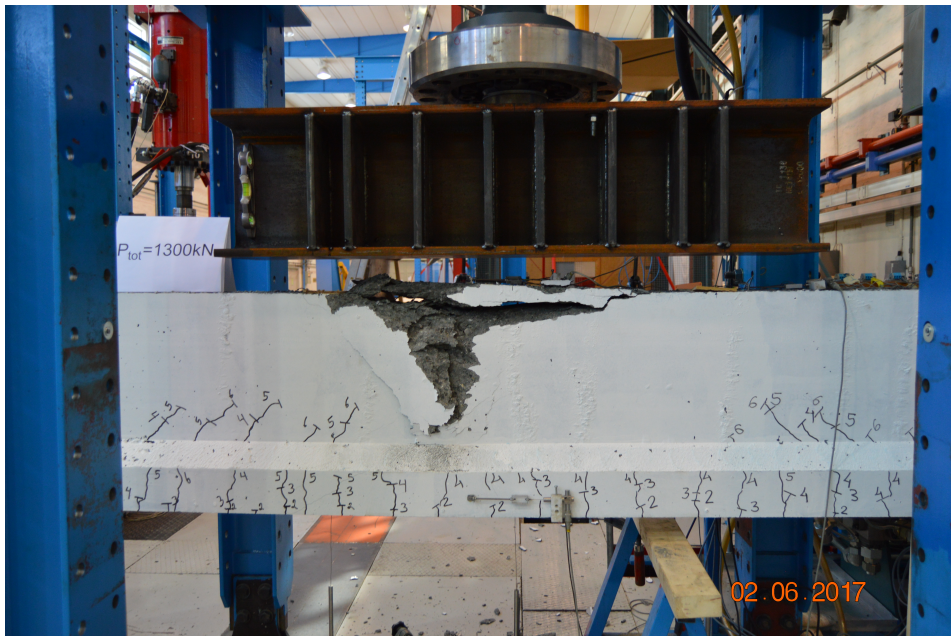


Figure 5.54: Beam 7 - Test zone, failure

Figure 5.53 and 5.47 shows beam 7 after failure as well as step wise crack development.

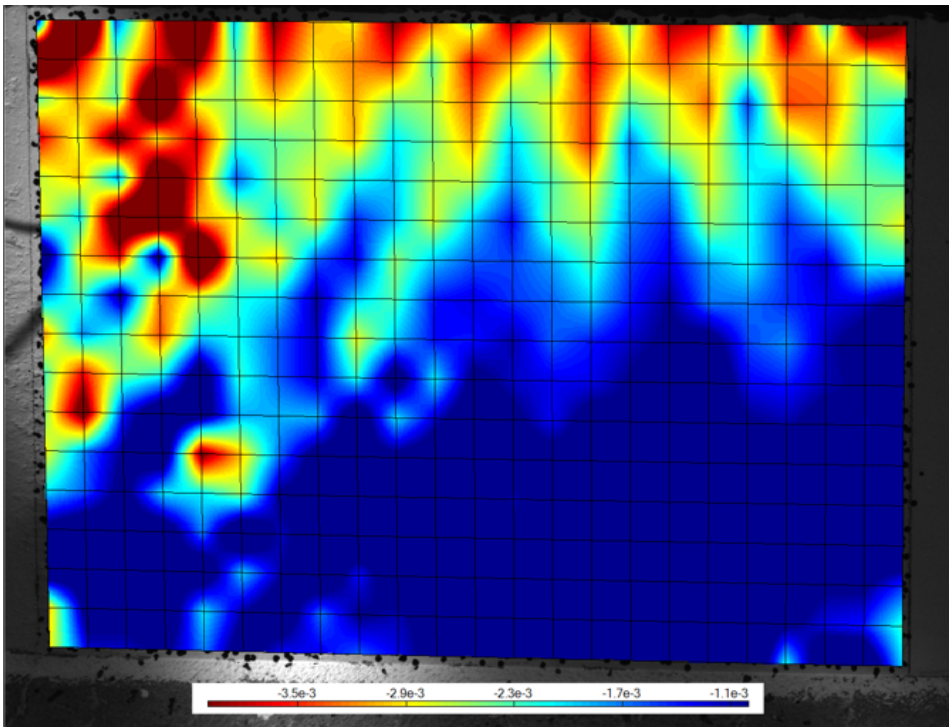


Figure 5.55: Strain field from DIC

Figure 5.55 shows the strain field of the compressive zone from DIC just before peak one.

5.3 Calculated Confined Concrete Capacity Revisited

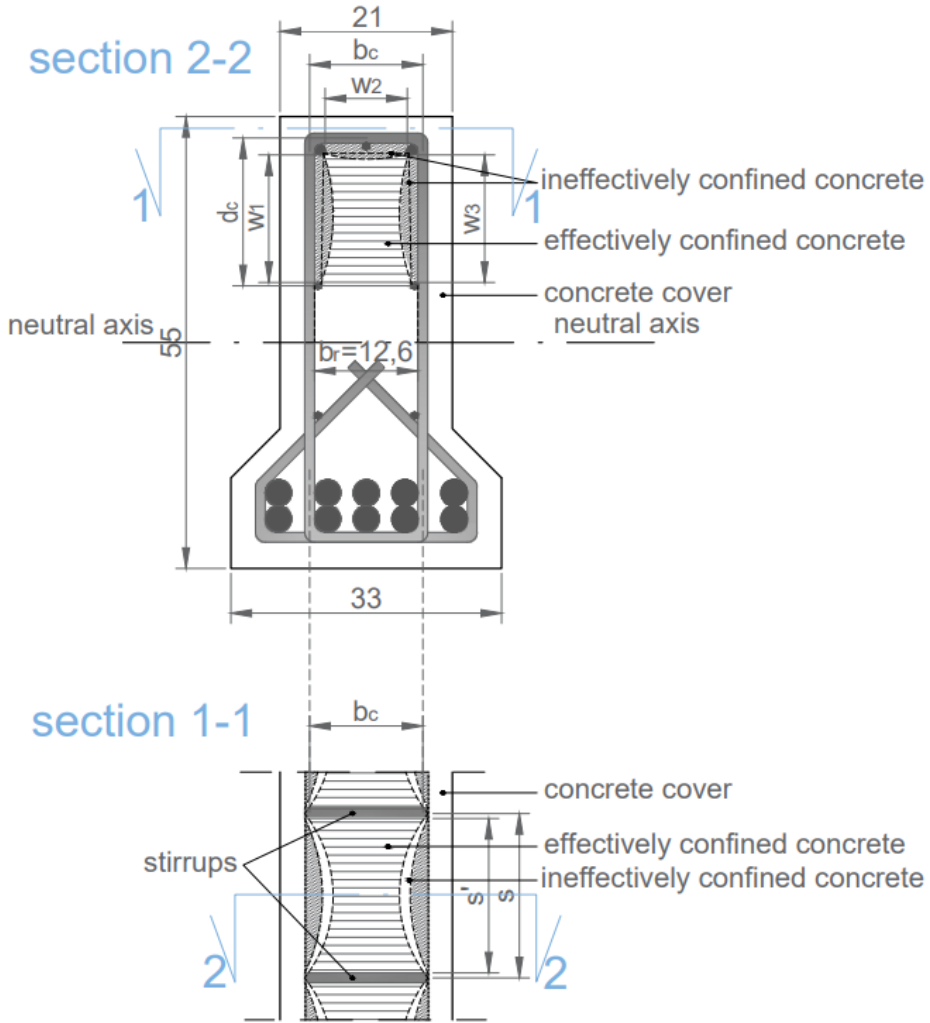


Figure 5.56

After the beam testing it was concluded that the confined concrete area that had been calculated was too large. By inspection of the fracture area, it was decided to exclude the rectangular concrete area below the construction reinforcement. Calculated results obtained from that cross section are in better agreement with experimental results.

Table 5.7: Confined concrete compressive capacity

Beam number	Beam identification	Confined compressive capacity [MPa]	Increase of capacity [%]
1	LWAC65_20_0	65	0
2	LWAC65_20_200	66.8	2.8
3	LWAC65_20_60	89.7	38.1
4	LWAC65_20_100	76.5	17.7
5	LWAC65_20_60	89	36.9
6	LWAC65_20_100	75.9	16.8
7	LWAC65_20_200	68.8	5.8

Table 5.7 shows the confined concrete capacity calculated without the lower rectangular part. The calculations are given in appendix C.4.

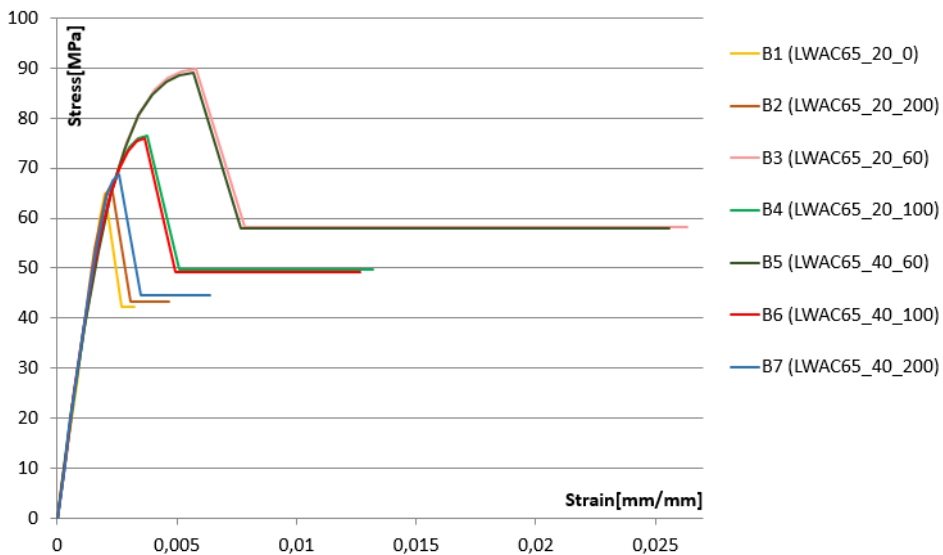
**Figure 5.57:** Updated calculated stress-strain curves for all the tested beams

Figure 5.57 shows the updated stress-strain curves for all the tested beams. When compared to Figure 4.16 it can be observed that the maximum stresses are reduced.

Chapter 6

Discussion

The following chapter will be a discussion of the results presented in chapter 5. All the parameters varied in the testing will be discussed separately. The parameters that were varied in this test were stirrup spacing, size of concrete cover and amount of compressive reinforcement. The results will also be compared with earlier experimental work.

6.1 Stirrup Spacing

Confinement can be described as a set of parameters improving concrete utilization. Stirrup spacing is one of these parameters. According to the model presented in chapter 3, the concrete will be more confined when the free distance between the stirrups is reduced. From Figure 3.1, confinement leads to failure at both higher stress and strain level. EC2 states that increased confinement leads to increased ductility [26].

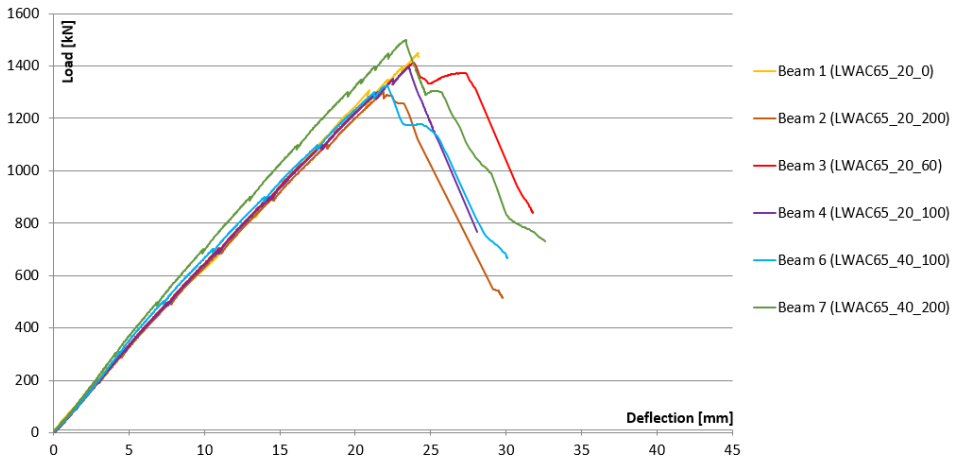


Figure 6.1: Load-deflection curves for all the beams

Figure 6.1 shows the load-deflection curves for all the beams at midspan. Table 6.1 shows deflections at midspan at first and second peak and the difference between them. Beam 1 only reached one peak as the failure was brittle and explosive. Beam 2 showed a certain ductile behaviour and reached a small second peak. Beam 3 had the most ductile behaviour and the largest increase in loading between peak one and two. Beam 4 showed a slow failure that cannot be defined as ductile as there was no inelastic deflection without strength loss. Beam 6 showed a ductile failure and a displacement plateau. Beam 7 showed a ductile failure and the largest load difference between first and second peak.

As beam 1 had no stirrups between the loading points, a brittle failure was expected. As beam 2 had large stirrup spacing, the ductility should only be slightly increased or not affected at all. Beam 3 was expected to be the most ductile as the stirrup spacing was small. Beam 1, 2 and 3 showed expected results. After testing beam 2 and 3, beam 4 was expected to show a ductile behaviour that was superior to beam 2 and inferior to beam 3. Beam 4 did not show ductile behaviour, but the capacity was larger than in beam 2. Beam 6, on the other hand, showed the behavior expected of beam 4. The only difference between beam 4 and 6 was the concrete cover. Even though they had the same stirrup spacing, they did not show the same ductile behaviour. Beam 7 also showed ductile behaviour and had the largest capacity due to the largest compressive reinforcement. From experimental investigation regarding the stirrup spacing, beams with smaller stirrup spacing showed more ductile behaviour.

Table 6.1: Deflections at peaks and deflection plateaus

Beam number	Beam identification	Defl. at midspan			Avg. defl. under load		
		$\delta_{M,1}$ [mm]	$\delta_{M,2}$ [mm]	$\delta_{M,2} - \delta_{M,1}$ [mm]	$\delta_{P,1}$ [mm]	$\delta_{P,2}$ [mm]	$\delta_{P,2} - \delta_{P,1}$ [mm]
1	LWA65_20_0	24,2	-	-	21,9	-	-
2	LWA65_20_200	22,1	23,1	1	19,7	20,8	1,1
3	LWA65_20_60	23,9	27,2	3,3	21,3	23,9	2,6
4	LWA65_20_100	23,6	-	-	20,7	-	-
6	LWA65_40_100	22,2	24,4	2,2	20,2	21,8	1,6
7	LWA65_40_200	23,4	25,4	2	21,5	22,7	1,2

From Table 6.1 it can be observed that the difference in deflections at midspan and at the loading points ranges from 1.0-3.3 mm between peak one and peak two. When looking at how much the deflections change between peak one and peak two, while comparing the midspan point to the loading points, the values represent high curvature for just one meter. It can be observed that beam 3, 6 and 7 have larger differences compared to beam 2. Increased curvature indicates increased ductility.

6.2 Concrete Cover

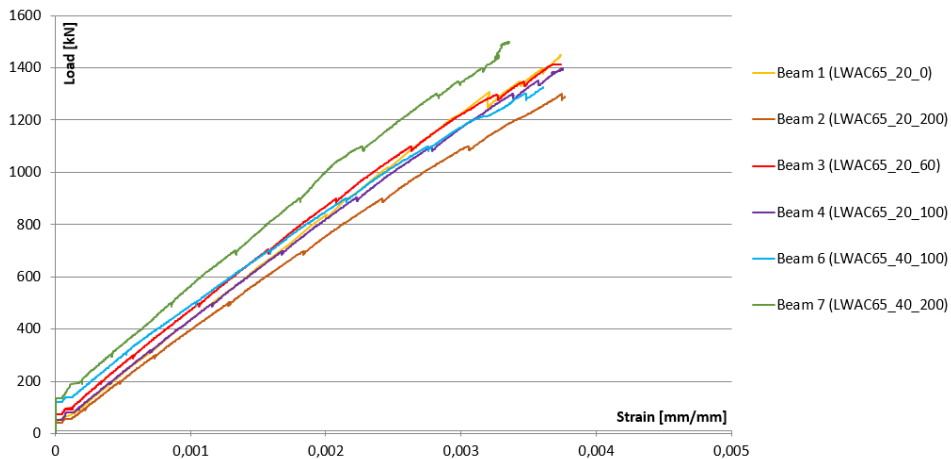
**Figure 6.2:** Load-average top strain curves for all the beams

Figure 6.2 shows the load-average top strain curves for all the beams. Equal strain levels for beam 1-4 can be observed at peak one. The strain levels observed for beam 6 and 7 were lower than for beam 1-4. This indicates that beams with concrete cover 40 mm spalled at a lower strain level. In Figure 6.1 we can observe a larger drop for the load

between peak one and two for beam 6 and 7. This was due to smaller remaining cross section after spalling. The reduction of the cross section led to a smaller internal moment arm for the remaining cross section. Generally, the confined concrete area becomes smaller by increasing the size of the concrete cover. This implies that increase of concrete cover reduces ductility.

Table 6.2 shows experimental values of the strains at peak one on the top surface of the beams at midspan. These values are far larger than allowed maximum concrete strain used in the calculations given in appendix C.1 and C.4. The maximum allowed concrete compressive strains for this type of concrete is 2.52 ‰ according to EC2 [26]. Table 6.2 shows how the measured maximum strains are 1.3-1.5 times larger than the allowed maximum strain.

Table 6.2: Maximum concrete compressive strains on the top surface

Beam number	Beam Identification	Maximum strains [‰]		Average concrete compressive strain [‰]
		LVDT-top-W	LVDT-top-E	
1	LWAC65_20_0	3,70	3,74	3,72
2	LWAC65_20_200	3,78	3,75	3,77
3	LWAC65_20_60	3,84	3,64	3,74
4	LWAC65_20_100	3,70	3,67	3,69
6	LWAC65_40_100	3,53	3,61	3,57
7	LWAC65_40_200	3,10	3,49	3,30

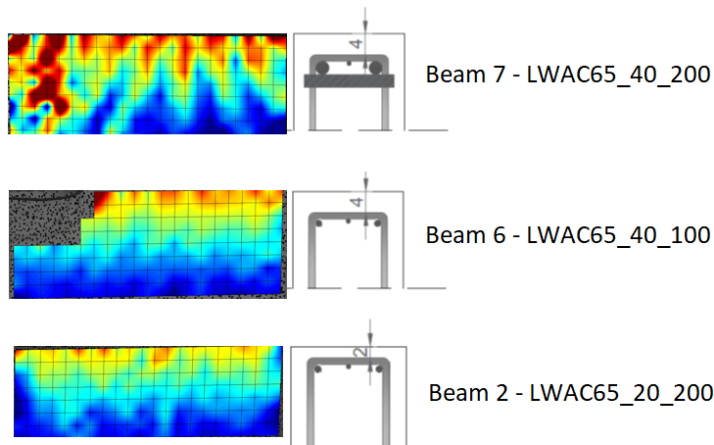


Figure 6.3: DIC-pictures of max strain longitudinally with accompanying cross sections

Figure 6.3 shows the compressive zone of beam 2, 6 and 7. Larger strains closer to the neutral axis and larger strains in concentrated areas were measured in beam 6 compared

to beam 2. Beam 7 shows the largest strains in concentrated areas and the largest strains closest to the neutral axis. This contradicts the average top strains measured from LVDTs.

6.3 Amount of Compressive Reinforcement

Compressive reinforcement is one of the confinement parameters. As the compressive bar gets larger, the distance between the longitudinal bars gets smaller. According to the model presented in chapter 3, this will increase the effectively confined concrete area. This further implies that increased amount of compressive reinforcement increases ductility.

Beam 7 was more heavily reinforced in the compressive zone than the others. The diameter of the longitudinal compressive reinforcement was doubled and additional transversal reinforcement was placed at each stirrup between the loading points. This reinforcement layout strengthens the compressive zone leading to an increase of the compressive capacity. The largest capacity was measured in beam 7. Even though the tensile reinforcement of this beam did not yield, the largest tensile reinforcement strains were measured in beam 7.

From Figure 6.1 and Table 6.1 it can be observed that beam 7 showed more ductile behaviour than beam 2. This indicates that an increase of the compressive reinforcement increases the ductility.

From Figure 6.3, it can be observed that beam 7 showed larger strains in the compressive zone compared to the other two beams.

6.4 Confinement

Table 6.3: Compressive capacities

Beam number	Beam identification	Compressive capacity based on chap. 3 [MPa]	Compressive capacity from experiment: LVDTs [MPa]*
1	LWAC65_20_0	65	89.9
2	LWAC65_20_200	66.8	91.1
3	LWAC65_20_60	89.7	90.4
4	LWAC65_20_100	76.5	89.2
5	LWAC65_40_60	89	-
6	LWAC65_40_100	75.9	86.3
7	LWAC65_40_200	68.8	79.8

* Calculated using the Young's modulus from Table 5.1 and strains from Table 6.2.

Table 6.3 shows two different ways of calculating the maximum stress in the concrete. It is apparent that there is a difference between the two ways of calculating the maximum stress. The model presented in chapter 3 predicts an increase in compressive capacity

based on the improvements of the confinement parameters. The rightmost column in Table 6.3 is based on calculating the stress from the maximum strain in the concrete based on an assumed Young's modulus at peak one. The model from chapter 3 generally predicts varying maximum stresses with varying confinement parameters. The experimental results show very similar maximum strains and thus similar maximum stresses was calculated.

6.5 Comparison with Previous Experimental Work

Testing of beams with the same reinforcement layout and cross-sectional geometry has previously been conducted [18]. The following section will be a comparison of the trends between the two studies.

Table 6.4: Aggregate, compressive strength and reinforcement layout of compared beams

Beam number	Beam identification	Aggregate	Compressive cube strength [MPa]	Stirrup spacing [mm]	Concrete cover [mm]
-	ND115-12-60*	Coarse aggregate (8-11 mm) (8-16 mm)	108.4**	60	20
-	ND95-12-200*		87.6**	200	20
-	ND95-12-60*		87.6**	60	20
-	LWA75-12-200*	Liapor (4-8 mm)/(8-16 mm)	74.6**	200	20
-	LWA75-12-60*		74.6**	60	20
1	LWAC65_20_0	Stalite (max 12.7 mm)	74.2***	-	20
2	LWAC65_20_200		74.2***	200	20
3	LWAC65_20_60		74.2***	60	20
4	LWAC65_20_100		74.2***	100	20
5	LWAC65_40_60		74.2***	60	40
6	LWAC65_40_100		74.2***	100	40
7	LWAC65_40_200		74.2***	200	40

* Beams tested in previous experimental work[18].

** Mean cube strength from 3 batches at 28 days.

*** Mean cube strength from 1 batch at 28 days.

Table 6.4 shows the compared beams. The table includes the beams with comparable parameters between this and the previous study. The previous experimental study tested 11 beams. Seven beams were tested with two different types of NDC and four beams were tested with LWAC. The NDCs contained coarse aggregate with fractions 8-11 mm and 8-16 mm. The LWAC contained Liapor aggregate of fractions 4-8 mm and 8-16 mm. The compressive strength was 108.4, 87.6 and 74.6 MPa respectively for ND115, ND95 and LWA75. Type of aggregate, compressive strength, stirrup spacing and concrete cover is given in Table 6.4.

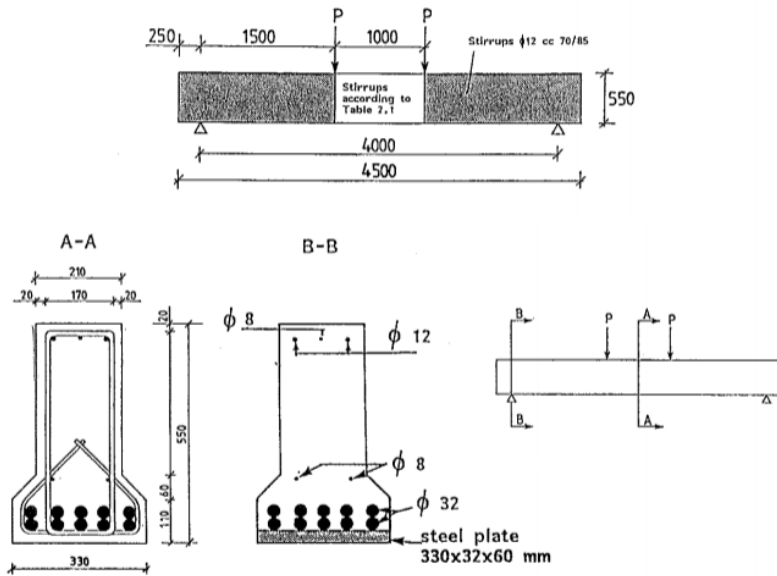


Fig 2.1 Geometry of the overreinforced beams with view of cross section at the mid-section and at the support

The numbering system of the beams is as follows:

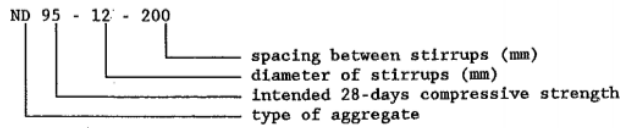


Figure 6.4: Test programme of previous experimental study [18].

Figure 6.4 shows the loading and layout of the beams in the previous experimental study. It is emphasized in this figure how the beam identification numbering system of this and the previous study was different. It can also be seen that the cross-sectional layout, length of the beams and load situation was equal in the two studies.

Table 6.5: Local maximum loads with corresponding deflections for all beams

Beam number	Beam Identification	First peak		Second peak		F_2/F_1	δ_2/δ_1
		Load F_1 [N]	Displacement δ_1 [mm]	Load F_2 [N]	Displacement δ_2 [mm]		
-	ND115-12-60 *	890	17.4	942	27.5	1.06	1.58
-	ND95-12-200 *	745	17.2	718	21.0	0.96	1.22
-	ND95-12-60 *	658	14.9	753	25.3	1.14	1.70
-	LWA75-12-200 *	682	16.9	-	-	-	-
-	LWA75-12-60 *	670	16.9	689	23.6	1.03	1.40
1	LWAC65_20_0	717	24.2	-	-	-	-
2	LWAC65_20_200	645	22.1	629**	23.1	0.98	1.05
3	LWAC65_20_60	707	23.9	687	27.2	0.97	1.14
4	LWAC65_20_100	691	23.6	-	-	-	-
5	LWAC65_40_60	-	-	-	-	-	-
6	LWAC65_40_100	663	22.2	589	24.4	0.89	1.10
7	LWAC65_40_200	742	23.4	653	25.4	0.88	1.09

* Beams tested in previous experimental work[18].

** Small peak.

Table 6.5 shows experimental values of loads and deflections for all the beams at first and second peak. The ratio between peak loads and peak deflections are also given to compare the beams. Two different trends can be observed. The loads at second peak in the previous study were generally larger than the loads at first peak. The beams in the previous study showed load-deflection curves where the beams were able to withstand more loading after the top cover spalled and a load redistribution occurred. The trend is the opposite in this study. None of the beams were able to resist a load level larger than for peak one. Beam 2 and 3 were close with load ratios of 0.98 and 0.97. The other difference observed is in deflections. The relative difference between deflections at peak one and peak two is generally larger in the previous study. It should be mentioned that the actual deflections at peak one are generally larger in this study compared to the previous study. When comparing LWAC65_20_200 to LWA75-12-200 and LWAC65_20_60 to LWA75-12-60, which are the most comparable beams, the capacities are not significantly different.

Table 6.6: Maximum concrete compressive strains on the top surface

Beam numbering	Beam identification	Maximum strains [‰]		Average concrete compressive strain [‰]
		LVDT-top-W	LVDT-top-E	
-	ND115-12-60*	3,42**	3,35**	3,38
-	ND95-12-200*	3,70**	4,00**	3,85
-	ND95-12-60*	2,88**	3,24**	3,06
-	LWA75-12-200*	3,56**	3,37**	3,47
-	LWA75-12-60*	3,20**	3,88**	3,54
1	LWA65_20_0	3,70	3,74	3,72
2	LWA65_20_200	3,78	3,75	3,77
3	LWA65_20_60	3,84	3,64	3,74
4	LWA65_20_100	3,70	3,67	3,69
6	LWA65_40_100	3,53	3,61	3,57
7	LWA65_40_200	3,10	3,49	3,30

* Beams tested in previous experimental work[18].

** Values are measured from strain gauges from previous experimental work[18].

Table 6.6 shows maximum strains measured on the top surface at midspan. These strains correspond to the concrete strains at peak one. It is apparent that the average strains at peak one in this study were generally larger than in the previous study. This is also seen when comparing LWAC65_20_200 to LWA75-12-200 and LWAC65_20_60 to LWA75-12-60. For beams with stirrup spacing 200 mm and concrete cover 20 mm, the strain in this study was 1.09 times larger than in the previous study. For stirrup spacing 60 mm and concrete cover 20 mm, the strain in this study was 1.06 times larger.

Summary and Conclusion

Seven over-reinforced LWAC beams have been tested in this study. Stalite with a fraction 1/2" was used as aggregate in the concrete. All the beams were loaded in a four point bending test. The test was deflection controlled with a loading rate of 1.2 mm/min until failure. The main test parameters were stirrup spacing, size of concrete cover and amount of compressive reinforcement. To find material properties of the LWAC, small specimens were tested. 22 cubes and 8 cylinders were tested from the same batch of concrete as the beams. One of the beams tested was not sufficiently casted and the results of this beam were therefore not analyzed. Four of the remaining six beams showed a ductile behavior. Contrary to the previous experimental study [18], the beams with stirrup spacing 200 mm showed a certain ductile behaviour. Structural LWAC are generally less ductile than NDC. The results indicated that by applying reinforcement in a way that increases the confinement of the concrete, LWAC beams can show ductile behaviour that is similar to NDC beams. Even though EC2 only allows for a maximum strain of 2.52 ‰ for the type of concrete used in this study, the compressive strains measured in all the beams ranged from 3.30-3.77 ‰. This indicates that EC2 underestimates the ultimate compressive strain of LWAC.

- The test results indicate that the beams with reduced stirrup spacing, which increased confinement, led to more ductile behaviour. LWAC65_20_100 (beam 4) was the exception. This beam showed a slow failure that cannot be defined as ductile.
- The main difference in behaviour between the beams with concrete cover 20 and 40 mm was the load drop from first to second peak. When more of the cross section spalled off at peak one, a smaller cross section was left to resist an increase of loading after the redistribution of forces. When the top concrete cover is increased, less of the cross section will generally be confined. A reduction of confinement will generally lead to less ductile behaviour.
- The beam containing the largest compressive reinforcement resisted the largest load. The confinement model presented in chapter 3 indicates that by increasing compressive reinforcement, the distance between each longitudinal bar decreases. This

results in more confinement and therefore increased ductility. By comparing the experimental results for LWAC65_20_200 (beam 2) and LWAC65_40_200 (beam 7), it was indicated that an increase of compressive reinforcement increased the ductility.

- The calculation of maximum stress, based on effectively confined concrete presented in chapter 3, gave varying results depending on the layout of the reinforcement. In the test, there was no measurement of compressive stress. Compressive stresses were calculated from Hooke's law and the average maximum strains measured on the top of the beams. The results from these two methods varied.
- DIC generally shows a detailed picture of a strain field. Localization of strains can be observed from the DIC pictures. LVDTs measure average strains over a given distance. For the beam with the largest compressive reinforcement, strain values measured by DIC and LVDTs varied. Larger strains and localization were measured using DIC, compared to the strain values measured with the LVDTs.
- EC2 has special rules for LWAC. The standard contains reduction factors and special rules that are applied to regular design criterion. The results in this study indicate that EC2 underestimates LWAC, as the recorded maximum strains in the beams were 1.3-1.5 times larger than the allowed maximum strain for this concrete.
- In this and the previous experimental study, beams with stirrup spacing 60 mm showed ductile behaviour. Beams with stirrup spacing 200 mm, in previous experimental work, only showed ductile behaviour for NDC. In this study both beams with stirrup spacing 200 mm and one of the beams with stirrup spacing 100 mm showed ductile behaviour.

Further Study

Considering the experimental results, literature and standards reviewed, it was concluded that some further study should be conducted.

- By using DIC, strain fields of the compressive zones have been measured. This methodology do not require complicated preparation compared to ordinary methodologies (LVDTs and strain gauges). DIC gives more detailed information as it provides a strain field. DIC gives varying strains in multiple dimensions as opposed to LVDTs, which gives an average value over a given distance in one dimension. Based on experience from this study, further investigation of DIC is proposed. Investigations could include DIC software understanding and application of DIC as a measuring device for concrete structures in general.
- Characteristics of LWAC mostly depend on the type of LWA used. EC2 do not differentiate between different types of LWAs used in LWAC. From the experimental results of this study, it is indicated that EC2 underestimates Stalite as an aggregate. Since LWAC showed behavior similar to NDC in this study, investigation of LWAC as a structural material should be continued. The way EC2 treats different types of LWAC should especially be investigated.

Bibliography

- [1] ACI 211.2-91. Standard Practice for Selecting Proportions for Structural LWAC. 1991.
- [2] ACI 304.5R-91. Batching, Mixing and Job Control of Lightweight Concrete. 1991.
- [3] H. Asgeirsson. Hekla Pumice in Lightweight Concrete. *IBRI*, 1994.
- [4] L. Bjerkeli. High-Strength Concrete SP1 Beams and Columns. *Report 1.1 Ductility of Spirall Reinforced Columns. SINTEF Report STF70 A92120*, 1992.
- [5] Y. Bouafia, A. Iddir, M.S. Kachi, and H. Dumontet. Stress Strain Relationship for the Confined Concrete.
- [6] R.W. Castrodale, R. Valum, and K.S. Harmon. High-Performance Lightweight Concrete Bridges and Buildings. 40, 2017.
- [7] R.W. Castrodale, J. Zivkovic, and R. Valum. Material Properties of High Performance Structural Lightweight Concrete. 2017.
- [8] Cembureau. Lightweight Aggregate Concrete - Technology and World Applications. 1974.
- [9] S. Chandra and L. Berntsson. Lightweight Aggregate Concrete. *Noyes Publications*, 2003.
- [10] D.D. Chapman and R.W. Castrodale. Sand Light-Weight Concrete for Prestressed Concrete Girders in Three Washington State Bridges. *Paper 81 Proceedings of the 2016 National Bridge Conference, Nashville. Precast/Prestressed Concrete Institute, Chicago, Ill. 2016. 22 p., 2016 Mar 3-6.*
- [11] Carolina Stalite Company. Structural Applications. *retrieved from: <http://www.stalite.com/applications.php?cat=21>, March 2017.*
- [12] T. Cousins, C. Roberts-Wollmann, and M.C. Brown. High-Performance/High-Strength Lightweight Concrete for Bridge Girders and Decks. *National Cooperative*

Highway Research Program Report 733. Transportation Research Board, Washington, DC., 2013.

- [13] F. Curcio, D. Galetota, A. Gallo, and M. Giammatteo. High-Performance Lightweight Concrete for the Precast Prestressed Concrete Industry. *Proc. 4th. Int. CANMET/ACI/JCI Symposium, To-kushima, Japan, pp. 389-406.*
- [14] EuroLightCon. Lwac Material Properties. *Document BE96-3942/R2*, December 1998.
- [15] T.M. Fayyada and J.M Leesb. Application of Digital Image Correlation to Reinforced Concrete Fracture. *Procedia Materials Science 3 (2014) 1585 1590*, 20th European Conference on Fracture (ECF20), 2014.
- [16] E. Filaj, A. Seranaj, and E. Leka. Confined Concrete Behavior Influencing Factors. *International Research Journal of Engineering and Technology (IRJET)*, 2016.
- [17] CUR Centre for Civil Engineering Research and Codes. Structural Behaviour of Concrete with Course Lightweight Aggregates. *Report 173, Gouda, Netherlands.*
- [18] E.A. Hansen. High-Strength Concrete. *SP1 - Beams and Columns. Report 1.6, Ductility of overreinforced beams*, 1993.
- [19] K.S. Harmon. Engineering Properties of Structural Lightweight Concrete.
- [20] T.M. Jensen and J.A. Øverli. Experimental study on flexural ductility in over-reinforced lightweight aggregate concrete beams. *COIN Project report*, 47, 2013.
- [21] S. Lin. Strain Measurement by Digital Image Correlation. 2015.
- [22] M. Lopez, L.F. Kahn, and K.E. Kurtis. Creep and Shrinkage of High-Performance Lightweight Concrete. *ACI Mater J. 2004;101(5):391-399.*
- [23] C. Lund and J.M. Sakshaug. Konstruktiv oppførsel av høyfast lettbetong. 2016.
- [24] N. McCormick and J. Lord. Digital Image Correlation for Structural Measurements. *ICE institution. Civil Engineering, 165 (CE4)*, pages 185–190, 2012.
- [25] J.B. Newman. Properties of Structural Lightweight Concrete in Structural Lightweight Concrete. pages 19–44, 1993.
- [26] Standard Norge. Eurokode 2: Prosjektering av betongkonstruksjoner.
- [27] American Society of the International Association for Testing and Materials (ASTM International). Standard Test Method for Density, Relative Density (specific gravity), and Absorption of Coarse Aggregate. C127-07:5, 2015.
- [28] P.L. Owens. Lightweight aggregates for Structural Concrete. pages 1–18, 1993.
- [29] J. Punkki and O.E. GjØrv. Effect of Water Absorption by Aggregate on Properties of High- Strength Lightweight Concrete. *CEB/FIP International Symposium on Structural Lightweight Ag- gregate Concrete, Sandefjord, Norway, pp 604-616. Editors: I. Holand et al., 1995.*

-
- [30] M. Rønne, T.A. Hammer, H. Justnes, I.S. Meland, V. Jensen, and S. Smeplass. Chemical Stability of LWAC Exposed to High Hydration Generated Temperatures. *CEB/FIP International Symposium on Structural Lightweight Aggregate, Sandefjord, Norway, pp 505-516. Editors: I.Holand, et al.*
- [31] M. Sargin. Stress-strain relationship for concrete and analysis of structural concrete sections. *PHD Thesis, University of Waterloo, Ontario, Canada, 1968.*
- [32] S. Smeplass. Mechanical Properties - Lightweight Concrete. *High Strength Concrete. SP4 - Materials Design, SINTEF, 1992.*
- [33] J. Spitzner. A Review of the Development of Lightweight Aggregate - History and Actual Survey. *CEB/FIP International Symposium on Structural Lightweight Aggregate Concrete, Sandefjord, Norway, pp 13-21. Editors: I. Holand, et al., 1995.*
- [34] S.I. Srensen. Betongkonstruksjoner, beregning og dimensjonering etter Eurokode 2. (2), 2013.
- [35] E. Thorenfeldt. Design Criteria of Lightweight Aggregate Concrete. *CEB/FIP International Symposium on Structural Lightweight Aggregate, Sandefjord, Norway, pp 244-255. Editors: I.Holand, et al.*
- [36] Dossier Técnico. Hormigones Ligeros Estructurales. 1997.
- [37] J.A. den Uijl, J. Stroband, and J.C. Walraven. Splitting Behavior of Lightweight Concrete. *CEB/FIP International Symposium on Structural Lightweight Aggregate, Sandefjord, Norway, pp 154-163. Editors: I.Holand, et al, 1995.*
- [38] https://en.wikipedia.org/wiki/Stolma_Bridge. April 2017.
- [39] <https://www.leca.no/om-leca/produksjon/>. March 2017.
- [40] <https://www.leca.no/produkter/leca-kuler/>. March 2017.
- [41] http://www.engineersedge.com/beam_bending/beam_bending4.htm. May 2017.
- [42] <http://www.kastell-pro.com/liapor-werkstoff.html>. April 2017.
- [43] http://www.weber.dk/fileadmin/user_upload/leca_com/greenroof/. April 2017.
- [44] M.H. Zhang and O.E. GjØrv. Properties of high-strength lightweight concrete. *CEB/FIP International Symposium on Structural Lightweight Aggregate, Sandefjord, Norway, pp 683-693. Editors: I.Holand, et al, 1995.*

Appendix **A**

Reinforcement Layout

A.1 Technical Drawings of Beams

BEAM 1
(without stirrups, concrete cover 20mm)

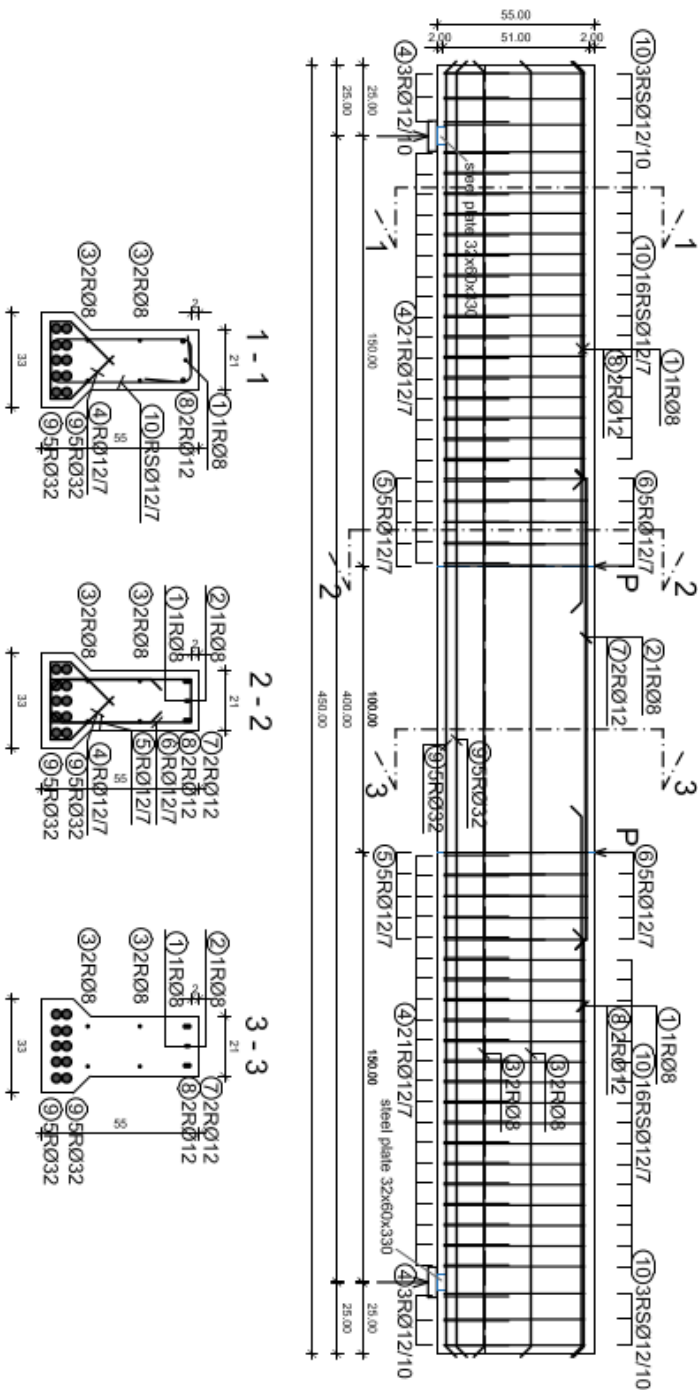


Figure A.1: Beam 1 - Reinforcement layout.

BEAM 2
 (stirrups distance 200mm, concrete cover 20mm)

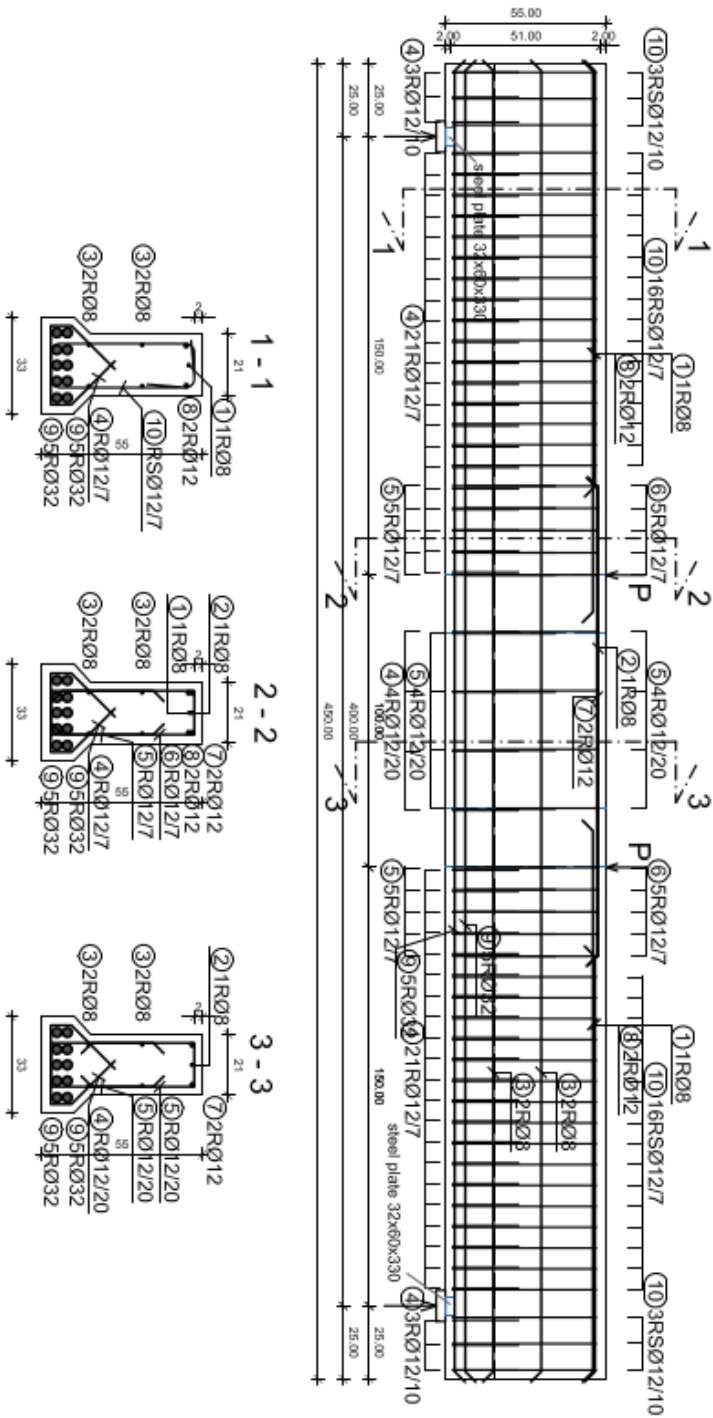


Figure A.2: Beam 2 - Reinforcement layout.

BEAM 3
 (stirrups distance 60mm, concrete cover 20mm)

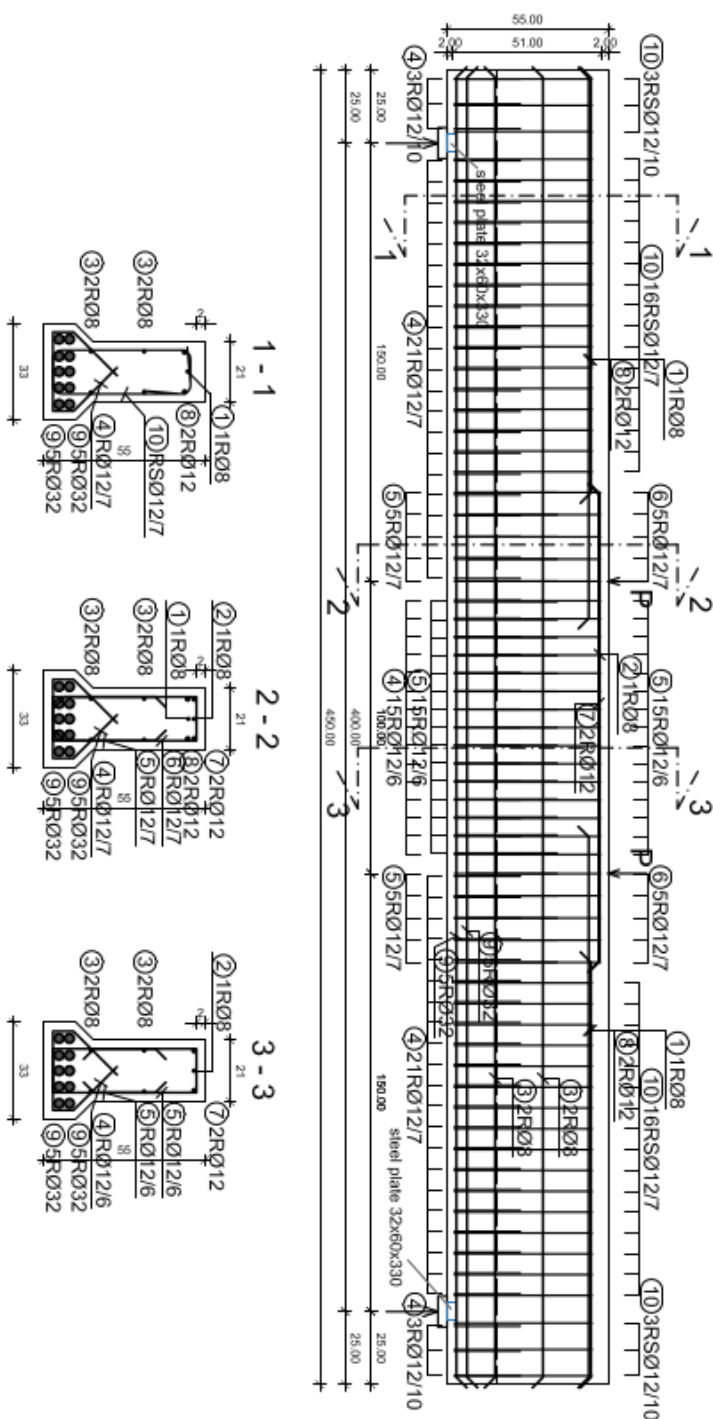


Figure A.3: Beam 3 - Reinforcement layout.

BEAM 4
 (stirrups distance 100mm, concrete cover 20mm)

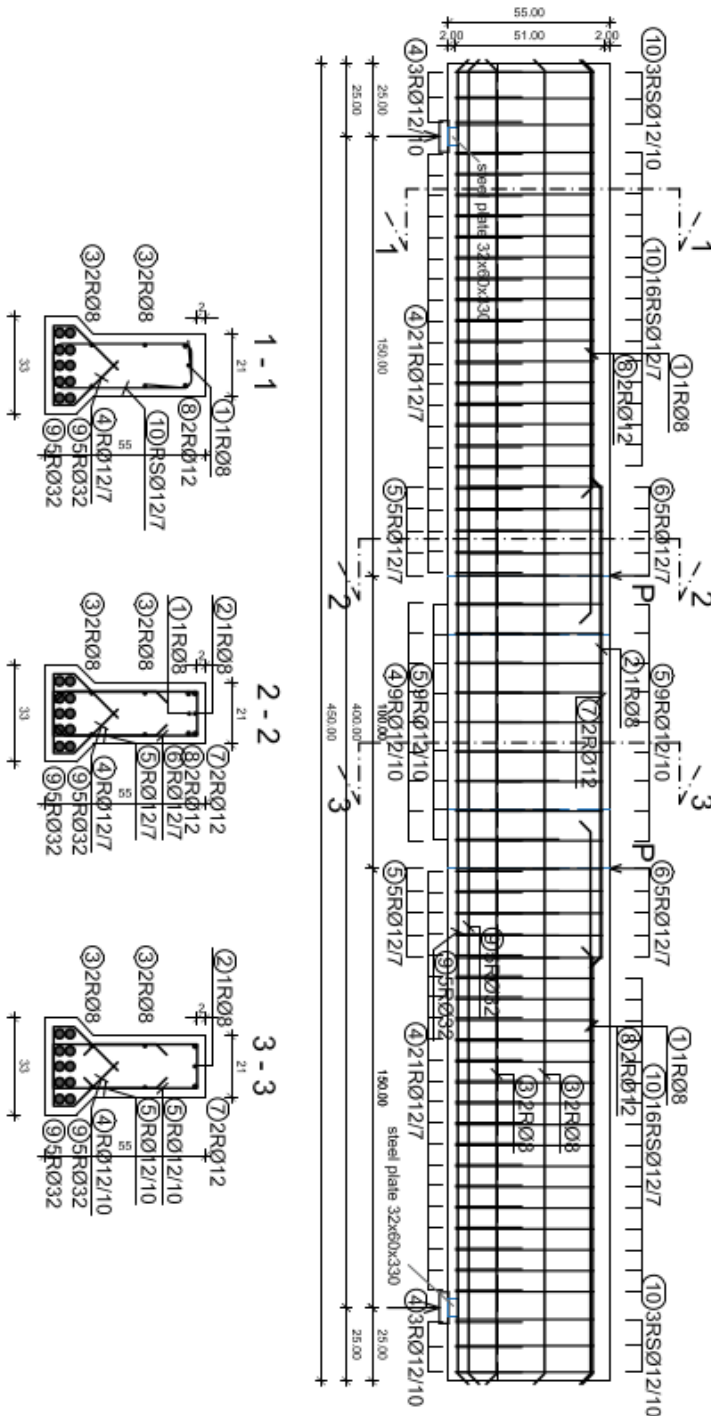


Figure A.4: Beam 4 - Reinforcement layout.

BEAM 5
 (stirrups distance 60mm, concrete cover 40mm)

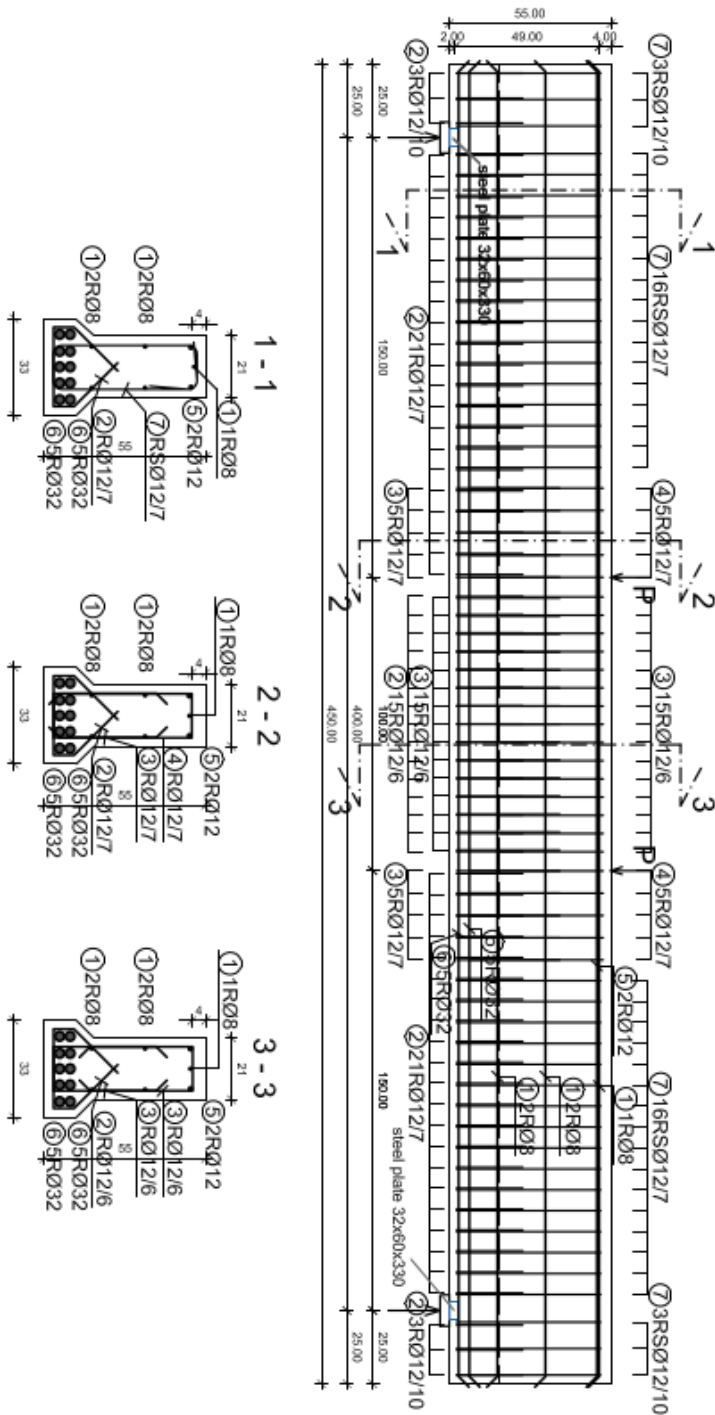


Figure A.5: Beam 5 - Reinforcement layout.

BEAM 6
 (stirrups distance 100mm, concrete cover 40mm)

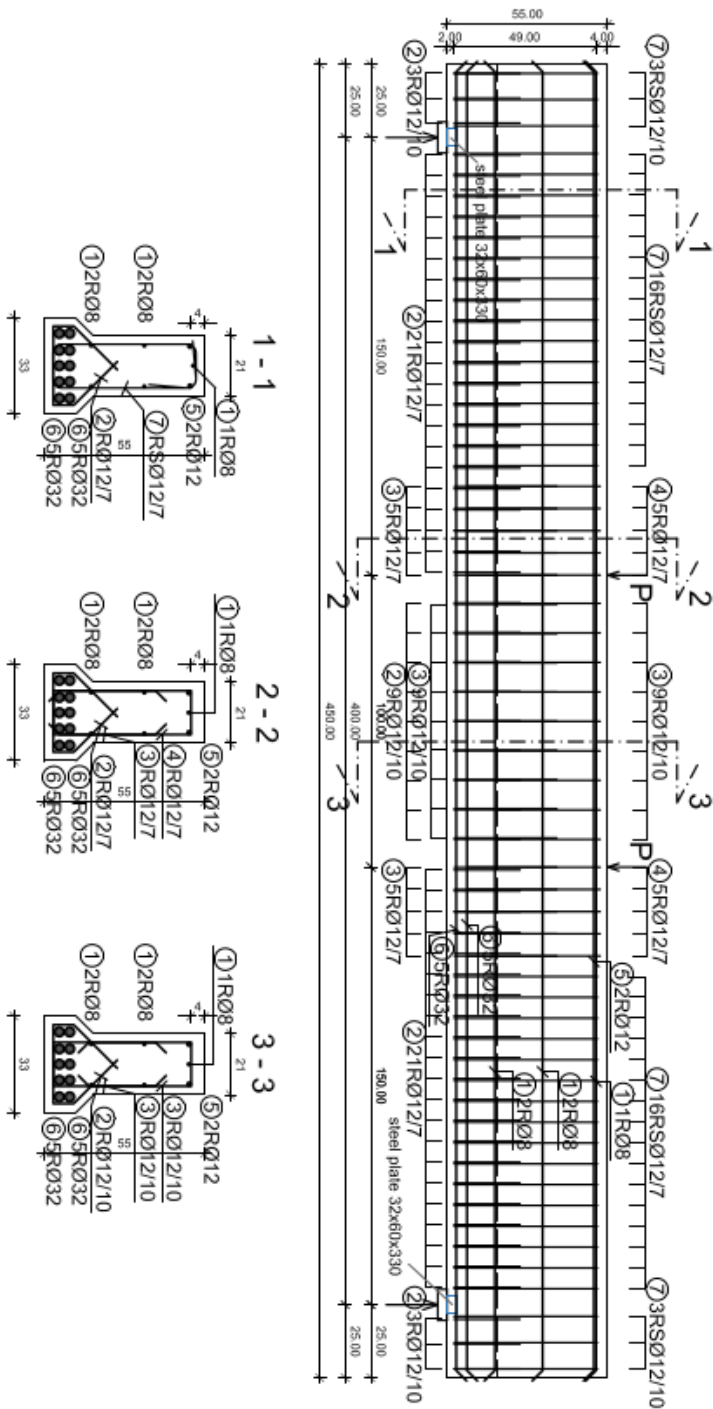


Figure A.6: Beam 6 - Reinforcement layout.

BEAM 7
 (stirrups distance 200mm, concrete cover 40mm)

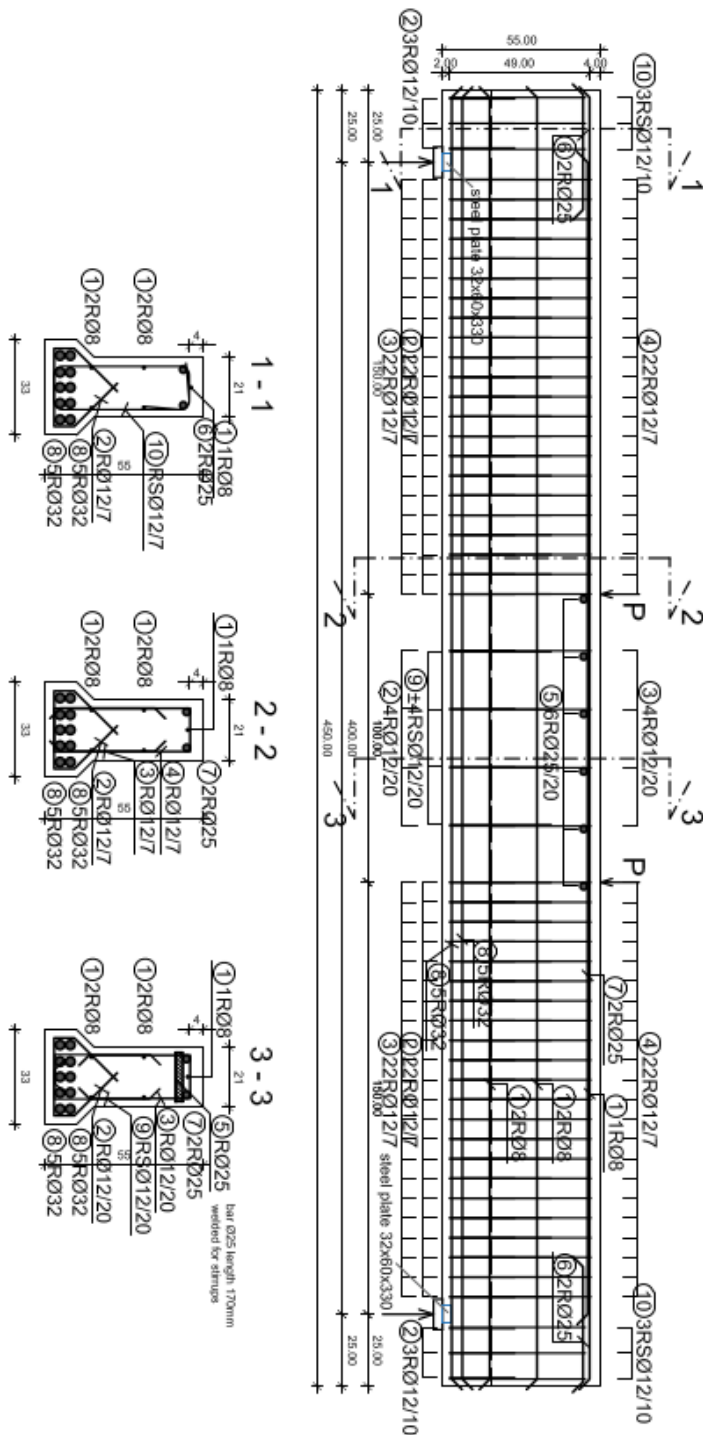


Figure A.7: Beam 7 - Reinforcement layout.




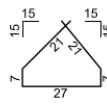
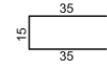
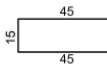

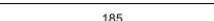


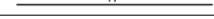
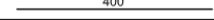
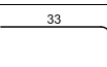
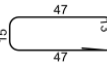
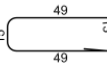

Bars-specification					
no	shape and dimensions (mm)	ø	l ₀ (m)	n (Barrs)	lgn (m)
BEAMS 1-7 (7 pcs.)					
1		8	1.42	8	11.36
2		8	1.60	4	6.40
3		8	4.45	31	137.95
4		12	0.83	394	327.02
5		12	0.85	212	180.20
6		12	1.05	104	109.20
7		12	1.60	8	12.80
8		12	1.85	16	29.60
9		12	4.45	4	17.80
10		25	0.17	6	1.02
11		25	4.00	2	8.00
12		32	4.45	70	311.50
13		12	0.43	8	3.44
14		12	1.50	82	123.00
15		12	1.54	152	234.08
16		25	0.40	4	1.60
Bars-recapitulation					
ø (mm)	lgn (m)	Unit weight (kg/m)	Weight (kg)		
S500					
8	155.71	0.40	61.51		
12	1037.14	0.89	923.05		
25	10.62	3.85	40.89		
32	311.50	6.31	1965.56		
Total (S500)				2991.01	
Total				2991.01	

Figure A.8: Recapitulation of total reinforcement for all beams.

A.2 Documentation of Cover and Spacing

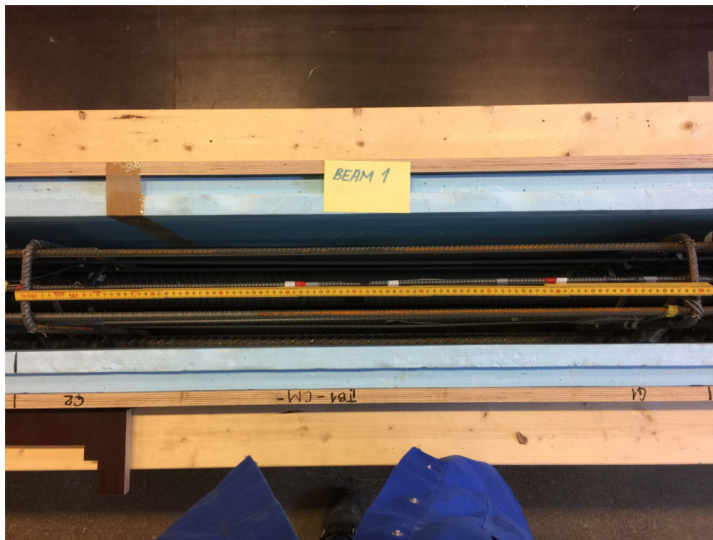


Figure A.9: Beam 1 - Stirrup spacing



Figure A.10: Beam 1 - Concrete cover



Figure A.11: Beam 2 - Stirrup spacing

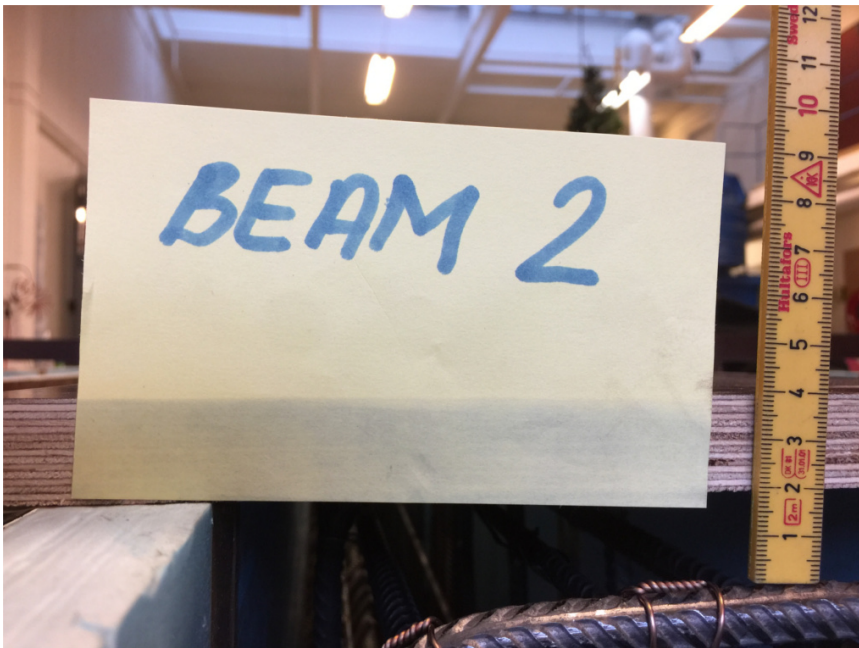


Figure A.12: Beam 2 - Concrete cover



Figure A.13: Beam 3 - Stirrup spacing

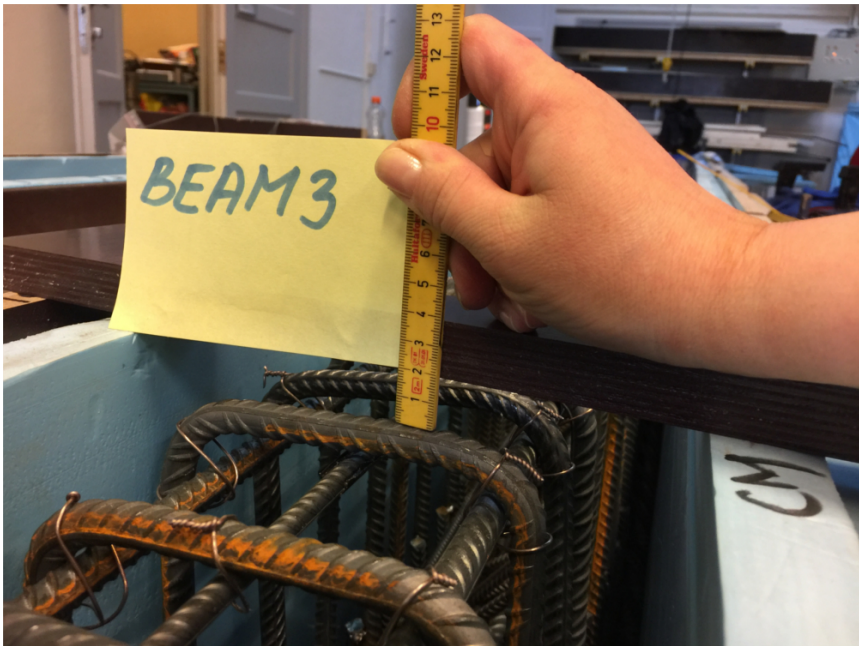


Figure A.14: Beam 3 - Concrete cover



Figure A.15: Beam 4 - Stirrup spacing

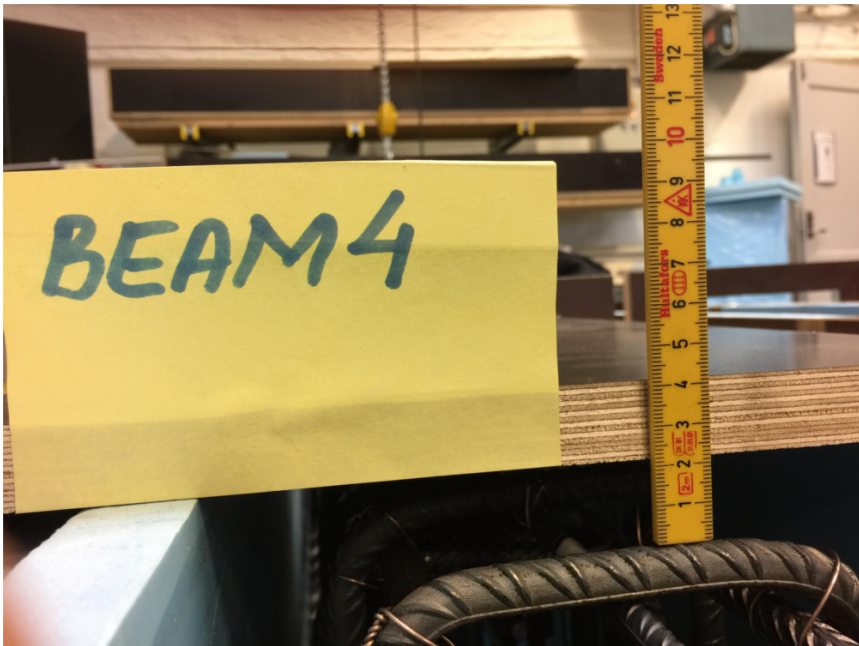


Figure A.16: Beam 4 - Concrete cover



Figure A.17: Beam 5 - Stirrup spacing



Figure A.18: Beam 5 - Concrete cover



Figure A.19: Beam 6 - Stirrup spacing

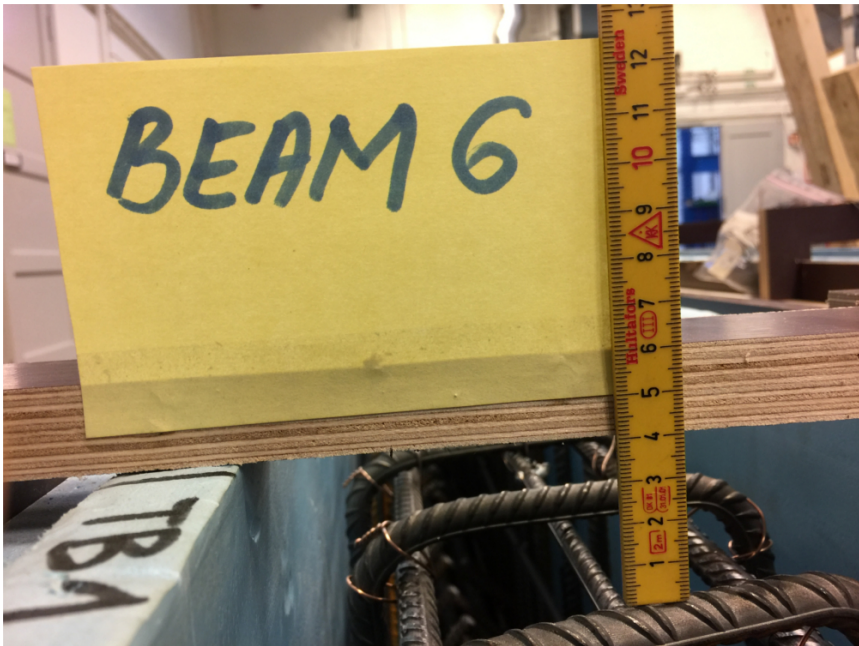


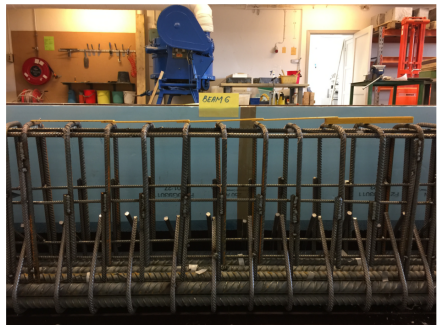
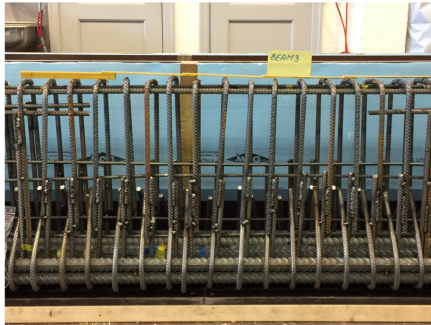
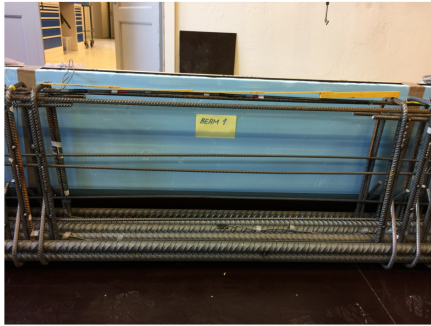
Figure A.20: Beam 6 - Concrete cover



Figure A.21: Beam 6 - Stirrup spacing



Figure A.22: Beam 7 - Concrete cover





Appendix **B**

Results

B.1 Beam Testing

Table B.1: Beam 1 - Steps, loads, deflections and strains

Step	1	2	3	4	5	6	7	8	9	10	11	Max	Failure
Load [kN]	100	200	300	500	700	900	1100	1200	1300	1350	1400	1448	1434
LVDT-M [mm]	1,52	2,91	4,29	7,50	11,08	14,50	17,93	20,00	21,45	22,2	23,17	24,17	24,18
LVDT-2 [mm]	1,41	2,69	3,96	6,91	10,21	13,40	16,54	18,46	19,23	19,91	20,8	21,7	21,69
LVDT-1 [mm]	1,22	2,49	3,75	6,66	9,92	13,04	16,16	18,08	19,67	20,34	21,23	22,14	22,15
LVDT-CW [% ϵ]	0	0,23	0,41	0,83	1,27	1,64	2,09	2,37	2,84	2,96	3,12	3,29	3,27
LVDT-TW [% ϵ]	0,01	0,23	0,39	0,66	1,0	1,36	1,66	1,84	1,70	1,75	1,79	1,83	1,82
LVDT-top-W [% ϵ]	0,13	0,34	0,57	1,08	1,61	2,13	2,67	3,01	3,21	3,35	3,53	3,72	3,70
LVDT-top-E [% ϵ]	0,18	0,43	0,68	1,22	1,77	2,34	2,92	3,29	3,41	3,53	3,69	3,76	3,74
LVDT-TE [% ϵ]	0,12	0,21	0,30	0,51	0,82	1,09	1,39	1,56	1,74	1,82	1,93	2,04	2,04
SG-C1 [% ϵ]	0,2	0,41	0,63	1,12	1,61	2,14	2,72	3,06	3,07	3,17	3,24	3,30	3,27
SG-C2 [% ϵ]	0,19	0,39	0,59	1,04	1,51	1,98	2,48	2,84	2,97	3,02	3,15	3,34	3,49
SG-CM [% ϵ]	0,19	0,39	0,59	1,03	1,48	1,93	2,40	2,80	-	-	-	-	-
SG-TB1 [% ϵ]	-	-	-	-	-	-	-	-	-	-	-	-	-
SG-TB2 [% ϵ]	-	-	-	-	-	-	-	-	-	-	-	-	-
SG-TT [% ϵ]	0,07	0,14	0,23	0,43	0,64	0,83	1,03	1,13	1,22	1,27	1,32	1,37	1,36

Table B.2: Beam 2 - Steps, loads, deflections and strains

Step Load [kN]	1 100	2 200	3 300	4 500	5 700	6 900	7 1100	Max 1300	Failure 1259
LVDT-M [mm]	1,57	3,11	4,61	7,77	11,17	14,65	18,14	21,88	23,06
LVDT-2 [mm]	1,30	2,65	3,93	6,67	9,67	12,76	15,94	19,31	20,08
LVDT-1 [mm]	1,39	2,72	4,02	6,81	9,89	13,01	16,25	19,68	20,77
LVDT-CW [% ₀₀]	0,24	0,45	0,66	1,09	1,55	2,03	2,54	3,11	-
LVDT-TW [% ₀₀]	0,09	0,14	0,25	0,52	0,79	1,04	1,36	1,63	1,75
LVDT-top-W [% ₀₀]	0,2	0,45	0,70	1,23	1,80	2,39	3,05	3,77	-
LVDT-top-E [% ₀₀]	0,25	0,51	0,78	1,33	1,88	2,45	3,05	3,73	-
LVDT-TE [% ₀₀]	0	0,17	0,27	0,52	0,83	1,12	1,41	1,71	1,80
SG-C1 [% ₀₀]	0,20	0,42	0,64	1,10	1,59	2,07	2,65	3,55	3,51
SG-C2 [% ₀₀]	0,19	0,37	0,58	1,02	1,50	1,66	2,18	2,92	-
SG-CM [% ₀₀]	0,20	0,42	0,65	1,11	1,60	2,02	2,61	-	-
SG-TB1 [% ₀₀]	0,10	0,23	0,36	0,68	0,99	1,37	1,63	1,95	2,03
SG-TB2 [% ₀₀]	0,10	0,24	0,37	0,68	0,99	1,37	1,65	1,97	2,05
SG-TT [% ₀₀]	0,08	0,17	0,26	0,54	0,76	1,05	1,24	1,46	1,48

Table B.3: Beam 3 - Steps, loads, deflections and strains

Step Load [kN]	1 100	2 200	3 300	4 500	5 700	6 900	7 1100	8 1300	Max 1414	Failure 1373
LVDT-M [mm]	1,59	3,01	4,47	7,59	10,91	14,27	17,79	21,42	23,89	27,18
LVDT-2 [mm]	1,35	2,55	3,79	6,49	9,46	12,46	15,63	18,89	21,08	23,65
LVDT-1 [mm]	1,41	2,68	3,99	6,77	9,75	12,79	15,99	19,29	21,52	24,21
LVDT-CW [% ₀₀]	0,18	0,38	0,60	1,04	1,50	1,97	2,48	3,06	3,55	20,73
LVDT-TW [% ₀₀]	0,08	0,28	0,51	0,97	1,37	1,72	2,01	2,31	2,47	3,00
LVDT-top-W [% ₀₀]	0,10	0,32	0,56	1,05	1,55	2,06	2,62	3,31	3,84	18,10
LVDT-top-E [% ₀₀]	0,15	0,37	0,60	1,09	1,58	2,10	2,64	3,22	3,64	0,40
LVDT-TE [% ₀₀]	0,16	0,28	0,40	0,68	0,94	1,21	1,48	1,75	1,96	2,04
SG-C1 [% ₀₀]	-	-	-	-	-	-	-	-	-	-
SG-C2 [% ₀₀]	0,19	0,38	0,59	1,03	1,51	2,00	2,55	3,49	-	-
SG-CM [% ₀₀]	0,21	0,41	0,63	1,07	1,53	2,00	2,51	2,85	3,23	-
SG-TB1 [% ₀₀]	0,08	0,20	0,34	0,67	0,98	1,29	1,60	1,92	2,13	2,41
SG-TB2 [% ₀₀]	-	-	-	-	-	-	-	-	-	-
SG-TT [% ₀₀]	0,09	0,17	0,27	0,53	0,74	0,96	1,18	1,40	1,53	1,60

Table B.4: Beam 4 - Steps, loads, deflections and strains

Step	1	2	3	4	5	6	7	8	Max	Failure
Load [kN]	100	200	300	500	700	900	1100	1300	1400	1381
LVDT-M [mm]	1,62	3,04	4,51	7,67	11,01	14,38	17,85	21,49	23,58	23,63
LVDT-2 [mm]	1,23	2,43	3,89	6,81	9,54	12,31	15,31	18,54	20,34	20,31
LVDT-1 [mm]	1,37	2,60	3,87	6,65	9,63	12,66	15,83	19,15	21,05	21,10
LVDT-CW [‰]	0	0,26	0,46	0,87	1,30	1,75	2,24	2,77	3,10	2,97
LVDT-TW [‰]	0,18	0,3	0,46	1,14	1,71	2,26	2,84	3,40	3,67	3,63
LVDT-top-W [‰]	0,21	0,44	0,68	1,18	1,70	2,24	2,82	3,44	3,82	3,64
LVDT-top-E [‰]	0,15	0,39	0,64	1,15	1,67	2,19	2,75	3,32	3,69	3,70
LVDT-TE [‰]	0,13	0,26	0,39	0,66	0,92	1,17	1,45	1,77	1,96	1,99
SG-C1 [‰]	0,19	0,39	0,61	1,07	1,53	2,00	2,52	3,22	3,81	3,81
SG-C2 [‰]	0,18	0,37	0,57	0,99	1,44	1,90	2,40	2,93	-	-
SG-CM [‰]	0,18	0,37	0,57	1,00	1,44	1,89	2,38	-	-	-
SG-TB1 [‰]	0,09	0,21	0,35	0,67	0,99	1,30	1,60	1,92	2,08	2,08
SG-TB2 [‰]	0,09	0,21	0,35	0,67	0,98	1,28	1,59	1,91	2,08	2,07
SG-TT [‰]	0,07	0,15	0,25	0,47	0,70	0,92	1,14	1,37	1,48	1,48

Table B.5: Beam 6 - Steps, loads, deflections and strains

Step	1	2	3	4	5	6	7	8	Max	Failure
Load [kN]	100	200	300	500	700	900	1100	1300	1327	1178
LVDT-M [mm]	1,60	3,01	4,30	7,27	10,56	14,00	17,52	21,29	22,15	24,35
LVDT-2 [mm]	1,34	2,56	3,76	6,53	9,59	12,74	15,91	19,28	20,01	21,59
LVDT-1 [mm]	1,30	2,54	3,73	6,53	9,61	12,80	16,06	19,55	20,36	22,06
LVDT-CW [‰]	0,11	0,26	0,44	0,85	1,28	1,73	2,20	2,73	2,81	-
LVDT-TW [‰]	0	0,23	0,35	0,68	0,92	1,15	1,39	1,64	1,67	1,98
LVDT-top-W [‰]	0	0,29	0,54	1,08	1,66	2,26	2,89	3,58	3,69	-
LVDT-top-E [‰]	0	0,24	0,46	0,97	1,50	2,05	2,61	3,37	3,53	-
LVDT-TE [‰]	0	0,22	0,37	0,78	1,11	1,47	1,82	2,16	2,24	2,21
SG-C1 [‰]	0,18	0,37	0,56	0,99	1,44	1,91	2,42	3,18	3,41	-
SG-C2 [‰]	0,16	0,36	0,55	0,98	1,43	1,90	2,41	3,35	3,93	3,80
SG-CM [‰]	0,14	0,35	0,54	0,98	1,43	1,89	2,38	3,14	3,45	-
SG-TB1 [‰]	0,14	0,25	0,37	0,68	0,99	1,31	1,62	1,94	2,01	2,18
SG-TB2 [‰]	0,13	0,25	0,38	0,70	1,02	1,34	1,66	1,98	2,04	2,16
SG-TT [‰]	0,10	0,18	0,26	0,46	0,68	0,92	1,13	1,34	1,37	1,32

Table B.6: Beam 7 - Steps, loads, deflections and strains

Step	1	2	3	4	5	6	7	8	9	10	11	Max	Failure
Load [kN]	100	200	300	500	700	900	1100	1300	1350	1400	1450	1500	1306
LVDT-M [mm]	1,42	2,76	4,07	6,90	9,92	13,01	16,18	19,48	20,42	21,31	22,22	23,38	24,57
LVDT-2 [mm]	1,30	2,53	3,72	6,30	9,02	11,80	14,61	17,53	18,34	19,11	19,90	20,90	21,21
LVDT-1 [mm]	1,39	2,69	3,94	6,63	9,46	12,35	15,30	18,36	19,23	20,05	20,90	21,98	22,92
LVDT-CW [% ϵ]	0,16	0,35	0,54	0,95	1,36	1,79	2,23	2,70	2,85	2,97	3,14	3,23	-
LVDT-TW [% ϵ]	0,11	0,24	0,37	0,68	0,98	1,27	1,56	1,87	1,95	2,04	2,12	2,18	2,23
LVDT-top-W [% ϵ]	0	0,25	0,47	0,92	1,40	1,87	2,32	2,89	3,07	3,26	3,35	3,25	-
LVDT-top-E [% ϵ]	0	0,12	0,34	0,79	1,26	1,73	2,22	2,74	2,89	3,05	3,21	3,46	-
LVDT-TE [% ϵ]	0	0,26	0,54	0,96	1,33	1,72	2,11	2,48	2,52	2,68	2,78	2,93	3,14
SG-C1 [% ϵ]	0,17	0,35	0,55	0,95	1,37	1,81	2,29	2,95	-	-	-	-	-
SG-C2 [% ϵ]	0,14	0,30	0,45	0,77	1,09	1,42	1,73	2,09	2,29	2,38	2,50	2,49	2,20
SG-CM [% ϵ]	0,14	0,32	0,51	0,88	1,27	1,67	2,08	2,57	2,73	3,04	3,26	3,45	3,53
SG-TB1 [% ϵ]	0,15	0,26	0,39	0,69	0,99	1,29	1,59	1,89	1,97	2,04	2,12	2,22	2,35
SG-TB2 [% ϵ]	0,24	0,39	0,52	0,75	0,92	1,06	1,21	1,38	1,42	1,46	1,51	1,56	1,62
SG-TT [% ϵ]	0,07	0,15	0,26	0,50	0,73	0,96	1,19	1,42	1,48	1,54	1,60	1,67	1,54

B.2 Crack Development



Figure B.1: Beam 1 - Setup 1 - Load steps with drawn crack development.

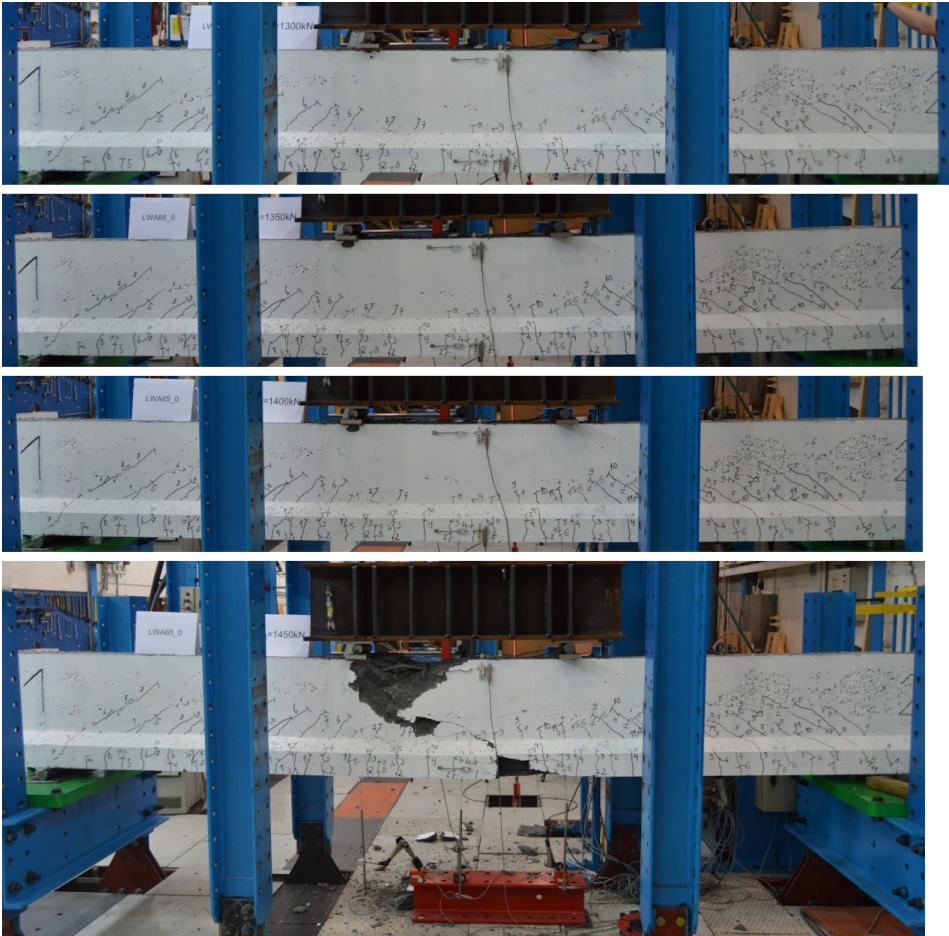


Figure B.2: Beam 1 - Setup 2 - Load steps with drawn crack development.



Figure B.3: Beam 2 - Load steps with drawn crack development.



Figure B.4: Beam 3 - Load steps with drawn crack development.



Figure B.5: Beam 4 - Load steps with drawn crack development.



Figure B.6: Beam 6 - Load steps with drawn crack development.

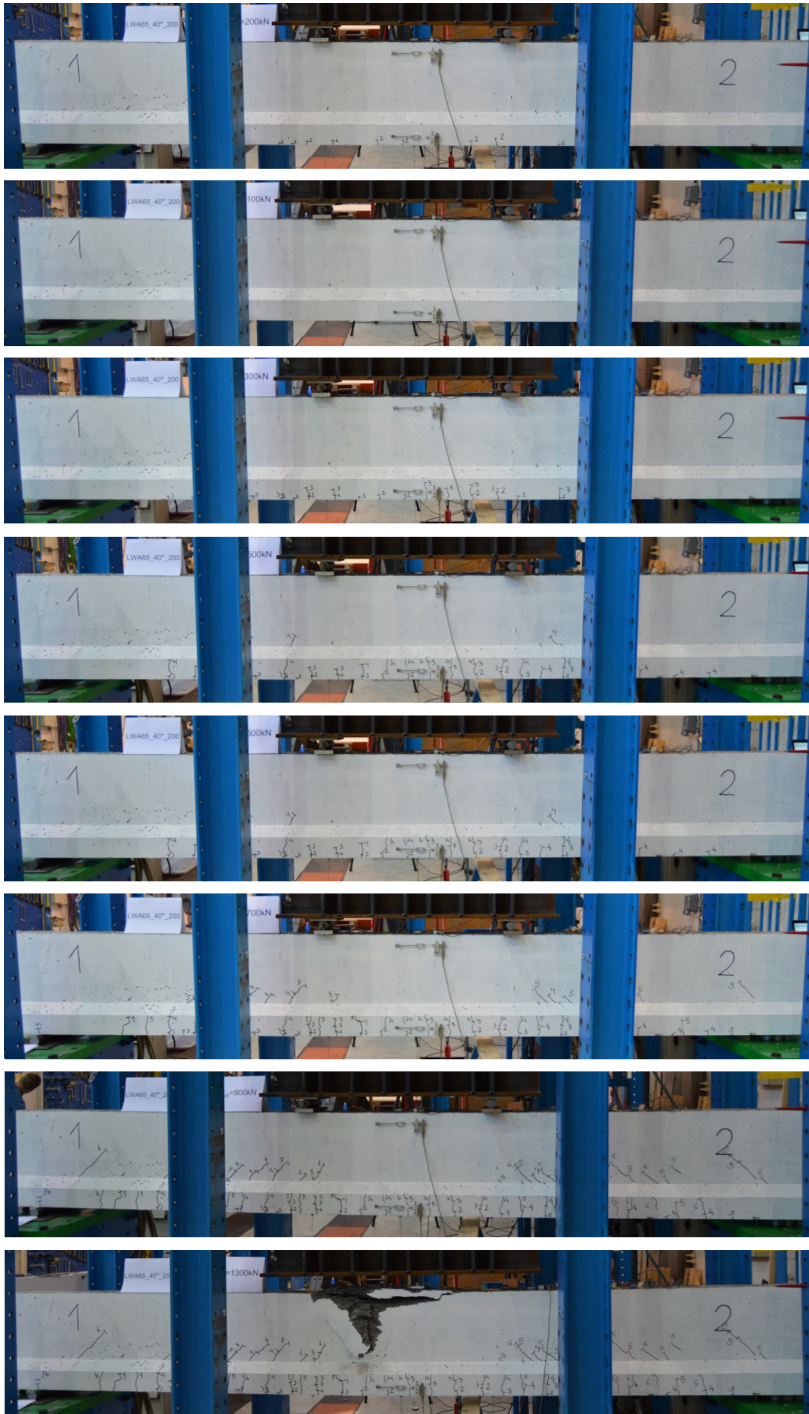
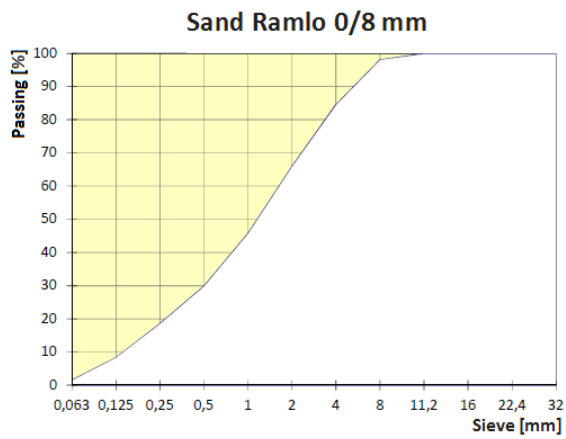
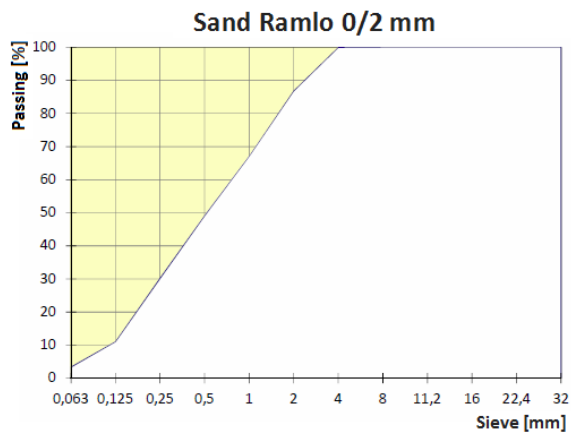


Figure B.7: Beam 7 - Load steps with drawn crack development.

B.3 Material Properties



**STALITE Lightweight Aggregate Properties and Gradations
for Structural Applications**

	3/4" (18mm)		1/2" (12.5mm)		3/8" (9.5mm)		MS16 Fines (#4 - 0)	
	lbs/cf	kg/m ³	lbs/cf	kg/m ³	lbs/cf	kg/m ³	lbs/cf	kg/m ³
Typical Density (Unit Weight)								
Dry Loose (ASTM C 29)	48	768	50	800	52	832	60	960
Dry Rodded (ASTM C 29)	55	880	56	896	58	928	65	1040
Saturated Surface Dry Loose (ASTM C 29)	50	800	52	832	53	848	55	880
Maximum Dry Density (ASTM D 4253)	60	960	-		-		-	
Damp Loose (ASTM C 29)	48-52	768-832	50-54	800-864	51-55	816-880	53-57	848-912
Typical Relative Density (Specific Gravity)								
Dry (ASTM C 127)	1.46		1.47		1.54		1.69	
Saturated Surface Dry (ASTM C 127)	1.52		1.53		1.60		1.75	
Range in Saturated Surface Dry (ASTM C 127)	1.47 - 1.54		1.49 - 1.55		1.57 - 1.64		1.70 - 1.80	
Sieve Size	% Passing		% Passing		% Passing		% Passing	
1" (25mm)	100		100		100		100	
3/4" (19mm)	90-100		100		100		100	
1/2" (12.5mm)	-		90-100		100		100	
3/8" (9.5mm)	10-50		40-80		80-100		100	
#4 (4.75mm)	0-15		0-20		5-40		97-100	
#8 (2.36mm)	-		0-10		0-20		89-100	
#16 (1.18mm)	-		-		0-10		46-66	
#30 (600um)	-		-		-		28-41	
#50 (300um)	-		-		-		17-25	
#100 (150um)	-		-		-		8-16	



Revised 11/2011

Proporsjonering av betong
SKANSKA

Prosjekt	Regnearktutvikling
Reseptnummer	Resept A
Tilsiktet kvalitet	B65 M40
Utført av	Stalite
Dato	01.04.2017

Initialparametre	Verdi	
$m = v/(c+\Sigma kp)$	0,39	
Luftinnhold	3,0 %	

Sementtype	Andel	Andel klinker	Andel FA	Andel slagg	[kg/m ³]	Alkalier	Klorider
	0,0 %	82,0 %	18,0 %	0,0 %	3000	1,4 %	0,1 %
Norcem Anlegg FA	100,0 %	100,0 %	0,0 %	0,0 %	3140	0,6 %	0,1 %
	0,0 %	100,0 %	0,0 %	0,0 %	1000	0,0 %	0,0 %

Tilsetningsmaterialer	Type	Andel (av b)	k	[kg/m ³]	Alkalier	Klorider
Elkem Microsilica	Silika	5,0 %	1,0	2200	0,1 %	0,1 %
	FA	0,0 %	0,7	2200	1,0 %	0,3 %
	Slagg	0,0 %	0,6	1000	1,0 %	0,3 %

Tilsetningsstoff	% av b	[kg/m ³]	Tørrstoff	[kg/m ³] TS	Alkalier	Klorider
	0,0 %	1050	16,0 %	1424	0,0 %	0,0 %
Mapel Dynamon SR-N	1,2 %	1040	19,0 %	1254	0,7 %	0,0 %
	0,0 %	1000	46,0 %	1000	0,2 %	0,1 %
	0,0 %	1000	100,0 %	1000	0,0 %	0,0 %

Fiber	Vol %	[kg/m ³]
	0,0 %	7800
	0,0 %	1050

Matriks	Verdi
Ønsket matriksvolum [l/m ³]	360
Oppnådd matriksvolum [l/m ³]	360
Klinkerandel i bindemiddel	95,0 %
Total FA- andel av bindemiddel	0,0 %
Total slaggandel av bindemiddel	0,0 %
Volum sementlim [l/m ³]	325,4
Effektivt vanninnhold [l/m ³]	177,0
v/p	0,34
Effektivt bindemiddel [kg/m ³]	454
Totalt bindemiddel [kg/m ³]	454

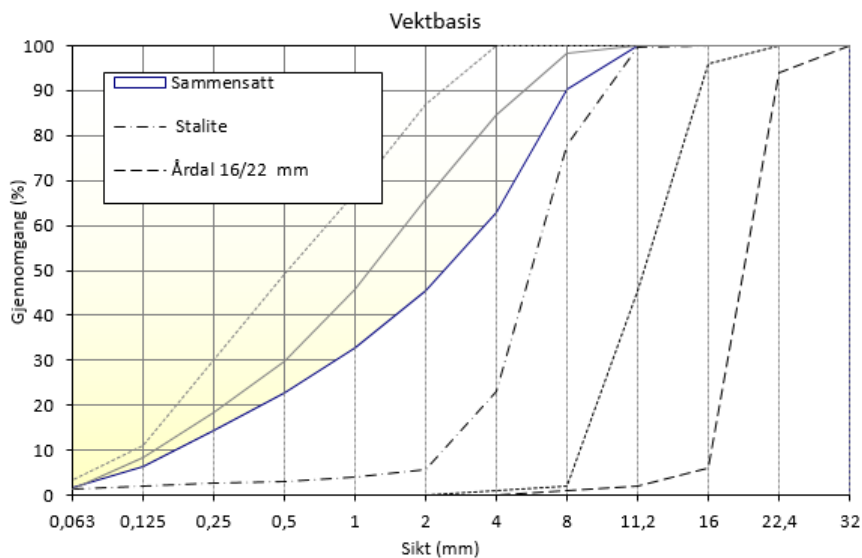
Blandeskjema	SKANSKA
---------------------	----------------

Prosjekt	Regnearkutvikling
Reseptnummer	Resept A
Tilsiktet kvalitet	B65 M40

Blandevolum	1000 liter
Dato:	Recipe for Norbetong
Tidspunkt for vanntilsetning:	
Ansvarlig:	
Utført av:	

Materialer	Resept kg/m ³	Sats kg	Fukt* %	Korr. kg	Oppveid** kg	
	0,0	0,000			0,000	
Norcem Anlegg FA	431,1	431,102			431,102	
	0,0	0,000			0,000	
Elkem Microsilica	22,7	22,690	0,0	0,000	22,690	
	0,0	0,000			0,000	
	0,0	0,000			0,000	
Fritt vann	177,0	176,979		-59,911	117,068	
Absorbert vann	6,3	6,315			6,315	123,383
Sand Ramlo 0/8 mm	552,6	552,579	7,7	42,549	595,128	
Sand Ramlo 0/2 mm nat. vask	236,8	236,820	5,5	13,025	249,845	
Årdal 8/16mm	0,0	0,000	0,5	0,000	0,000	
Årdal 16/22 mm	0,0	0,000	0,5	0,000	0,000	
Stalite	530,5	530,476	0,0	0,000	530,476	
	0,0	0,000	0,0	0,000	0,000	
	0,0	0,000	0,0	0,000	0,000	
	0,0	0,000	0,0	0,000	0,000	
	0,0	0,000	0,0	0,000	0,000	
	0,0	0,000	0,0	0,000	0,000	
	0,0	0,000	0,0	0,000	0,000	
	0,0	0,000	84	0,000	0,000	
Mapei Dynamon SR-N	5,4	5,355	81	4,337	5,355	
	0,0	0,000	54	0,000	0,000	
	0,0	0,000	0	0,000	0,000	
	0,0	0,000			0,000	
	0,0	0,000			0,000	

Fraksjon	Navn	Densitet [kg/m ³]	Abs. fukt [%]	Alk. reakt. Sv[%]	Klorider [%]	Andel		Bruk
						volum	vekt	
I	Sand Ramlo 0/8 mm	2650	0,8	0,0	0,00	0,323	0,420	ok
II	Sand Ramlo 0/2 mm na	2650	0,8	0,0	0,00	0,139	0,180	ok
III	Årdal 8/16mm	2700	0,0	0,0	0,00	0,000	0,000	
IV	Årdal 16/22 mm	2700	0,0	0,0	0,00	0,000	0,000	
V	Stalite	1530	0,0	0,0	0,00	0,538	0,400	ok
VI		2700	0,0	0,0	0,00	0,000	0,000	
VII		2700	0,0	0,0	0,00	0,000	0,000	
VIII		2700	0,0	0,0	0,00	0,000	0,000	
IX		2700	0,0	0,0	0,00	0,000	0,000	
X		2700	0,0	0,0	0,00	0,000	0,000	
Sammensatt		2050		0,0	0,00	1,000	1,000	



Appendix **C**

Calculations

C.1 Moment Capacity

Beam 1-4

Concrete cover: 20 mm Compr. reinf.: 2 ϕ 12

Sectional area of the tensile reinforcement	A_s	8042 mm ²	
Sectional area of the compressive reinforcement	A_s'	226 mm ²	
Height of the cross section	h	550 mm	
Width of the top part of the cross section	b	210 mm	
Compressive zone part of effective height	α	0,596	
Effective height	d	486 mm	
Neutral axis depth	αd	289 mm	
Distance from center of the compr. reinforcement to the top edge	d'	38 mm	
Oven-dry density	ρ	1834 kg/m ³	
Mean characteristic cylinder compressive strength after 28 days	f_{ck}	65 MPa	
Reduction factor	η_1	0,900	
	η	0,925	
	λ	0,763	
Young's modulus of the reinforcement	E_s	210000 MPa	
Characteristic yield strength of the reinforcement	f_{yk}	550 MPa	
Tensile reinforcement strain	ϵ_s	1,71 ‰	
Compressive reinforcement strain	ϵ_s'	2,19 ‰	(4.14)
Ultimate concrete strain (from tab. 11.3.1 in NS-EN 1992-1-1)	ϵ_{icu2}	2,52 ‰	
Concrete stress	σ_c	60 MPa	(4.15)
Compressive reinforcement stress	σ_s'	460 MPa	(4.16)
Tensile reinforcement stress	σ_s	359 MPa	(4.17)
Concrete force	F_c	2787 kN	(4.18)
Compressive reinforcement force	F_s'	104 kN	(4.19)
Tensile reinforcement force	F_s	2891 kN	(4.20)
Moment arm from the tensile reinforcement to the bottom edge	z_s	64 mm	
Moment arm from the compr. reinforcement to the bottom edge	z_s'	512 mm	
Moment arm from the concrete force to the bottom edge	z_c	440 mm	
Horizontal force equilibrium	ΣF_x	0 kN	
Moment capacity	M_R	1093 kNm	(4.21)
Maximum point load	P_{calc}	729 kN	

Beam 5-6

Concrete cover: 40 mm Compr. reinf.: 2 ϕ 12

Sectional area of the tensile reinforcement	A_s	8042 mm ²	
Sectional area of the compressive reinforcement	A_s'	226 mm ²	
Height of the cross section	h	550 mm	
Width of the top part of the cross section	b	210 mm	
Compressive zone part of effective height	α	0,596	
Effective height	d	486 mm	
Neutral axis depth	αd	290 mm	
Distance from center of the compr. reinforcement to the top edge	d'	58 mm	
Oven-dry density	ρ	1834 kg/m ³	
Mean characteristic cylinder compressive strength after 28 days	f_{ck}	65 MPa	
Reduction factor	η_1	0,900	
	η	0,925	
	λ	0,763	
Young's modulus of the reinforcement	E_s	210000 MPa	
Characteristic yield strength of the reinforcement	f_{yk}	550 MPa	
Tensile reinforcement strain	ϵ_s	1,71 ‰	
Compressive reinforcement strain	ϵ_s'	2,02 ‰	(4.14)
Ultimate concrete strain (from tab. 11.3.1 in NS-EN 1992-1-1)	ϵ_{icu2}	2,52 ‰	
Concrete stress	σ_c	60 MPa	(4.15)
Compressive reinforcement stress	σ_s'	423 MPa	(4.16)
Tensile reinforcement stress	σ_s	359 MPa	(4.17)
Concrete force	F_c	2789 kN	(4.18)
Compressive reinforcement force	F_s'	96 kN	(4.19)
Tensile reinforcement force	F_s	2885 kN	(4.20)
Moment arm from the tensile reinforcement to the bottom edge	z_s	64 mm	
Moment arm from the compr. reinforcement to the bottom edge	z_s'	492 mm	
Moment arm from the concrete force to the bottom edge	z_c	440 mm	
Horizontal force equilibrium	ΣF_x	0 kN	
Moment capacity	M_R	1088 kNm	(4.21)
Maximum point load	P_{calc}	726 kN	

Beam 7

Concrete cover: 40 mm Compr. reinf.: 2 ϕ 25

Sectional area of the tensile reinforcement	A_s	8042 mm ²	
Sectional area of the compressive reinforcement	A_s'	981 mm ²	
Height of the cross section	h	550 mm	
Width of the top part of the cross section	b	210 mm	
Compressive zone part of effective height	α	0,578	
Effective height	d	486 mm	
Neutral axis depth	αd	281 mm	
Distance from center of the compr. reinforcement to the top edge	d'	58 mm	
Oven-dry density	ρ	1834 kg/m ³	
Mean characteristic cylinder compressive strength after 28 days	f_{ck}	65 MPa	
Reduction factor	η_1	0,900	
	η	0,925	
	λ	0,763	
Young's modulus of the reinforcement	E_s	210000 MPa	
Characteristic yield strength of the reinforcement	f_{yk}	550 MPa	
Tensile reinforcement strain	ϵ_s	1,84 ‰	
Compressive reinforcement strain	ϵ_s'	2,00 ‰	(4.14)
Ultimate concrete strain (from tab. 11.3.1 in NS-EN 1992-1-1)	ϵ_{lcu2}	2,52 ‰	
Concrete stress	σ_c	60 MPa	(4.15)
Compressive reinforcement stress	σ_s'	420 MPa	(4.16)
Tensile reinforcement stress	σ_s	387 MPa	(4.17)
Concrete force	F_c	2702 kN	(4.18)
Compressive reinforcement force	F_s'	412 kN	(4.19)
Tensile reinforcement force	F_s	3114 kN	(4.20)
Moment arm from the tensile reinforcement to the bottom edge	z_s	64 mm	
Moment arm from the compr. reinforcement to the bottom edge	z_s'	492 mm	
Moment arm from the concrete force to the bottom edge	z_c	443 mm	
Horizontal force equilibrium	ΣF_x	0 kN	
Moment capacity	M_R	1200 kNm	(4.21)
Maximum point load	P_{calc}	800 kN	

C.2 Shear Capacity

Oven-dry density	ρ	1834 kg/m ³	
	η_{I1}	0,9	
	k_2	1	
Width of the top part of the cross section	b_w	210 mm	
Effective height	d	486 mm	
Mean characteristic cylinder compressive strength after 28 days	$f_{cd} = f_{cm}$	65 MPa	
Sectional area of the tensile reinforcement	A_{sl}	8042 mm ²	
Internal moment arm	z	437 mm	
Sectional area of the shear reinforcement	A_{sw}	226 mm ²	
Angle between compressive strut and horizontal axis	θ	40 degrees	
	$\tan\theta$	0,84	
	$\cot\theta$	1,19	
Yield strength of the shear reinforcement	$f_{ywk} = f_{ywd}$	550 Mpa	
	α_{cw}	1	
Without shear reinforcement			
	$C_{R,c}$	1	
	k	1,64	
Reinforcement ratio	ρ_l	0,02	
Shear capacity without shear reinforcement	$V_{R,c}$	764 kN	(4.22)
From table 11.6.1N in EC2	$V_{l,min}$	0,466 MPa	
	$V_{l,R,c}$	48 kN	(4.23)
With shear reinforcement			
Assumed shear force	$V_{l,R,s}$	900 kN	
Required stirrup spacing	s	72 mm	(4.24)
Strength reduction factor	v_1	0,37	
	$V_{l,R,max}$	1088 kN	(4.25)
Applied stirrup spacing	s	70 mm	
Final shear capacity	$V_{l,R,s}$	925 kN	(4.24)

C.3 Load-Deflection Curve

Young's modulus of the reinforcement	E_s	210000 MPa
Oven-dry density	ρ	1834 kg/m ³
	η_E	0,695
Young's modulus of LWAC	E_{lcm}	24175 MPa
Material stiffness ratio	η	8,687
Reinforcement ratio	ρ_l	0,079
Sectional area of the tensile reinforcement	A_{sl}	8042 mm ²
Sectional area of the concrete	A_c	115500 mm ²
Height of the cross section	h	550 mm
Width of the top part of the cross section	b	210 mm
Effective height	d	486 mm
Total length of the span	L	4000 mm
The length from the support to the point load	a	1500 mm

Stadium 1

Neutral axis depth	αd	355 mm
The concrete's contribution to the second moment of area	I_d	3,64E+09 mm ⁴
The reinforcement's contribution to the second moment of area	I_{s1}	1,39E+08 mm ⁴
Bending stiffness	$(EI)_1$	1,17E+14 Nmm ²
Maximum point load	P_{max}	800 kN
Deflection at midspan	δ_1	16,6 mm

Stadium 2

	$\rho_l \eta$	0,684
Compressive zone part of effective height	α	0,671
The equivalent second moment of area of the concrete	I_c	4,21E+09 mm ⁴
Bending stiffness	$(EI)_2$	1,02E+14 Nmm ²
Maximum point load	P_{max}	800 kN
Deflection at midspan	δ_{II}	19,1 mm

Cracking moment	M_{cr}	100 kNm
Tensile splitting strength of LWAC	f_{lctm}	4,03 MPa
Total cracking load	$P_{cr,tot}$	133 kN

Values used to calculate the load-deflection curve:

Total load $P_{,tot}$ [kN]	Uncracked	Cracked	Tension stiffening
0	0,00	0,00	0,00
50	0,52	0,60	0,52
100	1,04	1,20	1,04
133	1,39	1,59	1,39
200	2,08	2,39	2,25
300	3,12	3,59	3,50
400	4,16	4,79	4,72
500	5,20	5,98	5,93
600	6,24	7,18	7,13
700	7,28	8,38	8,34
800	8,32	9,57	9,54
900	9,36	10,77	10,74
1000	10,40	11,96	11,94
1100	11,44	13,16	13,14
1200	12,47	14,36	14,33
1300	13,51	15,55	15,53
1400	14,55	16,75	16,73
1500	15,59	17,95	17,93
1600	16,63	19,14	19,13

C.4 Confinement

Beam 1 - LWAC65_20_0

Width of stirrup center to centre	b_c	138 mm
Height of stirrup center to centre	d_c	180 mm
Distance from centre of reinforcement to neutral axis	d_{tot}	253
Free distance between long. reinf. 1	w'_1	158 mm
Free distance between long. reinf. 2	w'_2	102 mm
Free distance between long. reinf. 3	w'_3	158 mm
Distance of free concrete between stirrups	s'	276 mm
Distance between stirrups centre to centre	s	288 mm
Yield strength of stirrups	f_{yh}	550 MPa
Compressive strength of unconfined concrete	f_{c0}	65 MPa
Area of compressive longitudinal reinforcement	A_{sl}	226 mm ²
Area of stirrups in x-direction	A_{sx}	0 mm ²
Area of stirrups in y-direction	A_{sy}	0 mm ²
Ineffectively confined concrete area	A_i	10055 mm ²
Effectively confined concrete area	A_e	0 mm ²
Area of concrete within stirrups (long. reinf. area removed)	A_{cc}	24614
Longitudinal reinforcement ratio	ρ_{cc}	0,009
Effective confinement coefficient	k_e	0,000
Effective lateral stress in x-direction	f'_{lx}	0,00 MPa
Effective lateral stress in y-direction	f'_{ly}	0,00 MPa
Effective lateral stress	f'_l	0,00 MPa
Confined concrete capacity	f_{cc}	65,00 MPa
Increase of concrete capacity due to confinement		0,0 %
Unconfined concrete strain corresponding to the peak stress	ϵ_{c0}	0,002
Confined concrete strain corresponding to the peak stress	ϵ_{cc0}	0,0020
	η_E	0,746
Calculated Young's modulus in the first interval	E_{bc0}	32988 MPa
	k_c	1,015
	$k_{c'}$	0,015
Reinforcement ratio in x-direction	ρ_x	0
Reinforcement ratio in y-direction	ρ_y	0
The sum of the reinforcement ratio in x- and y-direction	ρ_s	0
The slope of the descending curve after peak stress	E_{slope}	32500 MPa
The strain corresponding to the stress equal to $0.65f_{cc}$	ϵ_{65}	0,0027
	η_1	0,918
Confined concrete ultimate strain	ϵ_{ccu}	0,0032

Beam 2 - LWAC65_20_200

Width of stirrup center to centre	b_c	138 mm
Height of stirrup center to centre	d_c	180 mm
Distance from centre of reinforcement to neutral axis	d_{tot}	253
Free distance between long. reinf. 1	w'_1	158 mm
Free distance between long. reinf. 2	w'_2	102 mm
Free distance between long. reinf. 3	w'_3	158 mm
Distance of free concrete between stirrups	s'	188 mm
Distance between stirrups centre to centre	s	200 mm
Yield strength of stirrups	f_{yh}	550 MPa
Compressive strength of unconfined concrete	f_{c0}	65 MPa
Area of compressive longitudinal reinforcement	A_{sl}	226 mm ²
Area of stirrups in x-direction	A_{sx}	226 mm ²
Area of stirrups in y-direction	A_{sy}	113 mm ²
Ineffectively confined concrete area	A_l	10055 mm ²
Effectively confined concrete area	A_e	2252 mm ²
Area of concrete within stirrups (long. reinf. area removed)	A_{cc}	24614
Longitudinal reinforcement ratio	ρ_{cc}	0,009
Effective confinement coefficient	k_e	0,092
Effective lateral stress in x-direction	f'_{lx}	0,32 MPa
Effective lateral stress in y-direction	f'_{ly}	0,21 MPa
Effective lateral stress	f'_l	0,26 MPa
Confined concrete capacity	f_{cc}	66,80 MPa
Increase of concrete capacity due to confinement		2,8 %
Unconfined concrete strain corresponding to the peak stress	ϵ_{c0}	0,002
Confined concrete strain corresponding to the peak stress	ϵ_{cc0}	0,0023
	η_E	0,746
Calculated Young's modulus in the first interval	E_{bc0}	33289 MPa
	k_c	1,134
	$k_{c'}$	0,134
Reinforcement ratio in x-direction	ρ_x	0,006
Reinforcement ratio in y-direction	ρ_y	0,008
The sum of the reinforcement ratio in x- and y-direction	ρ_s	0,014
The slope of the descending curve after peak stress	E_{slope}	29343 MPa
The strain corresponding to the stress equal to $0.65f_{cc}$	ϵ_{65}	0,0031
	η_1	0,918
Confined concrete ultimate strain	ϵ_{ccu}	0,0047

Beam 3 - LWAC65_20_60

Width of stirrup center to centre	b_c	138 mm
Height of stirrup center to centre	d_c	180 mm
Distance from centre of reinforcement to neutral axis	d_{tot}	253
Free distance between long. reinf. 1	w'_1	158 mm
Free distance between long. reinf. 2	w'_2	102 mm
Free distance between long. reinf. 3	w'_3	158 mm
Distance of free concrete between stirrups	s'	48 mm
Distance between stirrups centre to centre	s	60 mm
Yield strength of stirrups	f_{yh}	550 MPa
Compressive strength of unconfined concrete	f_{c0}	65 MPa
Area of compressive longitudinal reinforcement	A_{s1}	226 mm ²
Area of stirrups in x-direction	A_{sx}	226 mm ²
Area of stirrups in y-direction	A_{sy}	113 mm ²
Ineffectively confined concrete area	A_i	10055 mm ²
Effectively confined concrete area	A_e	10585 mm ²
Area of concrete within stirrups (long. reinf. area removed)	A_{cc}	24614
Longitudinal reinforcement ratio	ρ_{cc}	0,009
Effective confinement coefficient	k_e	0,430
Effective lateral stress in x-direction	f'_{lx}	4,95 MPa
Effective lateral stress in y-direction	f'_{ly}	3,23 MPa
Effective lateral stress	f'_l	4,09 MPa
Confined concrete capacity	f_{cc}	89,74 MPa
Increase of concrete capacity due to confinement		38,1 %
Unconfined concrete strain corresponding to the peak stress	ϵ_{c0}	0,002
Confined concrete strain corresponding to the peak stress	ϵ_{cc0}	0,0058
	η_E	0,746
Calculated Young's modulus in the first interval	E_{bc0}	36732 MPa
	k_c	2,376
	$k_{c'}$	1,376
Reinforcement ratio in x-direction	ρ_x	0,021
Reinforcement ratio in y-direction	ρ_y	0,027
The sum of the reinforcement ratio in x- and y-direction	ρ_s	0,048
The slope of the descending curve after peak stress	E_{slope}	15457 MPa
The strain corresponding to the stress equal to $0.65f_{cc}$	ϵ_{65}	0,0078
	η_1	0,918
Confined concrete ultimate strain	ϵ_{ccu}	0,0263

Beam 4 - LWAC65_20_100

Width of stirrup center to centre	b_c	138 mm
Height of stirrup center to centre	d_c	180 mm
Distance from centre of reinforcement to neutral axis	d_{tot}	253
Free distance between long. reinf. 1	w'_1	158 mm
Free distance between long. reinf. 2	w'_2	102 mm
Free distance between long. reinf. 3	w'_3	158 mm
Distance of free concrete between stirrups	s'	88 mm
Distance between stirrups centre to centre	s	100 mm
Yield strength of stirrups	f_{yh}	550 MPa
Compressive strength of unconfined concrete	f_{c0}	65 MPa
Area of compressive longitudinal reinforcement	A_{sl}	226 mm ²
Area of stirrups in x-direction	A_{sx}	226 mm ²
Area of stirrups in y-direction	A_{sy}	113 mm ²
Ineffectively confined concrete area	A_i	10055 mm ²
Effectively confined concrete area	A_e	7609 mm ²
Area of concrete within stirrups (long. reinf. area removed)	A_{cc}	24614
Longitudinal reinforcement ratio	ρ_{cc}	0,009
Effective confinement coefficient	k_e	0,309
Effective lateral stress in x-direction	f'_{lx}	2,14 MPa
Effective lateral stress in y-direction	f'_{ly}	1,39 MPa
Effective lateral stress	f'_l	1,77 MPa
Confined concrete capacity	f_{cc}	76,49 MPa
Increase of concrete capacity due to confinement		17,7 %
Unconfined concrete strain corresponding to the peak stress	ϵ_{c0}	0,002
Confined concrete strain corresponding to the peak stress	ϵ_{cc0}	0,0038
	η_E	0,746
Calculated Young's modulus in the first interval	E_{bc0}	34828 MPa
	k_c	1,716
	k'_c	0,716
Reinforcement ratio in x-direction	ρ_x	0,013
Reinforcement ratio in y-direction	ρ_y	0,016
The sum of the reinforcement ratio in x- and y-direction	ρ_s	0,029
The slope of the descending curve after peak stress	E_{slope}	20299 MPa
The strain corresponding to the stress equal to $0.65f_{cc}$	ϵ_{65}	0,0051
	η_1	0,918
Confined concrete ultimate strain	ϵ_{ccu}	0,0132

Beam 5 - LWAC65_40_60

Width of stirrup center to centre	b_c	138 mm
Height of stirrup center to centre	d_c	160 mm
Distance from centre of reinforcement to neutral axis	d_{tot}	233
Free distance between long. reinf. 1	w'_1	158 mm
Free distance between long. reinf. 2	w'_2	102 mm
Free distance between long. reinf. 3	w'_3	158 mm
Distance of free concrete between stirrups	s'	48 mm
Distance between stirrups centre to centre	s	60 mm
Yield strength of stirrups	f_{yh}	550 MPa
Compressive strength of unconfined concrete	f_{c0}	65 MPa
Area of compressive longitudinal reinforcement	A_{sl}	226 mm ²
Area of stirrups in x-direction	A_{sx}	226 mm ²
Area of stirrups in y-direction	A_{sy}	113 mm ²
Ineffectively confined concrete area	A_i	10055 mm ²
Effectively confined concrete area	A_e	8443 mm ²
Area of concrete within stirrups (long. reinf. area removed)	A_{cc}	21854
Longitudinal reinforcement ratio	ρ_{cc}	0,010
Effective confinement coefficient	k_e	0,386
Effective lateral stress in x-direction	f'_{lx}	5,01 MPa
Effective lateral stress in y-direction	f'_{ly}	2,90 MPa
Effective lateral stress	f'_l	3,95 MPa
Confined concrete capacity	f_{cc}	89,00 MPa
Increase of concrete capacity due to confinement		36,9 %
Unconfined concrete strain corresponding to the peak stress	ϵ_{c0}	0,002
Confined concrete strain corresponding to the peak stress	ϵ_{cc0}	0,0057
	η_E	0,746
Calculated Young's modulus in the first interval	E_{bc0}	36632 MPa
	k_c	2,343
	k'_c	1,343
Reinforcement ratio in x-direction	ρ_x	0,024
Reinforcement ratio in y-direction	ρ_y	0,027
The sum of the reinforcement ratio in x- and y-direction	ρ_s	0,051
The slope of the descending curve after peak stress	E_{slope}	15634 MPa
The strain corresponding to the stress equal to $0.65f_{cc}$	ϵ_{65}	0,0077
	η_1	0,918
Confined concrete ultimate strain	ϵ_{ccu}	0,0256

Beam 6 - LWAC65_40_100

Width of stirrup center to centre	b_c	138 mm
Height of stirrup center to centre	d_c	160 mm
Distance from centre of reinforcement to neutral axis	d_{tot}	233
Free distance between long. reinf. 1	w'_1	158 mm
Free distance between long. reinf. 2	w'_2	102 mm
Free distance between long. reinf. 3	w'_3	158 mm
Distance of free concrete between stirrups	s'	88 mm
Distance between stirrups centre to centre	s	100 mm
Yield strength of stirrups	f_{yh}	550 MPa
Compressive strength of unconfined concrete	f_{c0}	65 MPa
Area of compressive longitudinal reinforcement	A_{sl}	226 mm ²
Area of stirrups in x-direction	A_{sx}	226 mm ²
Area of stirrups in y-direction	A_{sy}	113 mm ²
Ineffectively confined concrete area	A_i	10055 mm ²
Effectively confined concrete area	A_e	5938 mm ²
Area of concrete within stirrups (long. reinf. area removed)	A_{cc}	21854
Longitudinal reinforcement ratio	ρ_{cc}	0,010
Effective confinement coefficient	k_e	0,272
Effective lateral stress in x-direction	f'_{lx}	2,11 MPa
Effective lateral stress in y-direction	f'_{ly}	1,22 MPa
Effective lateral stress	f'_l	1,67 MPa
Confined concrete capacity	f_{cc}	75,90 MPa
Increase of concrete capacity due to confinement		16,8 %
Unconfined concrete strain corresponding to the peak stress	ϵ_{c0}	0,002
Confined concrete strain corresponding to the peak stress	ϵ_{cc0}	0,0037
	η_E	0,746
Calculated Young's modulus in the first interval	E_{bc0}	34738 MPa
	k_c	1,683
	k'_c	0,683
Reinforcement ratio in x-direction	ρ_x	0,014
Reinforcement ratio in y-direction	ρ_y	0,016
The sum of the reinforcement ratio in x- and y-direction	ρ_s	0,031
The slope of the descending curve after peak stress	E_{slope}	20640 MPa
The strain corresponding to the stress equal to $0.65f_{cc}$	ϵ_{65}	0,0050
	η_1	0,918
Confined concrete ultimate strain	ϵ_{ccu}	0,0126

Beam 7 - LWAC65_40_200

Width of stirrup center to centre	b_c	138 mm
Height of stirrup center to centre	d_c	160 mm
Distance from centre of reinforcement to neutral axis	d_{tot}	233
Free distance between long. reinf. 1	w'_1	158 mm
Free distance between long. reinf. 2	w'_2	102 mm
Free distance between long. reinf. 3	w'_3	158 mm
Distance of free concrete between stirrups	s'	188 mm
Distance between stirrups centre to centre	s	200 mm
Yield strength of stirrups	f_{yh}	550 MPa
Compressive strength of unconfined concrete	f_{c0}	65 MPa
Area of compressive longitudinal reinforcement	A_{sl}	982 mm ²
Area of stirrups in x-direction	A_{sx}	604 mm ²
Area of stirrups in y-direction	A_{sy}	226 mm ²
Ineffectively confined concrete area	A_i	10055 mm ²
Effectively confined concrete area	A_e	1582 mm ²
Area of concrete within stirrups (long. reinf. area removed)	A_{cc}	21098
Longitudinal reinforcement ratio	ρ_{oc}	0,044
Effective confinement coefficient	k_e	0,075
Effective lateral stress in x-direction	f'_{lx}	0,78 MPa
Effective lateral stress in y-direction	f'_{ly}	0,34 MPa
Effective lateral stress	f'_l	0,56 MPa
Confined concrete capacity	f_{cc}	68,79 MPa
Increase of concrete capacity due to confinement		5,8 %
Unconfined concrete strain corresponding to the peak stress	ϵ_{c0}	0,002
Confined concrete strain corresponding to the peak stress	ϵ_{cc0}	0,0026
	η_E	0,746
Calculated Young's modulus in the first interval	E_{bc0}	33618 MPa
	k_c	1,263
	$k_{c'}$	0,263
Reinforcement ratio in x-direction	ρ_x	0,019
Reinforcement ratio in y-direction	ρ_y	0,022
The sum of the reinforcement ratio in x- and y-direction	ρ_s	0,041
The slope of the descending curve after peak stress	E_{slope}	26625 MPa
The strain corresponding to the stress equal to $0.65f_{cc}$	ϵ_{65}	0,0035
	η_1	0,918
Confined concrete ultimate strain	ϵ_{ccu}	0,0064